Università di Pisa

Facoltà di Scienze Matematiche Fisiche e Naturali

Corso di Laurea Magistrale in Fisica

Anno Accademico 2010/2011

Tesi di Laurea Magistrale

Electronic Quantum Interference - Diffraction Effects

Candidato
Stefano Valentini

Relatore
Prof. Vittorio Giovannetti

Contents

Chapter 1

Introduction

One of the most surprising and most discussed features of quantum mechanics is quantum entanglement [1]. The classic example of a two-particle entangled state was given by Einstein, Podolsky, and Rosen (EPR) in their famous 1935 gedankenexperiment [2], where the measurement of an observable on one of the particles determined the value of that observable for the other particle with unit probability.

In their paper EPR pointed out that quantum mechanics allows a two-particle state where the position of each particle is undetermined, but the measurement of one particle at a certain location implies that the other must be found at a specific corresponding location. Furthermore, a similar argument holds in momentum space. This interesting "nonlocal" phenomenon can never be understood from a classical point of view. To EPR this kind of nonlocality consitutes a paradox.

In the past century several efforts were made, trying to prove or disprove the existance of such effect [3] [4][5]. Quantum entanglement (or more precisely the violation of the strictly related Bell's inequality [6] in CHSH form [7]) was experimentally demonstrated by Aspect et al. [8] in 1982. Although questions regarding fundamental issues of quantum theory still exist, quantum entanglement has started to play an important role in practical applications, from quantum computation [9] to several other engineering applications.

Quantum imaging is one of these exciting areas. It implements ideas and techniques from the fields of quantum optics and nonlinear optics in order to, among other things, enhance the spatial resolution of imaging beyond the diffraction limit [10] and reproduce image in a nonlocal manner [11]. In addition, quantum imaging offers significant opportunities within the broader field of quantum information science. For instance quantum lithography benefits of the use of entangled N-photon states to improve the spatial resolution

of an imaging system by a factor of N, despite the Rayleigh diffraction limit. The idea was proposed by Bolo et al. [12] in 2000 and experimentally demonstrated by D'Angelo et al. [10] in 2001 by taking advantage of an entangled two-photon state of spontaneous parametric down-conversion (SPDC) [13]. Many practical applications of the subdiffraction-limited imaging techniques can be easily thought [14].

Actually, this wasn't the first realization of quantum imaging. In fact, the idea was introduced in the late 80's by Klyshko [15] , who proposed to study and test the two-particle EPR correlation in position and in momentum for an entangled two-photon system. The first experimental realization of this idea was made by Pittman et al. [11] in 1995 and immediately named "ghost imaging" due to its nonlocal feature.

Although it wasn't its main purpose, this work demonstrated that by joint-detection of two SPDC correlated photons it is possible to reconstrunct the image of an object, even if the photon that actually interacts with the object is counted by a fixed detector (no spatial resolution), while the scansion is made on the other side of the source by a moving detector, which captures the second photon of the pair (that seems not to "see" the object). On the contrary, in a classic imaging setup spatial-resolving detector and object are on the same side with respect to the light source.

Another quantum imaging setup is the one proposed by Strekalov et al. [16] in 1995. They demonstrated that it is possible to observe diffraction and interference by two-photon correlation measurements. The SPDC light beam is split by a polarization beam splitter into two beams (called signal and idler) and detected by two distant pointlike photon counting detectors for coincidences. A single- or double-slit aperture is inserted into the signal beam. A diffraction or interference pattern is observed in the coincidence counts by scanning the detector in the idler beam.

Both ghost imaging and ghost interference setups will be illustrated and discussed further in Chapter 2.

The advent of nanotechnology and nanostructures in the last few decades required imaging techniques that allow to inspect samples of atomic scale (nanometers). Of course optical microscopy in the visible or near-infrared range is of no use in this case because it cannot guarantee a sufficient resolution. X-ray and, most of all, electron microscopy have been used to image and characterize nanostructures [17].

The main idea of this thesis work is to combine the advantages of electron imaging and quantum imaging. In particular, we would like to introduce and study a model for a quantum imaging setup with an electronic source instead of a photonic one. As we already saw, a quantum imaging technique takes advantage of the entanglement of its two-particle probe. As far as

we know, only optical setups have been studied and experimentally demonstrated. They exploits the correlation of an SPDC photon pair.

In analogy with this kind of setups, we need a correlated pair of electrons to use as a probe for the sample. Our proposal is to use electron pairs field-emitted from a superconductor [18].

The superconducting state [19] is fully characterized by a set of correlation functions, that take into account long-range coherence and Cooper-pair correlations. If some particles are emitted from the superconductor, they retain some features of the correlation in the source. When a Cooper pair is emitted, its singlet spin state is a useful resource of entanglement [20]-[28], hence the idea of using it in our quantum imaging setup.

The process of electron field-emission was first theoretically explained by Fowler and Nordheim [29] in 1928. An experimental implementation of this process from a superconductor was realized by Nagaoka et al. [30] in 1998. Following the line proposed in the paper by Yuasa [18], we would like to treat the problem of emission as a tunneling process. We will use the transfer hamiltonian approach first introduced by Bardeen [31] in 1961. A brief review of the concepts of BCS ground state, field-emission and transfer hamiltonian approach will be given in Chapter 3.

Our model is studied in details in Chapter 4. The general setup is composed of a superconducting tip that emits correlated electrons in almost opposite directions, an object (for example a double-slit) and two detectors that work in coincidence. The detector on the object's side will be held fixed, while a spatial scansion will be done by the second, very distant detector on the other side with respect to the tip.

The aim of this work is to see if it is possible to observe any kind of ghost image or ghost interference / diffraction effect for slightly different configurations of the setup (like changing the tip's or the object's shape).

The whole setup is described in the framework of quantum field theory. After introducing the 3D effective Hamiltonian for the system, the dynamics is solved in the non-equilibrium stationary limit. The correlation functions and their spectra are computed and the image is reconstructed from them. The particular cases of infinite plane source and finite spherical source are presented in details.

A conclusive summary of the obtained results is given in Chapter 5.

Chapter 2

Quantum imaging

An image is a representation of an object by means of the spatial distribution $\varphi(\boldsymbol{r})$ of some physical quantity[32]. If an object is described by a function $f(\boldsymbol{r'})$, constructing the image of that object in some region of space means defining the functional relation $\varphi(\boldsymbol{r}) = I(\boldsymbol{r}, f)$, which associates to each point of the image region a function of the object distribution.

From an experimental point of view, often one would like to reconstruct the image on a screen by directly or indirectly measuring the intensity of some illuminating field over it, after that such field somehow is modified by the presence of the object.

In a classical, quite general setup, the field (photonic, electronic,etc...) generates from a source, interacts with the object and has its intensity measured by some scanning detector over the screen surface. Usually the object is placed between the source and the detector.

In a ghost imaging setup, one measures the coincidence countings of two detectors placed in different directions with respect to a source that emits correlated particles. The detector that is on the same side of the object is held fixed, while the scansion is done by the other one. In that case the position of the first detector can be considered as an external parameter and formally one still gets an image distribution like $\varphi(\boldsymbol{r}) = I(\boldsymbol{r}, f)$, where $\boldsymbol{r}$ is the position of the second detector.

In this chapter the first two important quantum imaging setups are discussed: the ghost imaging experiment by Pittman et al. [11] and the ghost interference setup by Strekalov et al. [16]. For each of them, first the experimental apparatus is illustrated and the observed data are shown and discussed. Then, we explain the results by introducing some simple theoretical models that exploit the formalism of Fourier optics [32].

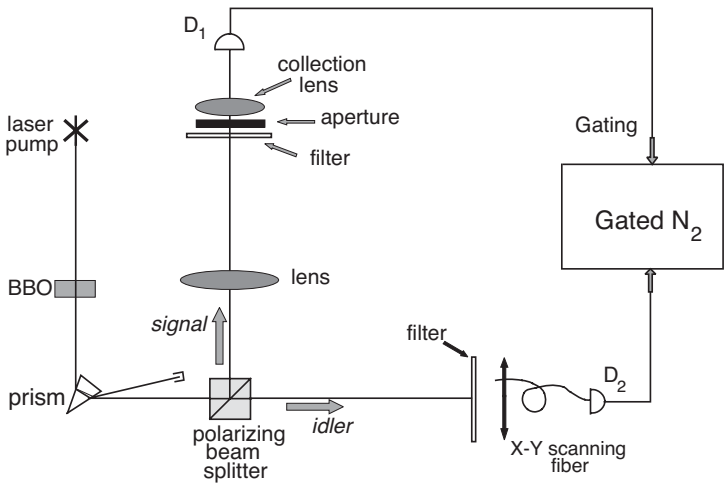

Figure 2.1: Schematic setup of the first ghost image experiment. Source: [11]

2.1 Pittman's experiment: ghost imaging

The schematic setup of the experiment is shown in Fig. 2.1. A continuous wave (CW) laser is used to pump a Beta Barium Borate (BBO) nonlinear crystal to produce an entangled pair of orthogonally polarized signal (e-ray of the crystal) and idler (o-ray of the crystal) photons in the nonlinear optical process of II-type spontaneous parametric down-conversion (SPDC) [13]. The pair emerges from the crystal collinearly with $\omega_s \cong \omega_i \cong \omega_p/2$ (degenerate SPDC) [11]. The pump is separated from the signal-idler pair by a dispersion prism, and then signal and idler are sent in different directions by a polarization beam splitting Thompson prism. The signal photon passes through a convex lens of 400mm focal length and illuminates a chosen aperture (mask).

As an example, one of the demonstrations used the letters "UMBC"[1] for the object mask. Behind the aperture is the "bucket" detector package D_1, which is made by an avalanche photodiode placed at the focus of a short-focal-length collection lens. During the experiment D_1 is kept in a fixed position. The idler photon is captured by detector package D_2, which consists of an optical fiber coupled to another avalanche photodiode. The input tip of the fiber is scannable in the transverse plane by two step motors (along orthogonal directions). The output pulses of D_1 and D_2, both operate in the photon counting mode, are independently counted as the counting rate of D_1 and D_2, respectively, and simultaneously, sent to a coincidence

[1]UMBC stands for University of Maryland, Baltimore County, where Pittman did the experiment and still works.

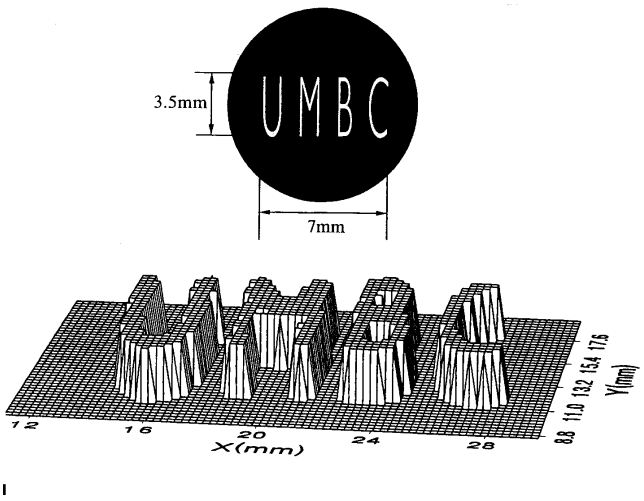

Figure 2.2: Upper: A reproduction of the actual aperture "UMBC" placed in the signal beam. Lower: The image of "UMBC": coincidence counts as a function of the fiber tip's transverse coordinates in the image plane. The step size is 0.25mm. The image shown is a "slice" at the half maximum value. Source: [11]

circuit for counting the joint-detection events of the pair. The single detector counting rates of D_1 and D_2 are both monitored to be constants during the measurement.

A "ghost" image of the chosen aperture is observed in coincidences during the scanning of the fiber tip, when the following two experimental conditions are met: (1) D_1 and D_2 always measure a pair; (2) the distances s_o, which is the optical distance between the aperture to the lens, s_i, which is the optical distance from the imaging lens going backward along the signal photon path to the two-photon source of SPDC then going forward along the idler photon path to the fiber tip, and the focal length of the imaging lens f satisfy the Gaussian thin lens equation:

$$\frac{1}{s_0} + \frac{1}{s_i} = \frac{1}{f}. \tag{2.1}$$

Figure 2.2 shows a typical measured ghost image. It is interesting to note that while the size of the "UMBC" aperture inserted in the signal path is only about 3.5mm×7mm, the observed image measures 7mm×14mm. The image is therefore magnified by a factor of 2 which equals the expected magnification $m = s_i/s_o$. In this measurement $s_o = 600$mm and $s_i = 1200$mm. When D_2 was scanned on transverse planes other than the ghost image plane the images blurred out.

As already anticipated in Chapter 1, the image of the object is reconstructed by joint-detection of correlated photon pairs, even if the photon that actually interacts with it is counted by a fixed detector (no spatial resolution), while the scansion is made on the other side of the source by a moving detector, which captures the second photon of the pair (that seems not to "see" the object).

A detailed theoretical explanation of the above results can be obtained as follows. We introduce the photon creation and annihilation operators that satisfy the commutation relation:

$$[a(\vec{\kappa}_l, \omega_l), a^\dagger(\vec{\kappa}_j, \omega_j)] = \delta_{l,j}\delta_{\vec{\kappa}_l,\vec{\kappa}_j}\delta_{\omega_l,\omega_j}, \tag{2.2}$$

where ω_l, $\vec{\kappa}_l$ $(l = s, i)$, are the frequency and transverse wavevector of the signal and idler, respectively. Specifically, $a(\vec{\kappa}_l, \omega_l)$ is the operator that destroys a photon of frequency ω_l and transverse momentum $\vec{\kappa}_l$ in the l beam, while $a^\dagger(\vec{\kappa}_j, \omega_j)$ creates a photon of frequency ω_j and transverse momentum $\vec{\kappa}_j$ in the beam j. Since $\omega/c = |k|$ for a photon in vacuum, where ω is the frequency, c is the light velocity and $|k|$ is the modulus of the momentum, specifying the couple $(\vec{\kappa}_l, \omega)$ is equivalent to say $(\vec{\kappa}_l, k_z)$. Let's recall that signal and idler are emitted with orthogonal polarization, hence the first δ in Eq.(2.2).

We also introduce the field operator $E^{(+)}(\vec{r}_j, t_j)$, or simply $E_j^{(+)}$, defined as

$$E^{(+)}(\vec{r}_j, t_j) = [E^{(-)}(\vec{r}_j, t_j)]^\dagger = \int d\vec{\kappa}_j\, d\omega_j\, a(\vec{\kappa}_j, \omega_j)\, \exp(-i\omega t_j)\, \varepsilon(\vec{\kappa}_j, \omega_j; \vec{r}_j), \tag{2.3}$$

where $j = s, i$ and $\varepsilon(\vec{\kappa}_j, \omega_j; \vec{r}_j)$ is the value of the classical field amplitude at $\vec{r}_j$; it takes into account the optical trasformations the photons undergo in their propagation due to the presence of lenses, filters, etc...(see the following paragraphs for the explicit expression of this function). Let's notice that $E^{(+)}$ is composed of only annihilation operators.

The quantity reported in Fig. 2.2 is the coincidence counting rate R_c, which is determined by the probability P_{12} of detecting a pair of photons by detectors D_1 and D_2 simultaneously. According to Glauber's quantum theory of photodetection [33], the latter is proportional to the square of the second order correlation function of the fields at points D_1 and D_2:

$$\begin{aligned} P_{12} &\propto \langle\Psi|E_1^{(-)}E_2^{(-)}E_2^{(+)}E_1^{(+)}|\Psi\rangle = |\langle 0|E_2^{(+)}E_1^{(+)}|\Psi\rangle|^2 = \\ &= |\Psi(\vec{\rho}_1, z_1, t_1; \vec{\rho}_2, z_2, t_2)|^2, \end{aligned} \tag{2.4}$$

where $E_1^{(+)}$ and $E_2^{(+)}$ are the field operators (2.3) evaluated at the detectors, while $\Psi(\vec{\rho}_1, z_1, t_1; \vec{\rho}_2, z_2, t_2)$ is the effective biphoton wavefunction [14],

and where finally $\vec{\rho}_1$ and $\vec{\rho}_2$ are the transverse coordinates of the point-like photodetector D_1 and D_2, on the object and image planes, respectively.

The expectation value is taken over the effective entangled biphoton state, which at the lowest order in the nonlinear coupling describes the nearly collinear signal-idler system generated by SPDC [14][34]:

$$\begin{aligned} |\,\Psi\,\rangle &= \Psi_0 \int d\vec{\kappa}_s\, d\vec{\kappa}_i\, \delta(\vec{\kappa}_s + \vec{\kappa}_i) \int d\omega_s\, d\omega_i \\ &\times \quad \delta(\omega_s + \omega_i - \omega_p)\, a^\dagger(\vec{\kappa}_s, \omega_s)\, a^\dagger(\vec{\kappa}_i, \omega_i)\,|\,0\,\rangle, \end{aligned} \tag{2.5}$$

where $|0\rangle$ represents the vacuum state of the fields, ω_j, $\vec{\kappa}_j$ $(j = s, i, p)$, are the frequency and transverse wavevector of the signal, idler, and pump, respectively, and where Ψ_0 is a normalization constant. [2] For simplicity a CW single mode pump with $\vec{\kappa}_p = 0$ is assumed. This state represents the equally probable creation of correlated photon pairs emitted in opposite transverse directions (hence $\delta(\vec{\kappa}_s + \vec{\kappa}_i)$) and whose frequencies add to give the pump frequency (hence $\delta(\omega_s + \omega_i - \omega_p)$, which is actually a statement of energy conservation). Equation (2.5) indicates that the biphoton state of the signal-idler pair is an entangled state, since it is not separable.

We will show that there exists a δ-function-like point-to-point correlation between the object and image planes, $\delta(\vec{\rho}_1 - \vec{\rho}_2/m)$. We will then show how the object function of $A(\vec{\rho}_o)$ is transferred to the image plane as a magnified image $A(\vec{\rho}_2/m)$.

We first calculate the effective biphoton wavefunction $\Psi(\vec{\rho}_1, z_1, t_1; \vec{\rho}_2, z_2, t_2)$, as defined in Eq. (2.4) . By inserting the field operators of Eq. (2.3) into $\Psi(\vec{\rho}_1, z_1, t_1; \vec{\rho}_2, z_2, t_2)$, and considering the commutation relations of the field operators, the effective biphoton wavefunction is calculated to be

$$\begin{aligned} \Psi(\vec{\rho}_1, z_1, t_1; \vec{\rho}_2, z_2, t_2) &= \Psi_0 \int d\vec{\kappa}_s\, d\vec{\kappa}_i\, \delta(\vec{\kappa}_s + \vec{\kappa}_i) \int d\omega_s\, d\omega_i\, \delta(\omega_s + \omega_i - \omega_p) \\ &\times \quad \varepsilon(\vec{\kappa}_s, \omega_s; \vec{\rho}_1, z_1)\, e^{-i\omega_s t_1} \varepsilon(\vec{\kappa}_i, \omega_i; \vec{\rho}_2, z_2)\, e^{-i\omega_i t_2}. \end{aligned} \tag{2.6}$$

Equation (2.6) indicates a coherent superposition of all the biphoton amplitudes. Next, we follow the unfolded experimental setup of Fig. 2.3 to establish the field amplitudes $\varepsilon(\vec{\kappa}_s, \omega_s, \vec{\rho}_1, z_1)$ and $\varepsilon(\vec{\kappa}_i, \omega_i, \vec{\rho}_2, z_2)$. For simplicity, in the following calculation we consider degenerate $(\omega_s = \omega_i = \omega)$ and collinear SPDC. Let's put the origin of the z-axis on the source plane and let's analyse the case of paraxial approximation: the source only emits photon with small transverse momentum, i.e. $|\vec{\kappa}| \ll \omega/c$. Using the transfer

[2] In writing Eq. (2.5), we dropped an irrelevant term proportional to the vacuum which doesn't contribute to the correlation measurements.

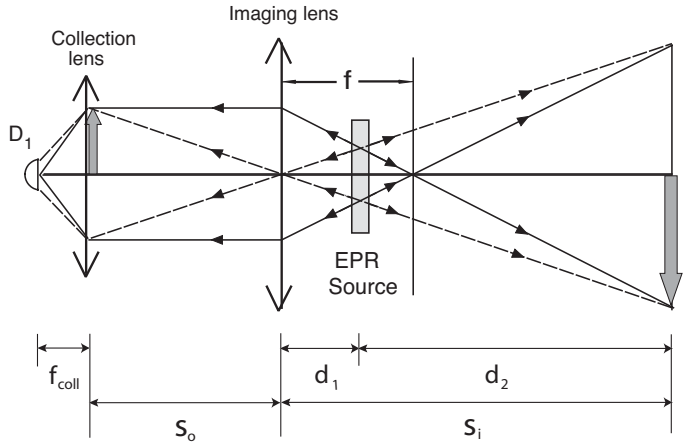

Figure 2.3: In arm-1 the signal propagates freely over a distance d_1 from the output plane of the source to the imaging lens, passes an object aperture at distance s_o, and then is focused onto photon-counting detector D_1 by a collection lens. In arm-2 the idler propagates freely over a distance d_2 from the output plane of the source to a point-like photon counting detector D_2. Source: [11]

function approach, we can write

$$\varepsilon(\vec{\kappa}_j, \omega; \vec{\rho}_j, z_j) = \int_{source} d\vec{\rho}_0 \varepsilon_0(\vec{\kappa}_j, \omega; \vec{\rho}_0) g(\vec{\kappa}_j, \omega, \vec{\rho}_j - \vec{\rho}_0, z_j), \tag{2.7}$$

where $g(\vec{\kappa}_j, \omega, \vec{\rho}_j - \vec{\rho}_0, z_j)$ is the single-mode Green's function [35][32] which propagates the field from the point $(\vec{\rho}_0, 0)$ on the source plane to the point $(\vec{\rho}_j, z_j)$ on the jth detector. We assume the field amplitude just outside the source ($z = 0$) having the free field form

$$\varepsilon_0(\vec{\kappa}_j, \omega; \vec{\rho}_0) = \exp(i\vec{k}_j \cdot \vec{\rho}_0). \tag{2.8}$$

In arm-1 the signal propagates freely over a distance d_1 from the output plane of the source to the imaging lens, passes an object aperture at distance s_o, and then is focused onto photon-counting detector D_1 by a collection lens. We will evaluate $g(\vec{\kappa}_s, \omega_s, \vec{\rho}_1 - \vec{\rho}_s, z_1)$ by propagating the field from the output plane of the biphoton source to the object plane. In arm-2 the idler propagates freely over a distance d_2 from the output plane of the biphoton source to a point-like detector D_2. $g(\vec{\kappa}_i, \omega_i, \vec{\rho}_2 - \vec{\rho}_{s'}, z_2)$ is thus a free propagator.

(I) Arm-1 (source to object):

The optical transfer function or Green's function in arm-1, which propagates the field from the source plane to the object plane, is given by:

$$\begin{aligned} g(\vec{\kappa}_s, \omega_s; \vec{\rho}_1 - \vec{\rho}_s, z_1 = d_1 + s_o) &= e^{i\frac{\omega_s}{c} z_1} \int_{lens} d\vec{\rho}_l \left\{ \frac{-i\omega_s}{2\pi c d_1} e^{i\frac{\omega_s}{2cd_1} |\vec{\rho}_s - \vec{\rho}_l|^2} \right\} \\ &\times \quad e^{-i\frac{\omega}{2cf} |\vec{\rho}_l|^2} \left\{ \frac{-i\omega_s}{2\pi c s_o} e^{i\frac{\omega_s}{2cs_o} |\vec{\rho}_l - \vec{\rho}_1|^2} \right\}, \quad (2.9) \end{aligned}$$

where $\vec{\rho}_s$ and $\vec{\rho}_l$ are the transverse vectors defined, respectively, on the output plane of the source and on the plane of the imaging lens. The terms in the first and second curly brackets in Eq. (2.9) describe free space propagation [32] from the output plane of the source to the imaging lens and from the imaging lens to the object plane, respectively. $e^{i\frac{\omega_s}{2cd_1} |\vec{\rho}_s - \vec{\rho}_l|^2}$ and $e^{i\frac{\omega_s}{2cs_o} |\vec{\rho}_l - \vec{\rho}_1|^2}$ are the Fresnel phases [32]. Here the imaging lens is treated as a thin-lens, and the transformation function of the imaging lens is approximated as a Gaussian, $l(|\vec{\rho}_l|, f) \cong e^{-i\frac{\omega}{2cf} |\vec{\rho}_l|^2}$ [32].

(II) Arm-2 (from source to image):

In arm-2, the idler propagates freely from the source to the plane of D_2, which is also the plane of the image. The Green's function is

$$g(\vec{\kappa}_i, \omega_i; \vec{\rho}_2 - \vec{\rho}_{s'}, z_2 = d_2) = \frac{-i\omega_i}{2\pi c d_2} e^{i\frac{\omega_i}{c} d_2} e^{i\frac{\omega_i}{2cd_2} |\vec{\rho_s'} - \vec{\rho}_2|^2} \quad (2.10)$$

where $\vec{\rho_s'}$ and $\vec{\rho}_2$ are the transverse vectors defined, respectively, on the output plane of the source and the plane of photodetector D_2.

(III) $\Psi(\vec{\rho}_1, \vec{\rho}_2)$ and P_{12} (object plane - image plane):

The effective transverse biphoton wavefunction $\Psi(\vec{\rho}_1, \vec{\rho}_2)$ is then evaluated by substituting the Green's functions $g(\vec{\kappa}_s, \omega; \vec{\rho}_1 - \vec{\rho}_s, z_1)$ and $g(\vec{\kappa}_i, \omega; \vec{\rho}_2 - \vec{\rho}_{s'}, z_2)$ into Eq. (2.6) using Eq. (2.7),

$$\begin{aligned} \Psi(\vec{\rho}_1, \vec{\rho}_2) &\propto \int d\vec{\kappa}_s \, d\vec{\kappa}_i \, \delta(\vec{\kappa}_s + \vec{\kappa}_i) \, g(\vec{\kappa}_s, \omega; \vec{\rho}_1, z_1) \, g(\vec{\kappa}_i, \omega; \vec{\rho}_2, z_2) \\ &\propto \int d\vec{\kappa}_s \, d\vec{\kappa}_i \, \delta(\vec{\kappa}_s + \vec{\kappa}_i) \int_{lens} d\vec{\rho}_l \int_{source} d\vec{\rho}_s \; e^{i\vec{\kappa}_s \cdot \vec{\rho}_s} e^{i\frac{\omega}{2cd_1} |\vec{\rho}_s - \vec{\rho}_l|^2} \\ &\times \; e^{-i\frac{\omega}{2cf} |\vec{\rho}_l|^2} \; e^{i\frac{\omega_s}{2cs_o} |\vec{\rho}_l - \vec{\rho}_1|^2} \int_{source} d\vec{\rho_s'} \; e^{i\vec{\kappa}_i \cdot \vec{\rho_s'}} \, e^{i\frac{\omega_i}{2cd_2} |\vec{\rho_s'} - \vec{\rho}_2|^2} \quad (2.11) \end{aligned}$$

where all the proportionality constants and overall phases have been ignored. After computing the double integral over $d\vec{\kappa}_s$ and $d\vec{\kappa}_i$

$$\int d\vec{\kappa}_s \, d\vec{\kappa}_i \, \delta(\vec{\kappa}_s + \vec{\kappa}_i) \, e^{i\vec{\kappa}_s \cdot \vec{\rho}_s} \, e^{i\vec{\kappa}_i \cdot \vec{\rho_s'}} \sim \delta(\vec{\rho}_s - \vec{\rho_s'}),$$

Eq. (2.11) becomes

$$\Psi(\vec{\rho}_1,\vec{\rho}_2) \propto \int_{lens} d\vec{\rho}_l \int_{source} d\vec{\rho}_s \, e^{i\frac{\omega}{2cd_2}|\,\vec{\rho}_2-\vec{\rho}_s\,|^2} \, e^{i\frac{\omega}{2cd_1}|\,\vec{\rho}_s-\vec{\rho}_l\,|^2} \, e^{-i\frac{\omega}{2cf}\,|\vec{\rho}_l|^2} \, e^{i\frac{\omega}{2cs_o}|\,\vec{\rho}_l-\vec{\rho}_o\,|^2}.$$

Next, we compute the integral for $d\vec{\rho}_s$,

$$\Psi(\vec{\rho}_1,\vec{\rho}_2) \propto \int_{lens} d\vec{\rho}_l \, e^{i\frac{\omega}{2cs_i}|\,\vec{\rho}_2-\vec{\rho}_l\,|^2} \, e^{-i\frac{\omega}{2cf}\,|\vec{\rho}_l|^2} e^{i\frac{\omega}{2cs_o}|\,\vec{\rho}_l-\vec{\rho}_1\,|^2}, \tag{2.12}$$

where we have replaced $d_1 + d_2$ with s_i (as depicted in Fig. 2.3). Although the signal and idler propagate in different directions along two optical arms, interestingly, the amplitude in Eq. (2.12) is equivalent to that of a classical imaging setup, as if the field starts from a point $\vec{\rho}_1$ on the object plane, propagates the lens and then arrives at point $\vec{\rho}_2$ on the imaging plane.

The finite integral on $d\vec{\rho}_l$ yields a point-to-"spot" relationship between the object plane and the image plane that is defined by the Gaussian thin-lens equation

$$\Psi(\vec{\rho}_1,\vec{\rho}_2) \propto \int_{lens} d\vec{\rho}_l \, e^{i\frac{\omega}{2c}[\frac{1}{s_o}+\frac{1}{s_i}-\frac{1}{f}]|\,\vec{\rho}_l|^2} \, e^{-i\frac{\omega}{c}(\frac{\vec{\rho}_1}{s_o}+\frac{\vec{\rho}_2}{s_i})\cdot\vec{\rho}_l} = \frac{2J_1\Big(\frac{R}{s_o}\,\frac{\omega}{c}|\vec{\rho}_1+\frac{\vec{\rho}_2}{m}|\Big)}{\Big(\frac{R}{s_o}\,\frac{\omega}{c}|\vec{\rho}_1+\frac{\vec{\rho}_2}{m}|\Big)}, \tag{2.13}$$

where R is the radius of the lens and $J_1(x)$ is the first kind Bessel function of order 1. If the integral is taken to infinity ($R \to \infty$), by imposing the condition of the Gaussian thin-lens equation the effective transverse biphoton wavefunction can be approximated as a δ function

$$\Psi(\vec{\rho}_1,\vec{\rho}_2) \sim \delta(\vec{\rho}_1+\vec{\rho}_2/m). \tag{2.14}$$

We now include an object-aperture function, a collection lens and a photon counting detector D_1 into the optical transfer function of arm-1 as shown in Fig. 2.1. The collection-lens+D_1 package can be simply treated as a "bucket" detector, i.e. a detector which only signals the arrival of the photon but which is insensitive to the exact position of the detection event. Therefore its action can be effectively accounted for by integrating the biphoton amplitudes $\Psi(\vec{\rho}_1,\vec{\rho}_2)$, which are modulated by the object aperture function $A(\vec{\rho}_1)$ into a joint photodetection event. This process is equivalent to the following convolution [14]

$$P_{12} \propto \int_{object} d\vec{\rho}_1 \, \big|A(\vec{\rho}_1)\big|^2 \, \big|\Psi(\vec{\rho}_1,\vec{\rho}_2)\big|^2 \simeq \big|A(\vec{\rho}_2/m)\big|^2. \tag{2.15}$$

Again, D_2 is scanned in the image plane. A ghost image of the object is thus reproduced on the image plane by means of the joint-detection between the point-like-detector D_2 and the bucket detector D_1.

The physical process behind the data of Fig. 2.2 is now clear. Suppose the point detector D_2 is triggered by an idler photon at a transverse position $\vec{\rho}_{\rm I}$ in a joint-detection event together with the bucket detector D_1 being triggered by the signal twin, that is either transmitted or reflected from a unique point $\vec{\rho}_{\rm o}$ on the object plane. This unique point-to-point determination comes from the non-factorizable correlation function $\delta(\vec{\rho}_{\rm o} + \vec{\rho}_I/m)$. Now, we move D_2 to another transverse position $\vec{\rho'}_I$ and register a joint-detection event. The signal photon that triggers D_1 must be either transmitted or reflected from another unique point $\vec{\rho'}_o$ on the object plane which is determined by $\delta(\vec{\rho'}_{\rm o}+\vec{\rho'}_{\rm I}/m)$. The chances of receiving a joint detection event at $\vec{\rho}_{\rm I}$ and at $\vec{\rho'}_{\rm I}$ would be modulated by the values of the aperture function $A(\vec{\rho}_{\rm o})$ and $A(\vec{\rho'}_{\rm o})$, respectively. By accumulating a large number of joint-detection events at each transverse coordinate on the image plane, the aperture function $A(\vec{\rho}_{\rm o})$ is thus reproduced in the joint-detection as a function of $\vec{\rho}_{\rm I}$.

2.2 Strekalov's experiment: ghost diffraction

The schematic setup of the experiment is shown in Fig. 2.4. As in the Pittman setting discussed before, a CW argon laser is used to pump a 3mm long BBO crystal to produce an entangled pair of orthogonally polarized signal (e-ray of the crystal) and idler (o-ray of the crystal) photons in the nonlinear optical process of SPDC. The pair emerges from the crystal collinearly with $\omega_s \cong \omega_i \cong \omega_p/2$ (degenerate SPDC). The pump beam has width 2mm FWHM (full width at half maximum) and divergence of about 0.3mrad. It is separated from the signal-idler pair by a fused quartz dispersion prism, and then signal and idler are sent in different directions by a polarization beam splitting prism (BS). The signal photon passes through a single- or double-slit aperture and then travels about 1m to a photon counting detector D_1 (0.5mm in diameter). During the experiment D_1 is kept in a fixed position along the axis of the signal beam. The idler photon travels a distance of about 1.2m from BS before being captured by detector package D_2, which consists of an optical fiber coupled to another photon counting detector (0.5mm in diameter). The input tip of the fiber is scannable in the horizontal transverse direction by an encoder driver. Two 702.2nm spectral filters f_1 and f_2 with 10nm FWHM bandwidth are inserted in front of each detector. The output pulses of D_1 and D_2 are simultaneously sent to a coincidence circuit for counting the joint-

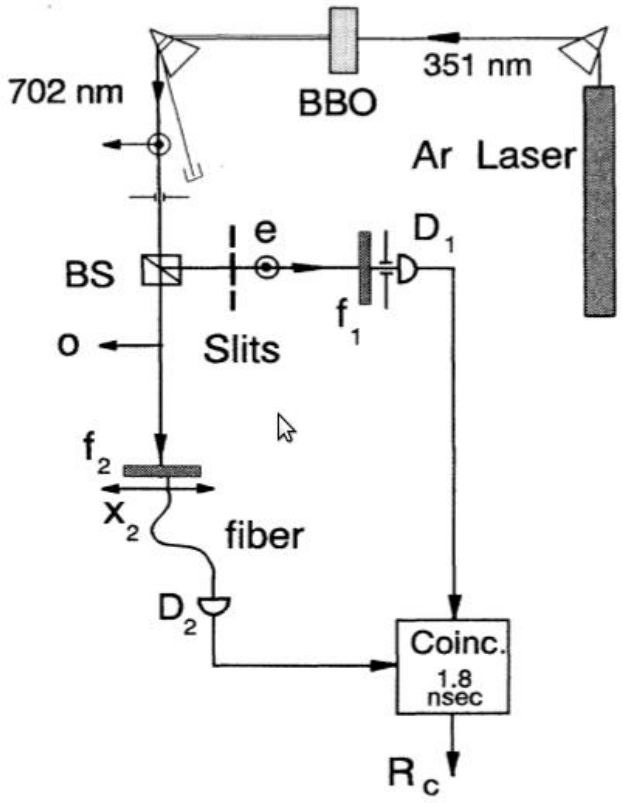

Figure 2.4: Schematic setup of the first ghost interference experiment. Source: [16]

detection events of the pair with a 1.8ns coincidence time window. The setup is similar to Pittman's [11] with the exception of losing the lens and moving the object in its place. The goal of this experiment is to obtain diffraction and/or interference patterns exploiting, as for the imaging case of Section 2.1, the correlation of SPDC photon pairs.

Let's examine the single-slit aperture case. The model can be derived from the one discussed for Pittman's experiment. After substituting the lens with the aperture, the first part can be used "mutatis mutandis". Eq. (2.12) thus becomes

$$\Psi(\vec{\rho}_1, \vec{\rho}_2) \propto e^{i\frac{\omega}{c}(z_1+z_2)} \int d\vec{\rho}_l \, e^{i\frac{\omega}{2cz_2}|\vec{\rho}_2-\vec{\rho}_l|^2} A(\vec{\rho}_l) e^{i\frac{\omega}{2cz_1}|\vec{\rho}_l-\vec{\rho}_1|^2}, \tag{2.16}$$

where z_1 is the distance from detector D_1 to the object and z_2 is the distance from detector D_2 to the object. Let's recall the fact that the detector D_1 is fixed on the axis of the signal beam, which means $\vec{\rho}_1 = 0$. In the case of an

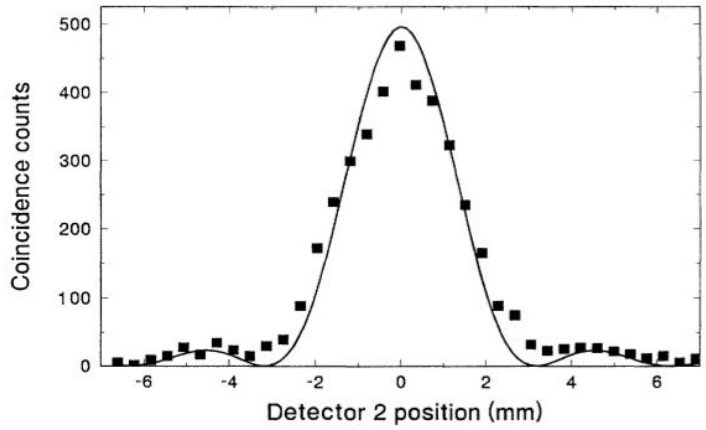

Figure 2.5: Two-photon diffraction pattern: coincidence counts (per 400s) vs the idler photon detection. A single slit of width a =0.4mm is in the signal beam. Source: [16]

infinitely long single slit with slit width a along the x-axis, we can describe the aperture with the following function:

$$A(\vec{\rho}_l) = \begin{cases} 1, & \text{if } |x| \leq a/2 \\ 0, & \text{otherwise.} \end{cases} \tag{2.17}$$

Under the assumption $\omega a^2 \ll z_1, z_2$, which is verified in this experiment, the integral in Eq. (2.16) gives the approximated result

$$\Psi(x_2) \propto \text{sinc}(x_2 \pi a / \lambda z_2), \tag{2.18}$$

where $\text{sinc}(x) = \sin(x)/x$ is the cardinal sine function and where we discarded some phases and proportionality constants.

From Eqs. (2.4),(2.18) we have

$$R_c(x_2) \propto \text{sinc}^2(x_2 \pi a / \lambda z_2), \tag{2.19}$$

that agrees with the curve extrapolated by a fitting of experimental data (see Fig. 2.5).

The latter show a diffraction pattern, observed in coincidences by scanning D_2 in the transverse direction of the idler beam even though single-slit aperture is in the other arm. Let's notice that this pattern is the same as one would observe illuminating the single slit directly, that is to say substituting the detector $D1$ with a point-like light source and placing a reflecting mirror instead of the BBO crystal in the setup of Fig. 2.4. Indeed, the relevant distance is the one from the slit to the second detector.

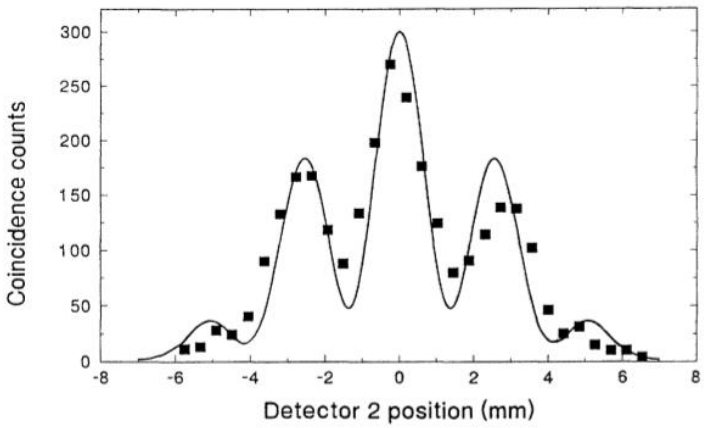

Figure 2.6: Two-photon double-slit "ghost" interference-diffraction pattern: the dependence of the coincidences (per 400s) on the position of detector D_2, which counts the idler photons, while the signal photons pass through a double-slit with a= 0.15mm and d= 0.47mm. The theoretical curve is calculated with corrections for the finite size of the detectors and the pump profile. Source: [16]

For the double-slit case we can use the same approach as before, after substituting the aperture function with

$$A(\vec{\rho_l}) = \begin{cases} 1, & \text{if } (d-a)/2 \leq |x| \leq (d+a)/2 \\ 0, & \text{otherwise.} \end{cases} \tag{2.20}$$

Adding to the previous ones the assumption $\omega d^2 \ll z_1, z_2$, after discarding some overall phases and proportionality constants we obtain

$$\Psi(x_2) \propto \text{sinc}(x_2 \pi a/\lambda z_2)(\exp(\frac{i\omega d}{2cz_2}) + \exp(\frac{-i\omega d}{2cz_2})), \tag{2.21}$$

which brings us to

$$R_c(x_2) \propto \text{sinc}^2(x_2 \pi a/\lambda z_2) \cos^2(x_2 \pi d/\lambda z_2), \tag{2.22}$$

that agrees with the curve extrapolated by a fitting of experimental data (see Fig. 2.6), after some corrections for the finite size of the detectors and the pump profile.

As in the previous case, the experimental results show an interference / diffraction pattern, observed in coincidences by scanning D_2 in the transverse direction of the idler beam, even though the double-slit aperture is in the other arm. Again, the pattern is the same as the one observed if we put a

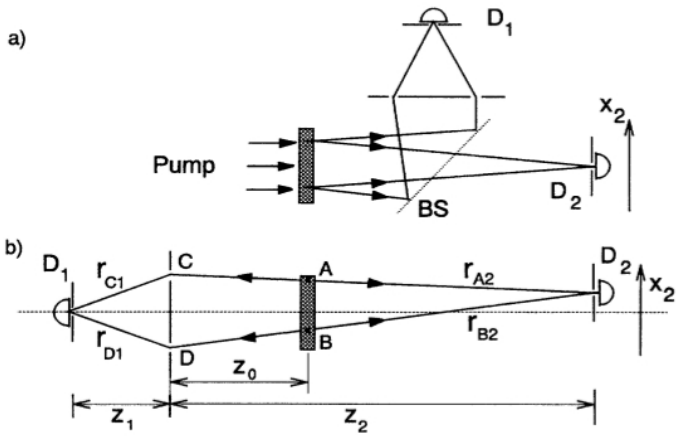

Figure 2.7: Simplified experimental scheme (a) and its "unfolded" version (b). Source: [16]

screen on the plane of D_2 and replace D_1 with a point-like source and the BBO crystal with a reflecting mirror.

The double slit interference can be explained also exploiting a different, but equivalent approach. In terms of the Copenaghen interpretation one can say that the interference is due to the uncertainty in the birth place (A or B in Fig. 2.7) of a photon pair. This is equivalent to say that the uncertainty is in the choice of the slit (C or D in Fig. 2.7), since the path from D_1 to D_2 is constrained by the condition that signal and idler photons emerge with opposite transverse momentum. As long as the interference is concerned, we are only interested in the independent modes of the signal and idler photons emitted in A and B. So the four-mode state vector of the SPDC field is

$$|\Psi\rangle = \Psi_0(a_s^\dagger a_i^\dagger \exp(i\phi_A) + b_s^\dagger b_i^\dagger \exp(i\phi_B))|0\rangle \tag{2.23}$$

where ϕ_A and ϕ_B are the phases of the pump field at A and B, $a_j^\dagger$ and $b_j^\dagger$ are the photon creation operators for the upper and lower mode in Fig. 2.7(b). Let's recall the fact that $\omega_s \cong \omega_i \cong \omega_p/2$. This means that the modulus k of the wavevector is fixed and is the same for both signal and idler. The fields at the detectors are given by

$$\begin{aligned} E_1^{(+)} &= a_s \exp(ikr_{A1}) + b_s \exp(ikr_{B1}), \\ E_2^{(+)} &= a_i \exp(ikr_{A2}) + b_i \exp(ikr_{B2}), \end{aligned} \tag{2.24}$$

where r_{Aj} and r_{Bj} are the optical path lengths from the source, along the upper or lower path, to the jth detector. For simplicity we assume $\phi_A = \phi_B$

(the transverse coherence of the pump beam at A and B is crucial in order to obtain interference, so this assumption is not totally arbitrary). Substituting Eqs. (2.23),(2.24) into Eq. (2.4), we have

$$R_c \propto 1 + \cos\left[k(r_A - r_B)\right], \tag{2.25}$$

where $r_A = r_{A1} + r_{A2}$ and $r_B = r_{B1} + r_{B2}$ are the overall optical lengths between the detectors. As we suggested before, it is equivalent to consider the points C and D in Fig. 2.7(b) instead of A and B. If we define r_{Cj} and r_{Dj} the path lengths from the slits to the jth detector, we have $r_A = r_{C1} + r_{C2}$ and $r_B = r_{D1} + r_{D2}$. In this experiment $r_{C1} = r_{D1}$ and the condition $z_2 \gg d^2/\lambda$ is verified, so $r_A - r_B \simeq x_2 d/z_2$ and Eq. (2.25) becomes

$$R_c(x_2) \propto \cos^2\left(\frac{x_2 \pi d}{\lambda z_2}\right), \tag{2.26}$$

that has the form of standard Young's double-slit interference pattern with z_2 as the distance from the double-slit to detector D_2, passing backwards through BS and BBO and forward through BS again.

If we consider the diffraction too, we have to multiply Eq. (2.26) by the factor $\mathrm{sinc}(x_2 \pi a/\lambda z_2)$ derived in Eq. (2.18) which takes into account the diffraction due to each one of the two slits. We thus obtain the same result as Eq. (2.22).

Chapter 3

Review of basic concepts

In the Introduction we have emphasized the need for an entangled two-electron state in order to realize an electronic ghost imaging experiment. We propose to exploit Cooper pairs field-emitted from a superconductor.

In the first section of this chapter, we introduce the concept of Cooper pair and write down the BCS Hamiltonian in order to describe the superconductive system. Following the same approach of Ref. [18], we will describe the emission process exploiting the method of the transfer matrix; this will be introduced in Section 3.2 together with an example of application to tunneling.

In Section 3.3 a formal analogy between field emission and junction tunneling is exploited to determine the emission spectrum from a superconductor, once again using the transfer matrix approach. An experiment that shows compatible results is then presented.

In the following subsection higher order effects on the emission spectra (like Andreev emission) are reviewed. These processes are important in the creation of entangled states. A proposal by Yuasa [18] for the observation of the latter by coincidence technique is discussed; as a hint that this setup is potentially implementable, in the last subsection a realized conicidence experiment on electron emission from a normal metal is presented.

3.1 BCS theory

3.1.1 Cooper pair

In his famous paper [36], Cooper demonstrated that the Fermi sea of electrons is unstable against the formation of at least one bound pair as long as there is an attractive interaction, regardless how weak.

A possible mechanism leading to mutual attraction is the indirect electron-electron interaction via phonons suggested by Frolich [37]. This coupling mechanism is operative among electrons near the Fermi energy E_F in an energy shell of the order of the Debye energy $\hbar\omega_D$, where ω_D is the Debye phonon frequency of the material. Anyway the specific mechanism is not important in this discussion.

Let's consider a simple model of two electrons added to the Fermi sea at $T = 0$; these two interact with each other but not with the electron sea except for the Pauli exclusion principle. The Schroedinger equation for this extra electrons is

$$[\frac{\boldsymbol{p}_1^2}{2m} + \frac{\boldsymbol{p}_2^2}{2m} + V(\boldsymbol{r}_1, \boldsymbol{r}_2)]\psi(\boldsymbol{r}_1, \sigma_1, \boldsymbol{r}_2, \sigma_2) = E\psi(\boldsymbol{r}_1, \sigma_1, \boldsymbol{r}_2, \sigma_2), \tag{3.1}$$

where $\boldsymbol{p}_i$ is the momentum operator for the i-th particle ($i = 1, 2$), m is the electron mass, $\psi(\boldsymbol{r}_1, \sigma_1, \boldsymbol{r}_2, \sigma_2)$ is the two-electron wavefunction, σ_i indicates the spin and $\boldsymbol{r}_i$ the position of the i-th electron, E is the energy of the solution, $V(\boldsymbol{r}_1, \boldsymbol{r}_2)$ is the attractive potential. The presence of the Fermi sea will be taken into account manually, by imposing the Pauli exclusion principle.

Let's start from a complete set of spin-orbitals formed by the product of plane waves and spin functions. We can obtain an antisymmetric solution for particle exchange (Fermi statistics) automatically considering two-particle Slater determinants composed by any two spin-orbitals of momenta $\boldsymbol{k}_1$ and $\boldsymbol{k}_2$ and spins σ_1 and σ_2 (we assume $\hbar = 1$). The total momentum for the Slater determinant is $\boldsymbol{K} = \boldsymbol{k}_1 + \boldsymbol{k}_2$ and is a constant of motion in an homogeneous system, because in that case the potential has the form $V(\boldsymbol{r}_1, \boldsymbol{r}_2) = V(\boldsymbol{r}_1 - \boldsymbol{r}_2)$ and only determinantal states with the same total momentum can be mixed. $\boldsymbol{K}$ describes the motion of the center of mass of the pair; since we are interested in the lowest energy possible, we neglect the motion of the center of mass by taking $\boldsymbol{K} = 0$. This means $\boldsymbol{k}_1 = -\boldsymbol{k}_2 \equiv \boldsymbol{k}$ and we can build up orbital wavefunction of the form $\sum_{\boldsymbol{k}} g(\boldsymbol{k}) e^{i\boldsymbol{k}\cdot(\boldsymbol{r}_1 - \boldsymbol{r}_2)}$, where g is some weighting function.

Taking into account the antisymmetry of the wavefunction for the exchange of particles, for a singlet spin ($S = 0$, where S is the total spin of the pair) wavefunction we must have a symmetric orbital wavefunction (cosinusoidal form); on the contrary for one of the triplet spin functions ($S = 1$) we must have antisimmetric orbital wavefunction (sinusoidal form). Since the potential is attractive, we have lower energy for the cosinusoidal state, where the probability for the electrons to be near each other is higher. So we consider a singlet spin state. From the Pauli exclusion principle, the pair can't be composed of electrons with momenta $\boldsymbol{k}$ smaller or equal to the Fermi momentum k_F. So the most general form for the pair wavefunction of total

spin zero and total momentum zero, after imposing the exclusion principle, is

$$\psi(\boldsymbol{r}_1, \sigma_1, \boldsymbol{r}_2, \sigma_2) = \sum_{|\boldsymbol{k}|>k_F} g(\boldsymbol{k}) cos(\boldsymbol{k} \cdot (\boldsymbol{r}_1 - \boldsymbol{r}_2))[\alpha(1)\beta(2) - \alpha(2)\beta(1)], \quad (3.2)$$

where α indicates spin up and β spin down. Substituting Eq. (3.2) in Eq. (3.1), we obtain the following equation for $g(\boldsymbol{k})$:

$$(E - 2\epsilon_k) g(\boldsymbol{k}) = \sum_{|\boldsymbol{k}'|>k_F} V_{\boldsymbol{k}\boldsymbol{k}'} g(\boldsymbol{k}'), \quad (3.3)$$

where ϵ_k is the unperturbed energy $\boldsymbol{k}^2/2m$ for a plane wave of momentum $\boldsymbol{k}$ and $V_{\boldsymbol{k}\boldsymbol{k}'}$ are the matrix elements of the interaction potential that characterize the scattering of a pair with momenta $(\boldsymbol{k}', -\boldsymbol{k}')$ to momenta $(\boldsymbol{k}, -\boldsymbol{k})$. A bound pair-state exists if a set of $g(\boldsymbol{k})$ that satisfies Eq. (3.3) with the condition $E < 2E_F$ can be found.

Let's consider the case where we can approximate the potential matrix element with a negative constant $-V$ for energies greater than the Fermi level E_F up to a cutoff ω_c, and zero elsewhere. The cutoff makes sense if we think to the Frolich mechanism, and it is of the order of the Debye frequency. In this case Eq. (3.3) leads to

$$\frac{1}{V} = \frac{1}{2} N(0) \ln \frac{2E_F - E + 2\omega_c}{2E_F - E}, \quad (3.4)$$

where $N(0)$ is the density of states at the Fermi level for electrons with one spin orientation. In the weak coupling approximation $N(0)V \ll 1$, we have

$$E \simeq 2E_F - 2\omega_c e^{\frac{-2}{N(0)V}} < 2E_F. \quad (3.5)$$

So a bound state exists; the binding energy is not analytic at $V = 0$: a perturbation theory is not possible. Due to the approximation on the matrix elements, $g(\boldsymbol{k})$ for our solution depends only on ω_k, which has spherical symmetry. Thus the orbital wavefunction has spherical simmetry, hence the Cooper pair state in this approximation is an S singlet state.

In second quantization formalism we can write the Cooper pair state as

$$|\psi\rangle = \sum_{|\boldsymbol{k}|>k_F} g(\boldsymbol{k}) a^\dagger_{\boldsymbol{k}\uparrow} a^\dagger_{-\boldsymbol{k}\downarrow} |\psi_N\rangle, \quad (3.6)$$

where $|\psi_N\rangle$ is the free-electron normal ground state defined as $|\psi_N\rangle = \prod_{|\boldsymbol{k}|<k_F} a^\dagger_{\boldsymbol{k}\uparrow} a^\dagger_{-\boldsymbol{k}\downarrow} |0\rangle$, with $|0\rangle$ being the vacuum state and $k_F = \sqrt{2mE_F}$ being the Fermi momentum. In this formalism $a^\dagger_{\boldsymbol{k}\sigma}$ creates an electron of momentum $\boldsymbol{k}$ and spin

σ, while its hermitian conjugate destroys it. They obeys the usual fermion anticommutations relations

$$\{a^\dagger_{\boldsymbol{k}\sigma}, a_{\boldsymbol{k}'\sigma'}\} = \delta_{\boldsymbol{k},\boldsymbol{k}'}\delta_{\sigma,\sigma'},$$
$$\{a^\dagger_{\boldsymbol{k}\sigma}, a^\dagger_{\boldsymbol{k}'\sigma'}\} = \{a_{\boldsymbol{k}\sigma}, a_{\boldsymbol{k}'\sigma'}\} = 0. \tag{3.7}$$

3.1.2 Model Hamiltonian and quasiparticle excitations

Since the Fermi sea is unstable when there is a net attractive interaction among electrons, we must expect pairs to condense until an equilibrium is reached, where the state is so different from the normal ground state that the binding energy has gone to zero. Handling a system of N electrons with the exact same method just illustrated for the single Cooper pair, is a difficult task because too many terms should be calculated. Bardeen, Cooper and Schrieffer (BCS) [19] proposed to relax the requirement that the number of particles is fixed. Moreover they proposed to use a Hartree-like approximation in which the probability of a specific configuration of pairs is given by the product of the occupancy probabilities for the individual pair state. A wavefunction that adequately describes this approximation is

$$|\psi_{BCS}\rangle = \prod_{\boldsymbol{k}}(u_{\boldsymbol{k}} + v_{\boldsymbol{k}} a^\dagger_{\boldsymbol{k}\uparrow} a^\dagger_{-\boldsymbol{k}\downarrow})|0\rangle, \tag{3.8}$$

where $u_{\boldsymbol{k}}$ and $v_{\boldsymbol{k}}$ are some coefficients that satisfy the relation $|u_{\boldsymbol{k}}|^2 + |v_{\boldsymbol{k}}|^2$. $v_{\boldsymbol{k}}$ represents the probability amplitude that the pair $(\boldsymbol{k}\uparrow, -\boldsymbol{k}\downarrow)$ is occupied, while $u_{\boldsymbol{k}}$ is the probability that it isn't occupied. In their original work, BCS determined this coefficients minimizing the ground state energy with variational method. Here we would like to present a different approach where u and v are coefficient of a Bogoliubov canonical transformation [38] and they will be determined by diagonalization of the Hamiltonian appropriately simplified.

The Hamiltonian of a system of interacting electrons usually includes terms that involve electrons not paired; their expectation value over the state of Eq. (3.8) is zero. In order to determine the ground state of the system those term can be dropped and the calculations can be done considering the so-called pairing or reduced hamiltionian:

$$H = \sum_{\boldsymbol{k}\sigma} \epsilon_k a^\dagger_{\boldsymbol{k}\sigma} a_{\boldsymbol{k}\sigma} + \sum_{\boldsymbol{k}\boldsymbol{k}'} V_{\boldsymbol{k}\boldsymbol{k}'} a^\dagger_{\boldsymbol{k}\uparrow} a^\dagger_{-\boldsymbol{k}\downarrow} a_{-\boldsymbol{k}'\downarrow} a_{\boldsymbol{k}'\uparrow}. \tag{3.9}$$

The product of two creation operators can always be expressed in the form

$$a^\dagger_{\boldsymbol{k}\uparrow} a^\dagger_{-\boldsymbol{k}\downarrow} = b_{\boldsymbol{k}} + (a^\dagger_{\boldsymbol{k}\uparrow} a^\dagger_{-\boldsymbol{k}\downarrow} - b_{\boldsymbol{k}}), \tag{3.10}$$

where we take $b_{\boldsymbol{k}}$ as the expectation value over the ground state $b_{\boldsymbol{k}} = \langle\psi_{BCS}|a^\dagger_{\boldsymbol{k}\uparrow}a^\dagger_{-\boldsymbol{k}\downarrow}|\psi_{BCS}\rangle$. The same thing can be done for annihilation operators. The term in the parentheses represents fluctuation around the average value and can be considered small because of the large number of particles in the system. Substituting this expression in the pairing hamiltonian, we drop the terms bilinear in the fluctuations (a procedure common in mean field theories) and obtain the model hamiltonian

$$H_B = \sum_{\boldsymbol{k}\sigma} \epsilon_k a^\dagger_{\boldsymbol{k}\sigma} a_{\boldsymbol{k}\sigma} + \sum_{\boldsymbol{k}\boldsymbol{k}'} V_{\boldsymbol{k}\boldsymbol{k}'}(b_{\boldsymbol{k}} a_{-\boldsymbol{k}'\downarrow} a_{\boldsymbol{k}'\uparrow} + b_{\boldsymbol{k}'} a^\dagger_{\boldsymbol{k}\uparrow} a^\dagger_{-\boldsymbol{k}\downarrow} - b_{\boldsymbol{k}} b_{\boldsymbol{k}'}). \tag{3.11}$$

Let's notice that this hamiltonian is explicitely number-non-conserving. One can define a new hamiltonian operator by shifting the zero of the single particle energy and choosing the new one as the Fermi level μ:

$$\mathcal{H}_B = H_B - \mu N = \sum_{\boldsymbol{k}\sigma} \varepsilon_k a^\dagger_{\boldsymbol{k}\sigma} a_{\boldsymbol{k}\sigma} + \sum_{\boldsymbol{k}\boldsymbol{k}'} V_{\boldsymbol{k}\boldsymbol{k}'}(b_{\boldsymbol{k}} a_{-\boldsymbol{k}'\downarrow} a_{\boldsymbol{k}'\uparrow} + b_{\boldsymbol{k}'} a^\dagger_{\boldsymbol{k}\uparrow} a^\dagger_{-\boldsymbol{k}\downarrow} - b_{\boldsymbol{k}} b_{\boldsymbol{k}'}), \tag{3.12}$$

where we defined $\varepsilon_k = \epsilon_k - \mu$ and the number operator $N = \sum_{\boldsymbol{k},\sigma} a^\dagger_{\boldsymbol{k}\sigma} a_{\boldsymbol{k}\sigma}$. Let's introduce the parameter $\Delta_{\boldsymbol{k}} = -\sum_{\boldsymbol{k}'} V_{\boldsymbol{k}\boldsymbol{k}'} b_{\boldsymbol{k}'}$ and perform the Bogoliubov transformation

$$\begin{pmatrix} a_{\boldsymbol{k}\uparrow} \\ a^\dagger_{-\boldsymbol{k}\downarrow} \end{pmatrix} = \begin{pmatrix} u_k & -v_k \\ v_k^* & u_k^* \end{pmatrix} \begin{pmatrix} \alpha_{\boldsymbol{k}\uparrow} \\ \alpha^\dagger_{-\boldsymbol{k}\downarrow} \end{pmatrix}. \tag{3.13}$$

Keeping in mind the condition $|u_{\boldsymbol{k}}|^2 + |v_{\boldsymbol{k}}|^2 = 1$, we can choose these coefficients such that the Hamiltionian is diagonalized:

$$\mathcal{H}_S = \sum_{\sigma=\uparrow,\downarrow} \int d^3\boldsymbol{k}\, E_{\boldsymbol{k}} \alpha^\dagger_{\boldsymbol{k}\sigma} \alpha_{\boldsymbol{k}\sigma} + W_G, \tag{3.14}$$

where W_G is the ground state energy and we have defined $E_{\boldsymbol{k}} = \sqrt{\varepsilon_k^2 + |\Delta_k|^2}$. In order to get the diagonal form, it can be demonstrated that [39] the coefficients should obey the following equation:

$$2\varepsilon_k u_{\boldsymbol{k}} v_{\boldsymbol{k}} + \Delta^* v_{\boldsymbol{k}}^2 - \Delta u_{\boldsymbol{k}}^2 = 0. \tag{3.15}$$

This equation has the solution $|v_{\boldsymbol{k}}|^2 = 1 - |u_{\boldsymbol{k}}|^2 = 1/2(1 - \varepsilon_k/E_{\boldsymbol{k}})$; let's notice that the relative phase between the coefficients is not fixed. In the following we assume $u_{\boldsymbol{k}}$ to be real. This is the same result that BCS obtained using the variational method [40].

As for the case of the single Cooper pair, we can assume the potential matrix element different from zero and constant only in the energy shell

$\pm\omega_c$ around the Fermi level. This leads to the "average gap approximation" $\Delta_{\boldsymbol{k}} = \Delta$ in that shell. The energies $E_{\boldsymbol{k}}$ of the quasiparticle excitations above the ground state become $\omega_k = \sqrt{\varepsilon_k^2 + |\Delta|^2}$ and we get, after shifting the zero of energy of the quantity W_G, the following Hamiltonian:

$$\mathcal{H}_S = \sum_{\sigma=\uparrow,\downarrow} \int d^3\boldsymbol{k}\, \omega_k \alpha^\dagger_{\boldsymbol{k}\sigma} \alpha_{\boldsymbol{k}\sigma}. \tag{3.16}$$

It is easy to demonstrate that in the limit $\Delta \to 0$ we recover the case of the normal metal.

3.1.3 Density of quasiparticle states

From the dispersion relation $\omega_k = \sqrt{\varepsilon_k^2 + |\Delta|^2}$ we can see that there is a gap in the energy spectrum of the quasiparticle excitations: there are no electron-like states with energy in the interval $[E_F, E_F + |\Delta|]$ and no hole-like states in $[E_F - |\Delta|, E_F]$. The Bogoliubov canonical transformation creates a one-to-one correspondence between the electrons in the normal metal created by $a^\dagger_{\boldsymbol{k}}$ and the quasiparticle excitations created by $\alpha^\dagger_{\boldsymbol{k}}$ [39], so the following equality holds:

$$\rho_s(\omega) d\omega = \rho_n(\varepsilon) d\varepsilon, \tag{3.17}$$

where ρ_s is the density of states of the quasiparticles in the superconductor, ω is the energy of the quasiparticle, $\rho_n(\varepsilon)$ is the density of states in the normal metal and ε is the energy of the particle inside the metal calculated with respect to the Fermi level. We are interested in a small interval near the Fermi level, so $\rho_n(\varepsilon)$ can be taken as a constant $\rho_n(E_F)$. From the dispersion relation $\omega_k = \sqrt{\varepsilon_k^2 + |\Delta|^2}$ we can compute

$$\frac{d\omega}{d\varepsilon} = \frac{\varepsilon}{\sqrt{\varepsilon^2 + |\Delta|^2}} = \begin{cases} \frac{\omega}{\sqrt{\omega^2 - |\Delta|^2}} \text{ if } \omega > |\Delta|, \\ 0 \text{ if } \omega < |\Delta|, \end{cases} \tag{3.18}$$

which then yields the following superconductive density of states

$$\rho_s(E) = \begin{cases} \rho_n(E_F) \frac{|E|}{\sqrt{E^2 - |\Delta|^2}} \text{ if } |E| > |\Delta|, \\ 0 \text{ if } |E| < |\Delta|. \end{cases} \tag{3.19}$$

3.2 Transfer Matrix Method

The Transfer Matrix method is an effective Hamiltonian approach for dealing with the phenomenon of tunneling. Bardeen first introduced this method in

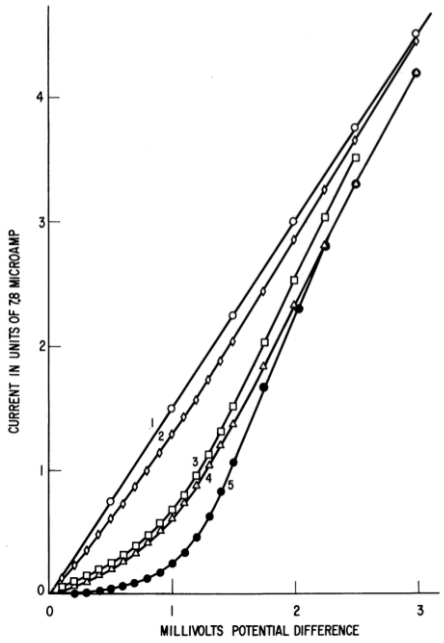

Figure 3.1: Tunnel current between Al and Pb through Al_2O_3 film as a function of voltage at various temperatures and magnetic fields. Source: [41]

1961 [31] in order to give an explanation for the observations by Giaever about the tunneling current flowing from a normal metal to another metal or a superconductor [41]. The theory was soon translated in the second quantization formalism [42] and has been used in several applications, e.g. a many-body approach to field emission [44] or a theory for scanning tunneling microscopes [45][46]. The basic idea is to treat the two conductors separately and add an effective term that describes the transfer from one side to the other. To understand how this method works, in this section we present its first application to the case of superconductor-metal tunneling.

The most interesting result that Giaever observed was the direct evidence for a gap in the quasiparticle spectrum of the superconductor. In fact, he saw that there was no current flow (or very low with respect to the ohmic behaviour that one has for normal metals, see Fig. 3.1) for values of the voltages smaller than the gap parameter divided by the electron charge. He was able to explain the results taking only into account the density of states in energy. One may think that, since we are dealing with superconductors, some BCS coherence factors should matter [19]. In the following we illustrate why that is not the case using the transfer matrix approach.

Bardeen noticed that if the process is regarded as in time-dependent per-

turbation theory, i.e. a transition from one set of nearly stationary states to another, the expression for the transition probability for the transfer of an electron from the metal to the superconductor is, by Fermi's golden rule, $(2\pi/\hbar)|T|^2\rho_f$, where T is the matrix element and ρ_f is the energy density of final states. Hence the assumption of Giaever is justified if T is independent of energy and is the same in the case of metal-metal or metal-semiconductor tunneling.

Using a many-particle point of view, Bardeen [31] computed the matrix element. The following line was adopted: suppose that a barrier extends from a point x_a to a point x_b with $x_a < x_b$. Let's call ϕ_0 the many-particle state for the entire system before the tunneling, while ϕ_{mn} is the state for the whole system after the tunneling. Suppose that both states can be defined in terms of quasi-particle states of both metals, so that ϕ_{mn} differs from ϕ_0 just in the transfer of an electron from the state m in the first metal a to the state n of the second metal b. The quasiparticle wavefunctions are not plane waves in the x direction, but are reflected at it, drop exponentially into the barrier region and go to zero smoothly in the other metal. So we have to assume that ϕ_0 is a good solution of the Schroedinger equation with energy W_0 for $x < x_b$, while it is not a good solution for $x > x_b$. The same thing is valid for ϕ_{mn} and the regions $x > x_a$ and $x < x_a$. Both are good solutions inside the barrier region.

If H is the entire hamiltonian of the system, by the time-dependent perturbation theory we have the following matrix element for the transition:

$$T_{mn} = \int \phi_0^*(H - W_{mn})\phi_{mn} d\tau = \int_a \phi_0^*(H - W_{mn})\phi_{mn} d\tau. \tag{3.20}$$

The subscript a means that we have to integrate only in the region a since, by our assumption, the integrand vanishes in the other regions, where ϕ_{mn} is a good solution; τ indicates the volume in the N-particles coordinate space. Let's notice that $\phi_{mn}(H - W_0)\phi_0^*$ vanishes in region a, so we can subtract this term in the integral for the matrix element:

$$T_{mn} = \int_a (\phi_0^*(H - W_{mn})\phi_{mn} - \phi_{mn}(H - W_0)\phi_0^*) d\tau \simeq \int_a (\phi_0^* H \phi_{mn} - \phi_{mn} H \phi_0^*) d\tau. \tag{3.21}$$

The last passage is valid if $W_{mn} \simeq W_0$, which is the case here. The potential part of the hamiltonian can be dropped because gives zero contribution to the integral. Actually performing the integration leads us to the form $T_{mn} = -iJ_{mn}(x_1)$ [31], where $J_{mn}(x)$ is the matrix element of the x-component of the current density operator and x_1 is inside the barrier (we refer to [31] for an explicit expression of this quantity). Let's notice two important results:

first, for charge conservation the current is constant inside the barrier, so $J_{mn}(x_1)$ is actually independent from position; second, by the definition of the current operator we can see that the actual value of the matrix element depends only on the overlap inside the barrier of the wavefunctions calculated for the separated systems.

Now let's switch to the second quantization formalism. This picture for the tunneling problem was first used by Cohen et al. [42] in 1962. Let's write down the hamiltonian for the system:

$$H = H_N + H_S + H_T, \tag{3.22}$$

where H_N and H_S are the exact hamiltonians for the normal metal and the superconductor, while the coupling term H_T transfers electrons between the two. Let's call $a_{q\sigma}$ and $b_{k\sigma}$ the annihilation operators for the electrons inside the superconductor and the metal; k and q represent the momenta, while σ is the spin. Let's also perform the Bogoliubov transformation of Eq. (3.13). In this representation we have

$$H_S = \sum_{q\sigma} \omega_q \alpha^\dagger_{q\sigma} \alpha_{q\sigma} + U + H_2 + H_{int}, \tag{3.23}$$

$$H_N = \sum_{k\sigma} \varepsilon_k b^\dagger_{k\sigma} b_{k\sigma}, \tag{3.24}$$

$$H_T = \sum_{kq\sigma} [T_{kq} b^\dagger_{k\sigma} a_{q\sigma} + h.c.]. \tag{3.25}$$

ε_k is the normal electron energy measured from the Fermi level;
$\omega_q = \sqrt{|\Delta|^2 + \varepsilon_q^2}$ is the superconducting quasiparticle energy, with Δ representing the gap parameter of the superconductor. U is the ground state energy for the superconductor; H_2 represents terms of the form $\alpha^\dagger_\sigma \alpha^\dagger_{-\sigma}$ or $\alpha_\sigma \alpha_{-\sigma}$, while H_{int} includes interactions between quasiparticles (terms with four quasiparticle operators). T_{kq} is the Bardeen matrix element; it relates normal electrons on both sides of the barrier. u_k and v_k are the BCS coherence factors [19] defined as

$$\begin{cases} u_k = \dfrac{1}{\sqrt{2}} \sqrt{1 + \dfrac{\varepsilon_k}{\omega_k}}, \\ v_k = \dfrac{e^{i\delta}}{\sqrt{2}} \sqrt{1 - \dfrac{\varepsilon_k}{\omega_k}}. \end{cases} \tag{3.26}$$

The tunneling current is determined by the average value of the rate of change of the number of electrons in the superconductor $\langle \dot{N}_S \rangle$. The Heisenberg equation of motion for the number operator N_S is

$$i\hbar \dot{N}_S = [N_S, H] = [N_S, H_T], \tag{3.27}$$

where the last passage makes sense, since we have adopted the complete superconductive hamiltonian, which conserves the number of electrons (therefore commutes with N_S). In the Hartree-Fock approximation [42] we obtain

$$\langle \dot{N}_S \rangle = \frac{2\pi}{\hbar} \sum_{kq} |T_{kq}|^2 [|u_q|^2 (f_k - g_q)\delta(\omega_q - \varepsilon_k) + |v_q|^2 (f_k + g_q - 1)\delta(\omega_q + \varepsilon_k)], \tag{3.28}$$

where f_k and g_q are the occupation numbers for the quasiparticles in the metal and the superconductor. Let's notice that there are two channels q and q' such that

$$|u_q|^2 + |u_{q'}|^2 = 1 \text{ if } q < k_F;\ q' > k_F;\ \omega_q = \omega_{q'}. \tag{3.29}$$

The same is possible for v_q. k_F is the Fermi momentum. Let's notice that the matrix element is almost a constant for the small energies involved in tunneling, assuming some particular geometries (e.g. a plane infinite interface) [42]. After introducing the energy density of states for the metal ($\rho_N(E)$) and the superconductor($\rho_S(E)$), we can replace the sum over momenta with an integral over energy, making explicit the voltage dependence of the Fermi-Dirac distribution for the occupation numbers:

$$\langle \dot{N}_S \rangle \propto \int dE\, |T|^2 (f(E - eV) - f_S(E)) \rho_N(E - eV) \rho_S(E), \tag{3.30}$$

where f is the Fermi-Dirac distribution, V is the voltage, T is the matrix element and $f_S(E)$ is defined as

$$\begin{cases} f_S(E) = g(E) \text{ for } E > 0, \\ f_S(E) = 1 - g(-E) \text{ for } E < 0. \end{cases} \tag{3.31}$$

So we can see that the tunneling current depends only on the density of states of the superconductor, while all coherence factors are ruled out by Eq. (3.29). This is the result experimentally found by Giaever [43]. At zero absolute temperature $f(x) = g(x) = \theta(-x)$, so $f(E - eV) = \theta(eV - E)$ and $f_S = 0$. This leads to

$$\begin{aligned} \langle \dot{N}_S \rangle &\propto \int dE\, |T|^2 \theta(eV - E) \rho_N(E - eV) \rho_S(E) \\ &= \int dE\, |T|^2 \theta(-E) \rho_N(E) \rho_S(E + eV). \end{aligned} \tag{3.32}$$

Since only electrons near the Fermi level contribute to tunneling ($E \simeq 0$) and since by BCS theory [19]

$$\begin{cases} \rho_S = \rho_N \frac{|E|}{\sqrt{E^2 - |\Delta|^2}} \text{ if } |E| > |\Delta|, \\ \rho_S = 0 \text{ if } |E| < |\Delta|, \end{cases} \tag{3.33}$$

we can notice that no current can flow until the applied voltage corresponds to the energy gap $|\Delta|$, as shown in Fig. 3.1.

3.3 Electron field emission

Field emission consists of the extraction of an electron, typically from a cold metal (or a superconductor) into vacuum, by the application of a strong electric field. Examples of applications for surface field emission include the construction of bright electron sources for high-resolution electron microscopes.

Formally there exists an analogy between the theory of junction tunneling and the theory of field emission from solids; so the theory presented in the previous section can be adapted to the case of field emission, provided some small changes.

In the free-electron model for a metal, an electron is confined to stay in the metal region by a potential barrier (details in the papers about the theory of work function by Wigner and Bardeen[47] [48]). If we apply a uniform electric field F, the surface potential profile seen by an electron is modified and decreases linearly with position far from the surface. In this case, even at zero temperature, an electron with energy lower than the Fermi energy can tunnel out of the metal into the vacuum. Let's call x the direction normal to the surface; the profile of the barrier, with a correction due to the image potential, can be modeled as [50] (see Fig. 3.2)

$$V(x) = V_0 - \frac{e^2}{4x} - eFx \text{ for } x > 0, \tag{3.34}$$

where we put the origin of the x axis at the surface and negative coordinates describe the bulk region of the metal, where the potential is assumed constant and of course lower than the Fermi energy, and where V_0 is the vacuum level.

This picture is totally equivalent to the tunneling one described before, if we use the barrier profile $V(x)$ and notice that, by definition, all the states in the vacuum region are unoccupied.

Once again let's approach the problem with a second quantization formalism and break the geometrical domain in three parts: left (normal metal or superconductor), right (vacuum) and barrier region. Let's assume that, within the limits by Prange [49][1], electrons are localized to the left or right hand side. Hence it is possible to introduce the effective hamiltonian $H =$

[1] In Ref. [49] Prange questions wheter it is correct to use Hamiltonians of the form (3.22) to describe tunneling and demonstrates that it is a good choice if intended as a perturbation theory.

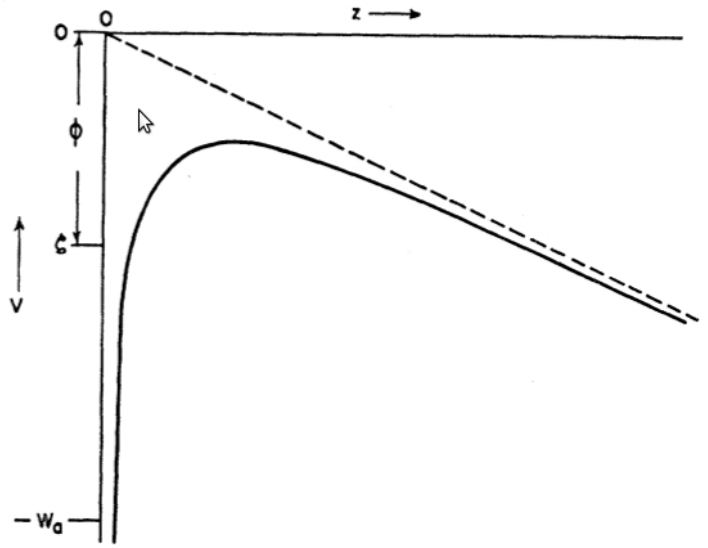

Figure 3.2: One-dimensional potential energy $V(z)$ of an electron near a metal surface (see Eq. (3.34)). In the picture Φ is the work function and ζ is the Fermi level. Source: [50]

$H_L + H_R + H_T$, where H_L and H_R are the unperturbed hamiltonians for each side, H_T is a coupling term that allows for mixing and thus for an effective flow of particles from one side to the other. This term is given by Eq. (3.25), assuming $b^\dagger_{k\sigma}$ to be the operator that creates an electron of momentum k (energy ε_k) and spin σ in the right side (vacuum region), while $a_{q\sigma}$ destroys an electron with momentum q (energy ε_q) in the metal. T_{kq} is the Bardeen matrix element introduced before, but some of the previous assumptions on the energy dependence are relaxed. If we assume the surface to be an infinite plane, we have [50]

$$|T_{\boldsymbol{kq}}|^2 \propto \frac{\delta(\boldsymbol{k}_\perp - \boldsymbol{q}_\perp)}{\rho_x^R \rho_x^L} D(\varepsilon_{qx}), \tag{3.35}$$

where $\boldsymbol{k}_\perp$ and $\boldsymbol{q}_\perp$ are the transverse momenta of the electrons and $\delta(\boldsymbol{k}_\perp - \boldsymbol{q}_\perp)$ implies the conservation of the transverse momenta in the tunneling process. This term is due to the particular chosen geometry. ρ_x^R and ρ_x^L are the densities of states with momentum normal to the surface. The term $D(\varepsilon_{qx})$ is a function of the "normal" energy (the contribution to the energy due to the motion normal to the barrier) of the electron destroyed in the metal; it takes into account the potential profile and in the WKB approximation, near the Fermi level, can be estimated to be

$$D(\varepsilon_{qx}) \simeq \exp(-c + (\varepsilon_{qx} - \mu)/d), \tag{3.36}$$

where μ is the Fermi energy, c and d [50] are two functions of the applied field and the work function; they do not depend on energy. The current can be calculated as the time rate change of the number of particles in the left hand side, when the probability of tunneling from the right to the left is negligible:

$$j = e\langle \dot{N}_L \rangle = -ei\langle [N_L, H_T] \rangle. \tag{3.37}$$

Following the line proposed by Gadzuk [44], one obtains the general expression

$$j = e \sum_{\boldsymbol{kq}} |T_{\boldsymbol{kq}}|^2 \int d\omega \, A_L(\boldsymbol{k}, \omega) A_R(\boldsymbol{q}, \omega) f(\omega), \tag{3.38}$$

where A_L and A_R are the spectral weight functions for the left and the right hand side, while f is the Fermi-Dirac distribution. Substituting the matrix element of Eq. (3.35) and performing integration over momenta, we get the following expression for the total energy distribution or current density per unit energy of emitted electrons:

$$J(\varepsilon_q) = \frac{\partial j}{\partial \varepsilon_q} \propto \int d\varepsilon_k \int d\omega \, A_L(\boldsymbol{k}, \omega) A_R(\boldsymbol{q}, \omega) f(\omega) e^{\frac{\varepsilon_k - \mu}{d}}. \tag{3.39}$$

If the electrons go to definite energy eigenstates, i.e. are measured by a non-resolution-limited apparatus, the right-hand-side spectral weight is sharp: $A_R(\boldsymbol{q}, \omega) = \delta(\varepsilon_q - \omega)$. For a noninteracting electron gas (simple model for a normal metal) the spectral weight is sharp too: $A_L(\boldsymbol{k}, \omega) = \delta(\varepsilon_k - \omega)$ [51]. Substituting in Eq. (3.39), we have

$$J(E) \propto f(E) e^{\frac{E - \mu}{d}}. \tag{3.40}$$

The case of the non-interacting electron gas is the one studied by Fowler and Nordheim [29] for the current and by Young [50] for the total energy density of states. Their results, also compatible with the data obtained by experiments [52][53], are the same as the one in Eq. (3.40), so this formalism is correct, at least in this simple case. In the superconductive case we have [51]

$$A_L(\boldsymbol{k}, \omega) = [(1 + \frac{\varepsilon_k}{\omega_k})\delta(\varepsilon_k - \omega) + (1 - \frac{\varepsilon_k}{\omega_k})\delta(\varepsilon_k + \omega)]/2, \tag{3.41}$$

where $\omega_k = \sqrt{\varepsilon_k^2 - |\Delta|^2}$ for $|\varepsilon_k| > |\Delta|$ and zero elsewhere. Δ is the superconductor gap parameter. This leads to [44]

$$\begin{aligned} J(E) \propto f(E) e^{-\mu/d} \frac{|E|}{\sqrt{E^2 - |\Delta|^2}} [\cosh(\frac{\sqrt{E^2 - |\Delta|^2}}{d}) \\ + \frac{\sqrt{E^2 - |\Delta|^2}}{E} \sinh(\frac{\sqrt{E^2 - |\Delta|^2}}{d})], \end{aligned} \tag{3.42}$$

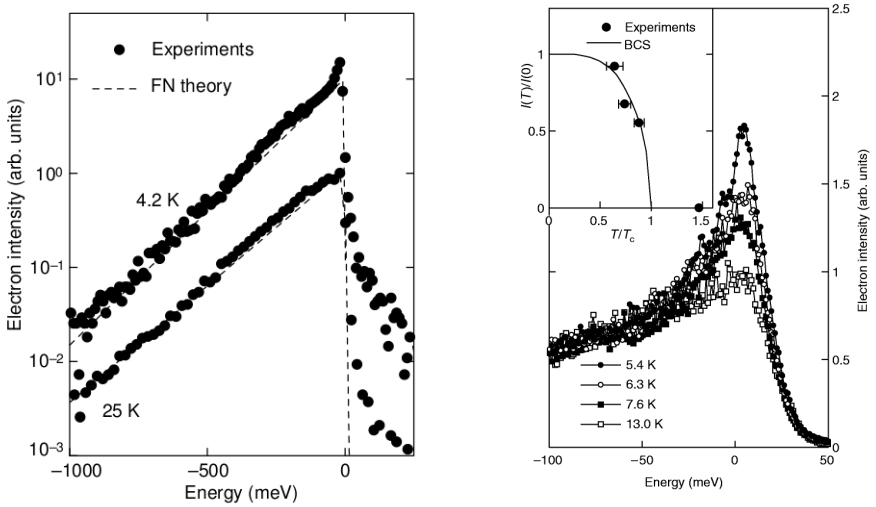

Figure 3.3: On the left: Typical field emission (FE) spectra from the Nb tip at 4.2 K and 25 K, which are respectively below and above Tc. The dashed curves are calculated on the basis of the Fowler-Nordheim theory [29]. A sharp peak appears at FE in the spectrum at 4.2 K. On the right: The observed FE spectra from the Nb tip at various temperatures around $T_c = 9.2K$. Inset, the intensity of the sharp peak plotted against the temperature normalized by T_c. Source: [30]

which is valid outside the gap. Inside the gap we should have zero current. Notice that, as one can expect, in the limit $\Delta = 0$ we recover the result of Eq. (3.40). With respect to this result, that has a linear behaviour in a logarithmic plot, we have a sharp peak near the gap. This means that the emission is essentially monochromatic.

This peak has been observed for the first time in 1998 by Nagaoka et al. [30] ; before that, all the experiments did not show any noticeable difference between normal and superconductive field emission. The peak disappeares for $T > T_c$, as reported in Fig. 3.3. The experiment was performed exploiting high-resolution electron spectroscopy techniques and a cryo-field-emission gun, working at a temperature of $4.2K$ and $25K$. The emitting tip was made of Niobium, that has a critical temperature $T_c = 9.2K$, so both the emission from the normal state and the superconductive state have been observed. The peak was observed only after several cleaning of the tip surface by field evaporation and tended to disappear after several hours of measurements, because of the condensation of residual gases onto the tip surface at $4.2K$. The experiment was conducted using a voltage of $6kV$ and a vacuum pres-

sure of $10^{-10}Pa$. Typical average current emitted was $10^{-7}A$. The radius tip was $100nm$, while the coherence length for Nb is $38nm$; this presumably means that the tails of wavefunctions can't penetrate the contaminated layer and so no extra emission results for dirty tips. The cleaning is one of the big differences between this experiment and the pioneering works.

The experimental data of Fig. 3.3 show an unexpected broadening of the peak of $20meV$ (wider than the gap), which prevents the gap from being directly visible on the spectrum of the emitted quasiparticles. The cause of this broadening is still to be investigated. Anyway, the trend of the observed total energy current density observed is compatible with the prevision made by Gadzuk [44]: a quasi-monochromatic electron beam is emitted from the tip. This result may be useful for applications as a source for microscopy and spectroscopy.

3.3.1 Higher order processes

In 2008 Iazzi [54] showed the possibility of having sub-gap current if higher order emission processes were taken into account. In fact, as we have just seen, no current due to single quasiparticle emission (first order tunneling process) is allowed in the gap, but double-particle tunneling should be considered. These terms are second-order tunneling events. Among these processes he analyzed the Andreev contributions [55], that describe processes which bring a full Cooper pair outside the superconductor.

He calculated that the Andreev contribution is concentrated near the borders of the gap. Experimentally it is quite difficult to detect such a contribution, because near the gap border the single particle contribution can make it impossible to be distinguished: one should have high resolution and little broadening of the single particle spectrum. Unfortunately, this was not the case for the experiment of Nagaoka et al., where a broadening larger than the gap was observed. Some improvements are needed to see such an effect; an idea has been proposed by Yuasa [18] and is described below.

The Andreev process that is relevant in field emission is the analogous to the one where a hole incident from a normal metal to a superconductor (in presence of a voltage) is reflected as an electron with spin and momentum opposite to the incident particle. In order for that to happen, a Cooper pair should be destroyed inside the superconductor, so that the total electric charge is conserved. Shifting the zero of the energy, a hole-Andreev-reflection can be seen as a two-electron emission (e.g. see [26], [25]).

A very similar process is also important in the creation of entangled two-electron states. Essentially, an Andreev reflection happens in a "nonlocal" manner: instead of being emitted from the same point, the electron pair is

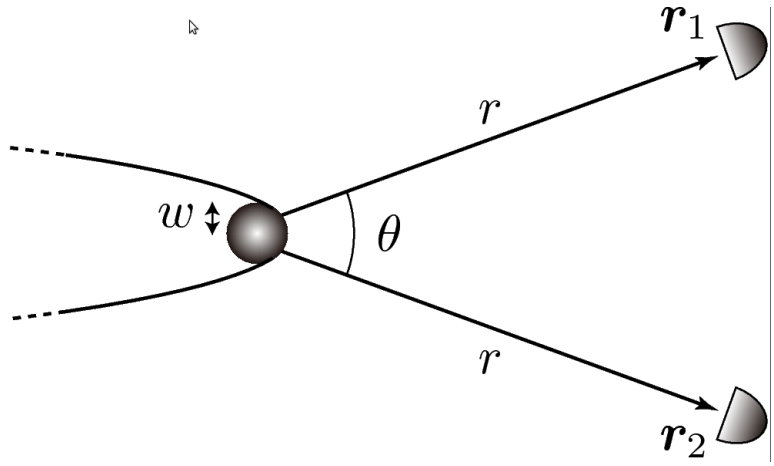

Figure 3.4: Setup proposed by Yuasa: emission of electrons from a superconductor in 3D space and detection of two electrons emitted in different directions. Spherical symmetry for the system is assumed. Source: [18]

emitted from two distant points on the surface of the superconductor. This effect is called "crossed Andreev reflection" and usually happens in normal-superconductor-normal junctions with the superconductor layer thinner than the Pippard coherence length. The dynamics is similar to the classic Andreev reflection, except for the fact that the pair is emitted in a singlet S state, i.e. the two electrons go in opposite directions. This entangled state, in the case of field emission, could be very useful for purposes of quantum information and has been studied in detail by Yuasa [18]. He proposed a coincidence experiment in the field emission from a superconductor. The idea comes from the experiment of Nagaoka et al. [30] on the field emission from a superconductor and from a coincidence experiment in field emission by Kiesel et al. [56]. The latter will be discussed at the end of this section.

In Yuasa's setup, electrons emitted in opposite directions by a superconducting tip are detected by two point-like single-particle detectors and the coincidences are counted. In the proposed scheme (Fig. 3.4) , the tip has spherical symmetry and the detectors are placed at the same distance from it. The far field limit is explored, imposing the detector-tip distance much greater than the Fermi wavelength. The two variables of the system are the angle between the detectors and the delay in the coincidence counting; this allows to study the correlation of the emitted pair both in space and time.

Without delay, a strong positive correlation is observed for angles close to π (this bunching effect is observable in Fig. 3.5). This has to be reconducted to the emission of Cooper pairs by Andreev events; a detailed explanation is

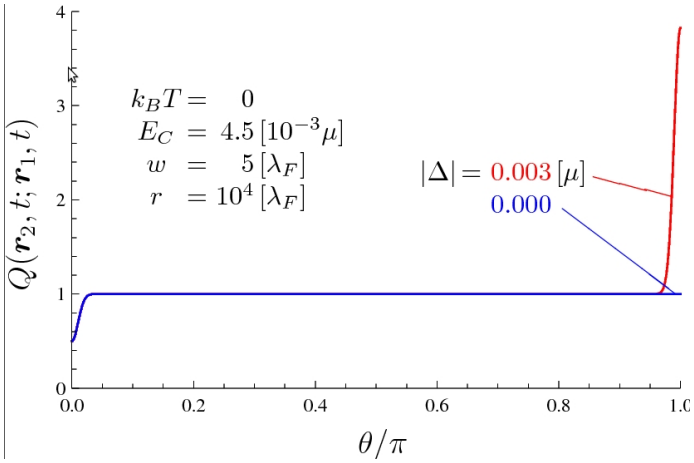

Figure 3.5: Normalized coincidence counts Q vs θ for normal and superconducting emitter. A bunching effect at $\theta \sim \pi$ is evident in the superconducting case. Source: [18]

given in terms of the dynamics of the emission, analyzed in the framework of quantum field theory in [18]. The spectrum of the Andreev emission, calculated for detectors in opposite directions, is shown in Fig. 3.6. Let's notice that the spectrum is non-zero inside the gap of the quasiparticle spectrum. In order to experimentally observe that, a coincidence technique may be a good choice since it allows to isolate second-order effects: one can measure the quasiparticle contributions to the current with a single detector and then subtract the result from the coincidence case. Exploiting this technique, it has been demonstrated that only the Andreev emission is relevant to the entanglement. This fact should be stressed, since it will be used in Chapter 4.

A field-theoretical description has also been given in the appendix of [18] and is here reported. Let's analyze the Andreev emission as a scattering process from an initial eigenstate of the unperturbed hamiltonian H_0 of the superconductor and the vacuum regions into a scattering state by the scattering hamiltonian $H = H_0 + H_T$, where H_T is the coupling (or tunneling) hamiltonian. The scattering can be described by the following wave operator $\mathcal{W}$:

$$\mathcal{W} = \lim_{t\to\infty} e^{-iHt} e^{iH_0 t}, \tag{3.43}$$

where t indicates the time. Let's assume that H doesn't have bound states and that H_0 admits only one discrete eigenvalue E_0 (corresponding to the state $|E_0\rangle$) besides a continuous spectrum. Let's also assume that

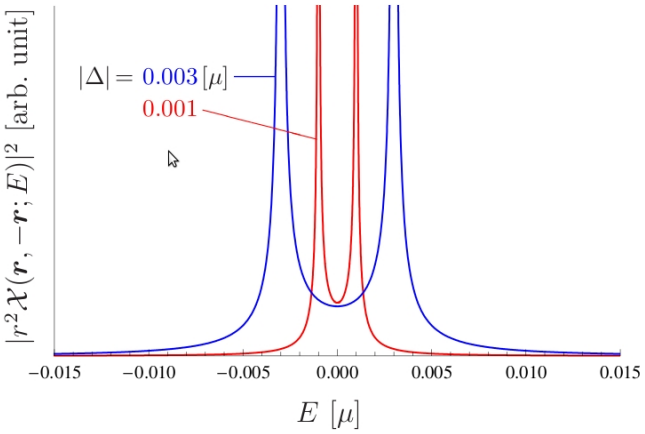

Figure 3.6: Spectrum of Andreev emission for $\theta = \pi$. Source: [18]

$\langle E_0|H_T|E_0\rangle = 0$. Then we have

$$\mathcal{W}|E_0\rangle = (1 + \frac{1}{E_0 - H - i0^+}H_T)|E - 0\rangle. \tag{3.44}$$

Exploiting the Lippman-Schwinger equation, we have the following matrix element of the wave operator:

$$\begin{aligned}\langle E|\mathcal{W}|E_0\rangle = \frac{1}{E_0 - E - i0^+}\Big(&\langle E|H_T|E_0\rangle + \langle E|H_T\frac{1}{E_0 - H_0 - i0^+}H_T|E_0\rangle \\ &+ \langle E|H_T\frac{1}{E_0 - H - i0^+}H_T\frac{1}{E_0 - H_0 - i0^+}H_T|E_0\rangle\Big),\end{aligned} \tag{3.45}$$

where $|E\rangle$ is an eigenstate of the continuous spectrum of H_0 with energy E. In the case of field emission from superconductor we should consider the hamiltonian of the form given by Eq. (3.22) with the specifications of Eqs. (3.13)-(3.25), after substituting the metal with the vacuum. The initial state $|E_0\rangle$ is the ground state of the whole system, i.e. $|0\rangle = |0\rangle_V|0\rangle_S$, where $|0\rangle_V$ is the vacuum state outside the superconductor and $|0\rangle_S$ is the BCS ground state. The final state is the one where a pair of electrons has been emitted in the vacuum: $|2\rangle = b^\dagger_{\boldsymbol{p}_2,\sigma_2}b^\dagger_{\boldsymbol{p}_1,\sigma_1}|0\rangle$, where $|2\rangle$ is the pair state, $b^\dagger_{\boldsymbol{p},\sigma}$ creates an electron of momentum $\boldsymbol{p}$ and spin σ outside the superconductor. The latter remains in the BCS state.

Yuasa proved the lowest nonzero contribution to be of second order in

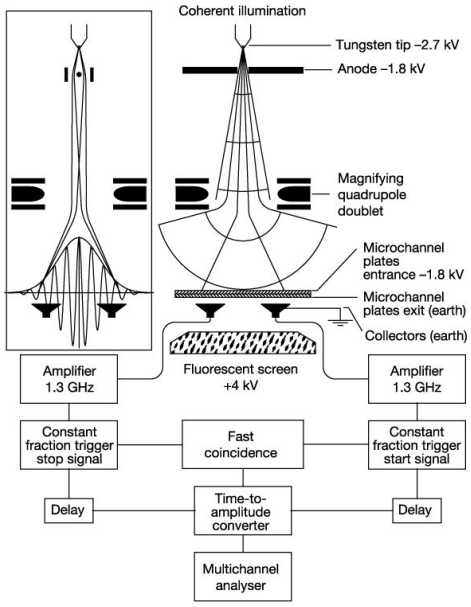

Figure 3.7: Kiesel's setup: electron optical set-up (top) and fast coincidence electronics (bottom) to measure electron anticorrelations. The quadrupoles produce an elliptically shaped beam of coherent electrons. Between the electron source and the quadrupole a biprism (inset) is inserted temporarily to check the coherence of illumination of the collectors. Source: [56]

H_T:

$$\langle 2|\mathcal{W}|0\rangle = \lambda^2(\delta_{\sigma_1\uparrow}\delta_{\sigma_2\downarrow} - \delta_{\sigma_1\downarrow}\delta_{\sigma_2\uparrow}) \int d^3\boldsymbol{k}\, u_k v_k \frac{T_{\boldsymbol{p}_1\boldsymbol{k}} T_{\boldsymbol{p}_2(-\boldsymbol{k})}}{\varepsilon_{p_1} + \varepsilon_{p_2} - i0^+} \times \left(\frac{1}{\varepsilon_{p_1} + \omega_k - i0^+} + \frac{1}{\varepsilon_{p_2} + \omega_k - i0^+} \right) + O(H_T^4), \tag{3.46}$$

where u_k and v_k are the BCS coherence factors introduced in Section 3.1, ε_k and ω_k are the quasiparticle energies outside and inside the superconductor, $T_{\boldsymbol{pk}}$ are the tunneling matrix elements. From the first parentheses it is clear that the pair is emitted in the singlet spin state. It is interesting to notice that virtual processes are involved in Andreev emission, since the last parentheses represent propagators between H_T's.

3.3.2 Coincidence measurements in field emission

As we already said, it is quite difficult to observe Andreev effects in field emission experiments like Nagaoka's. Andreev pairs can be isolated and studied

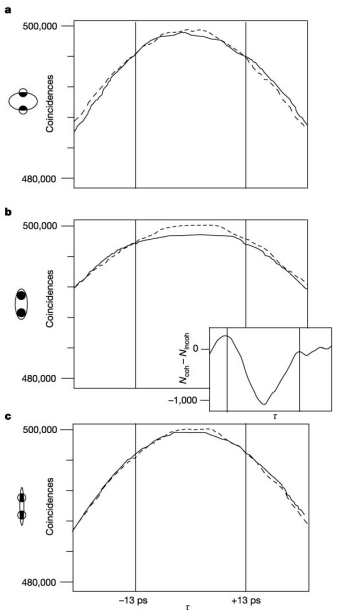

Figure 3.8: Antibunching as a function of coherence of illumination of the collectors. The coincidences per channel for incoherent illumination (dashed lines) is compared to that for partially coherent (a), coherent (b), and again partially coherent illumination (c) (full lines). Source: [56]

exploiting coincidence measurements. One example of this kind of experiment in electron field emission was realized in 2002 by Kiesel et al. [56]. They observed antibunching, which indicates negative correlation, between electrons field-emitted by a normal metal. The antibunching is observed using a coincidence method in which two detectors are coherently illuminated by an electron field emitter. This effect is essentially due to the Pauli exclusion principle: two electrons cannot occupy the same quantum state, that is they cannot arrive at both detectors simultaneously if the latter are close. The antibunching was difficult to observe due to very low degeneracy in the particle beam; the innovation of this experiment is to use high-brightness field electron emitters whose degeneracy is about 10^{-4} electrons per cell in phase space.

The setup is illustrated in Fig. (3.7). Instead of changing the position of the detectors, as proposed in Yuasa's setup, a magnifying quadrupole system is used to modify the beam size, so that the two detectors can be illuminated coherently, incoherently or with partial coherence. The magnifying factors have been calibrated measuring the overlap between the shadows cast by the collectors on the fluorescence screen and the interference fringes due to the insertion of an electron biprism (see Fig. (3.7)). Once the calibration is

done, the biprism is removed and the coincidences are measured in different coherence configurations. The results are shown in Fig (3.8).

The data showed less coincidence counts in case of coherent or partially coherent illumination with respect to the incoherent configuration. So the antibunching is verified. The relative reduction in the counts is compatible with the ratio of the apparatus time resolution and the coherence time, as one can expect. Specifically it was of order 10^{-3}. The setup had the following features: the emitter, made of tungsten, had a virtual diameter of $36nm$; the extraction potential was $900V$ and the total current $1.5\mu A$. Also the brightness was $4.4\times10^{7}Acm^{-2}sr^{-1}$, the coherence time was $3.25\times10^{-14}s$, the time resolution was $26ps$ and the coherent particle current was $4.7\times10^{9}s^{-1}$. The experiment was conducted in vacuum ($10^{-10}mbar$).

Chapter 4

Electron ghost diffraction and ghost imaging

In this chapter we present an electronic analogous of the "ghost" imaging setups we have introduced in Chapter 2. There, we saw that correlated pairs are a key ingredient. Indeed, in a ghost imaging setup, one measures the coincidence countings of two detectors placed in different directions with respect to a source that emits correlated particles. The detector that is on the same side of the object is held fixed, while the scansion is done by the other one. In that case the position of the first detector can be considered as an external parameter and formally one gets an image distribution like $\varphi(\boldsymbol{r}) = I(\boldsymbol{r}, f)$, where $\boldsymbol{r}$ is the position of the second detector and $f(\boldsymbol{r}')$ is the function that describes the object.

Now we would like to introduce a model that demonstrates the possibility of exploiting this kind of setup to reconstruct images by means of correlated electron-pairs. After discussing the Hamiltonian of the system and studying its dynamics, we will extrapolate approximated functional relations of the kind $\varphi(\boldsymbol{r})$ starting from the calculation of the two-particle distribution and the two-point correlation functions for different configurations of the setup. Some data have been obtained using numerical techniques, since analytical expressions are rather difficult to compute but for the limiting case of point-like apertures. In order to keep the discussion flowing, the calculations needed to derive some intermediate results have been omitted here and presented separately in Appendix A.

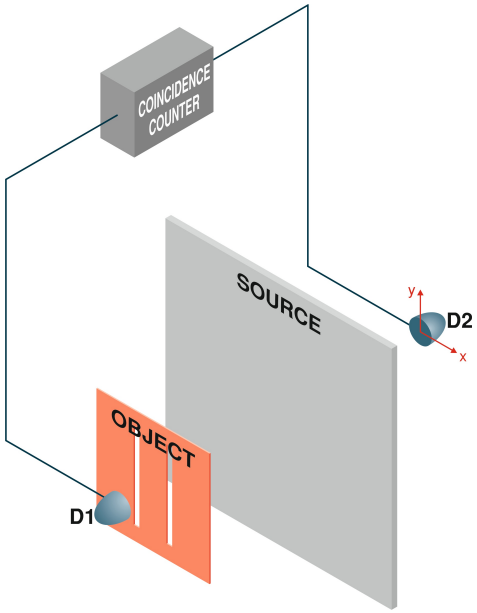

Figure 4.1: Correlated electrons are emitted in opposite directions from a very large superconducting tip and are detected in coincidence by two point-like detectors $D1$ and $D2$. An object is placed in front of $D1$, which is held fix. $D2$ moves on the transverse plane.

4.1 Hamiltonian

Let's consider a system in 3D space composed of a superconducting tip, an object (mask) placed far away from the tip and two detectors of electrons. A schematic representation is given in Fig. 4.1.

For the sake of simplicity, we make the hypothesis that the length of the tip in one direction (that we will call longitudinal) is much smaller than the other two (transverse directions). Since the tip is highly asymmetrical, the definition of the left and the right with respect to the tip is well-posed in the following discussion and has to be intended in the longitudinal direction.

Following the approach introduced in Ref. [18] we divide the system in four parts: 1) the superconductor, 2) the vacuum outside the superconductor on the left, 3) the vacuum outside the superconductor on the right and 4) the vacuum behind the object. Let's suppose that the object is on the right of the tip and that subsytems 2 and 3 are independent. This last assumption should be further discussed and will be justified later for some specific cases.

The Hamiltonians of these four subsystems can be then written as

$$H_S = \int d^3\boldsymbol{r} \left[\sum_{s=\uparrow,\downarrow} \phi_s^\dagger(\boldsymbol{r}) \left(-\frac{1}{2m}\nabla^2 \right) \phi_s(\boldsymbol{r}) - W\phi_\downarrow^\dagger(\boldsymbol{r})\phi_\uparrow^\dagger(\boldsymbol{r})\phi_\uparrow(\boldsymbol{r})\phi_\downarrow(\boldsymbol{r}) \right] \tag{4.1}$$

$$H_V^{(l)} = \sum_{s=\uparrow,\downarrow} \int d^3\boldsymbol{r}\, \psi_s^{\dagger(l)}(\boldsymbol{r}) \left(-\frac{1}{2m}\nabla^2 \right) \psi_s^{(l)}(\boldsymbol{r}) \tag{4.2}$$

$$H_B = \sum_{s=\uparrow,\downarrow} \int d^3\boldsymbol{r}\, \zeta_s^\dagger(\boldsymbol{r}) \left(-\frac{1}{2m}\nabla^2 \right) \zeta_s(\boldsymbol{r}) \tag{4.3}$$

where s denotes spin, l =left (L), right (R) and we set $\hbar = 1$. $\phi_s(\boldsymbol{r})$, $\psi_s^{(l)}(\boldsymbol{r})$ and $\zeta_s(\boldsymbol{r})$ are the fermionic field operators that annihilate an electron of spin s in position $\boldsymbol{r}$ in the subsystem where they are defined: region 1) for $\phi_s(\boldsymbol{r})$, region 2) for $\psi_s^{(L)}(\boldsymbol{r})$, region 3) for $\psi_s^{(R)}(\boldsymbol{r})$ and region 4) for $\zeta_s(\boldsymbol{r})$. These operators satisfy the canonical anticommutation relations

$$\{\phi_s(\boldsymbol{r}), \phi_{s'}^\dagger(\boldsymbol{r}')\} = \{\psi_s^{(l)}(\boldsymbol{r}), \psi_{s'}^{\dagger(l)}(\boldsymbol{r}')\} = \{\zeta_s(\boldsymbol{r}), \zeta_{s'}^\dagger(\boldsymbol{r}')\} = \delta_{ss'}\delta^3(\boldsymbol{r}-\boldsymbol{r}') \tag{4.4}$$

with other anticommutators vanishing. The Coulomb repulsion is neglected outside the conductor, while it is screened inside it [39][40].

Equations (4.2),(4.3) are the free-particle hamiltonians, while in Eq. (4.1) an electron-electron attractive term is added, which is fundamental for the superconductivity. Basically, Eq. (4.1) is the BCS hamiltonian introduced in Section 3.1 rewritten in terms of field operators.

If an electrostatic field is applied around the tip, the potential barrier is modified and the tip emits electrons. This process happens thanks to quantum tunneling through the barrier and, as discussed in Section 3.3, can be described by an Hamiltonian of the kind introduced in Eq. (3.25):

$$H_T = \sum_{s=\uparrow,\downarrow} \sum_{l=L,R} \int d^3\boldsymbol{p} \int d^3\boldsymbol{k} \left(T_{\boldsymbol{pk}}^{(l)} b_{\boldsymbol{p}s}^{\dagger(l)} a_{\boldsymbol{k}s} + T_{\boldsymbol{pk}}^{*(l)} a_{\boldsymbol{k}s}^\dagger b_{\boldsymbol{p}s}^{(l)} \right). \tag{4.5}$$

Similarly the scattering from the object can be described, in first approximation, as a tunneling process with Hamiltonian:

$$H_O = \sum_{s=\uparrow,\downarrow} \int d^3\boldsymbol{p} \int d^3\boldsymbol{k} \left(F_{\boldsymbol{pk}} c_{\boldsymbol{p}s}^\dagger b_{\boldsymbol{k}s}^{(R)} + F_{\boldsymbol{pk}}^* b_{\boldsymbol{k}s}^{\dagger(R)} c_{\boldsymbol{p}s} \right), \tag{4.6}$$

where $a_{\boldsymbol{k}s}$, $b_{\boldsymbol{k}s}^{(l)}$ and $c_{\boldsymbol{p}s}$ are the annihilation operators in momentum space of the electrons inside and outside the emitter and behind the object, respec-

tively, and are related to the fields in configuration space by the expressions

$$\phi_s(\boldsymbol{r}) = \int \frac{d^3\boldsymbol{k}}{\sqrt{(2\pi)^3}}\, a_{\boldsymbol{k}s} e^{i\boldsymbol{k}\cdot\boldsymbol{r}}, \tag{4.7a}$$

$$\psi_s(\boldsymbol{r})^{(l)} = \int \frac{d^3\boldsymbol{k}}{\sqrt{(2\pi)^3}}\, b^{(l)}_{\boldsymbol{k}s} e^{i\boldsymbol{k}\cdot\boldsymbol{r}}, \tag{4.7b}$$

$$\zeta_s(\boldsymbol{r}) = \int \frac{d^3\boldsymbol{p}}{\sqrt{(2\pi)^3}}\, c_{\boldsymbol{p}s} e^{i\boldsymbol{p}\cdot\boldsymbol{r}}. \tag{4.7c}$$

In characterizing the tunneling emission from the superconductor to the vacuum we assume that the only relevant areas of the emitter are the ones near the left and right surfaces. Moreover, the emitting regions are two identical very long (in the transverse directions) and thin (in the longitudinal direction) parts of the superconductor specified by the functions $g(\boldsymbol{r} \pm \boldsymbol{d}/2)$. The vector $\boldsymbol{d}$ takes into account the thickness of the emitter and represents mathematically the translation from one emitting region to the other.

The assumption of very long emitter gives us the possibility of considering the two regions on the left and on the right of the superconductor as independent, hence justifying the hypothesis of independence between the free fields on the left and right side of the superconductor, i.e. $\{\psi_s^{(l)}(\boldsymbol{r}), \psi_{s'}^{\dagger(l')}(\boldsymbol{r}')\} = \{\psi_s^{(l)}(\boldsymbol{r}), \psi_{s'}^{(l')}(\boldsymbol{r}')\} = 0$ for $l \neq l'$. This is consistent if the transverse length of the emitting tip is the largest scale of the system, even with respect to the detector-tip distance, so that no border effects can be observed.

Within the above assumptions the tunneling matrices can be expressed as

$$\begin{cases} T^{(R)}_{\boldsymbol{p}\boldsymbol{k}} = T_{\boldsymbol{p}\boldsymbol{k}} e^{-i(\boldsymbol{p}-\boldsymbol{k})\cdot\boldsymbol{d}/2}, \\ T^{(L)}_{\boldsymbol{p}\boldsymbol{k}} = T_{\boldsymbol{p}\boldsymbol{k}} e^{i(\boldsymbol{p}-\boldsymbol{k})\cdot\boldsymbol{d}/2}, \end{cases} \tag{4.8}$$

where

$$\begin{aligned} T_{\boldsymbol{p}\boldsymbol{k}} &= \langle \boldsymbol{p}|h(\boldsymbol{p})g(\boldsymbol{r})|\boldsymbol{k}\rangle \\ &= h(\boldsymbol{p}) \int \frac{d^3\boldsymbol{r}}{(2\pi)^3}\, g(\boldsymbol{r}) e^{-i(\boldsymbol{p}-\boldsymbol{k})\cdot\boldsymbol{r}} = h(\boldsymbol{p})\tilde{g}(\boldsymbol{p}-\boldsymbol{k}). \end{aligned} \tag{4.9}$$

The function $|h(\boldsymbol{p})|^2$ represents the momentum dependence of the tunneling probability through the potential barrier surrounding the emitting region.

All this implies that an electron with momentum $\boldsymbol{k}$ in the emitter is annihilated by $a_{\boldsymbol{k}s}$, filtered by $g(\boldsymbol{r} \pm \boldsymbol{d}/2)$ and $h(\boldsymbol{p})$, and created outside with momentum $\boldsymbol{p}$ by $b^{\dagger(l)}_{\boldsymbol{p}s}$.

In a similar fashion, for the scattering matrix of Eq. (4.6) we take

$$\begin{aligned} F_{\boldsymbol{pk}} &= \langle \boldsymbol{p}|M(\varepsilon_p)f(\boldsymbol{r})|\boldsymbol{k}\rangle \\ &= M(\varepsilon_p)\int \frac{d^3\boldsymbol{r}}{(2\pi)^3}\, f(\boldsymbol{r})e^{-i(\boldsymbol{p}-\boldsymbol{k})\cdot\boldsymbol{r}} = \tilde{f}(\boldsymbol{p}-\boldsymbol{k}). \end{aligned} \tag{4.10}$$

Accordingly an electron with momentum $\boldsymbol{k}$ in front of the object is annihilated by $b^{(R)}_{\boldsymbol{k}s}$, filtered by $f(\boldsymbol{r})$ and $M(\varepsilon_p)$ and created behind the object with momentum $\boldsymbol{p}$ by $c^\dagger_{\boldsymbol{p}s}$. The function $f(\boldsymbol{r})$ specifies the mask, while $M(\varepsilon_p)$ is an eventual monochromatizing filter placed behind the object.

Including all these terms the global hamiltonian can then be expressed as $H = H_S + H_V^{(L)} + H_V^{(R)} + H_B + \lambda_1 H_T + \lambda_2 H_O$ (here the dimensionless parameters λ_1 and λ_2 have been introduced to characterize the strength of the trasmissions).

4.2 Dynamics of emission

In order to solve the dynamics of the field emission, we find useful to introduce the number operators which refer to the four subsystems:

$$N_S = \sum_{s=\uparrow,\downarrow}\int d^3\boldsymbol{r}\, \phi^\dagger_s(\boldsymbol{r})\phi_s(\boldsymbol{r}), \tag{4.11a}$$

$$N_V^{(l)} = \sum_{s=\uparrow,\downarrow}\int d^3\boldsymbol{r}\, \psi^{\dagger(l)}_s(\boldsymbol{r})\psi^{(l)}_s(\boldsymbol{r}), \tag{4.11b}$$

$$N_B = \sum_{s=\uparrow,\downarrow}\int d^3\boldsymbol{r}\, \zeta^\dagger_s(\boldsymbol{r})\zeta_s(\boldsymbol{r}). \tag{4.11c}$$

and define the new operator

$$\mathcal{H} = H - \mu N \tag{4.12}$$

where $N = N_S + N_V^{(R)} + N_V^{(L)}$. Notice that $[\mathcal{H}, N] = 0$, so the time-evolution operator can be factorized as $e^{-iHt} = e^{-i\mu Nt}e^{-i\mathcal{H}t}$. In the Heisenberg representation, the field operators can therefore be factorized as

$$\phi_s(\boldsymbol{r},t) = e^{iHt}\phi_s(\boldsymbol{r})e^{-iHt} = \tilde{\phi}_s(\boldsymbol{r},t)e^{-i\mu t}, \tag{4.13}$$

$$\psi_s(\boldsymbol{r},t)^{(l)} = e^{iHt}\psi_s(\boldsymbol{r})^{(l)}e^{-iHt} = \tilde{\psi}_s(\boldsymbol{r},t)^{(l)}e^{-i\mu t}, \tag{4.14}$$

$$\zeta_s(\boldsymbol{r},t) = e^{iHt}\phi_s(\boldsymbol{r})e^{-iHt} = \tilde{\zeta}_s(\boldsymbol{r},t)e^{-i\mu t}, \tag{4.15}$$

where

$$\tilde{\phi}_s(\boldsymbol{r},t) = e^{i\mathcal{H}t}\phi_s(\boldsymbol{r})e^{-i\mathcal{H}t} \tag{4.16}$$

$$\tilde{\psi}_s(\boldsymbol{r},t)^{(l)} = e^{i\mathcal{H}t}\psi_s(\boldsymbol{r})^{(l)}e^{-i\mathcal{H}t} \tag{4.17}$$

$$\tilde{\zeta}_s(\boldsymbol{r},t) = e^{i\mathcal{H}t}\zeta_s(\boldsymbol{r})e^{-i\mathcal{H}t} \tag{4.18}$$

describe the dynamics of the fields in the picture introduced by the unitary transformation $e^{i\mu Nt}$.

In order to prove these results and some others afterwards, we can exploit the following rules which can be derived directly from the anticommutation relations:

$$[B_s^\dagger(\boldsymbol{r})A_s(\boldsymbol{r}), A_{s'}^\dagger(\boldsymbol{r}')] = \delta_{ss'}\delta^3(\boldsymbol{r}-\boldsymbol{r}')B_s^\dagger(\boldsymbol{r}) \tag{4.19a}$$

$$[A_s^\dagger(\boldsymbol{r})B_s(\boldsymbol{r}), A_{s'}(\boldsymbol{r}')] = -\delta_{ss'}\delta^3(\boldsymbol{r}-\boldsymbol{r}')B_s(\boldsymbol{r}) \tag{4.19b}$$

where $A_s(\boldsymbol{r})$ and $B_s(\boldsymbol{r})$ are any two fermionic field operators of the type $\phi_s(\boldsymbol{r})$, $\psi_s(\boldsymbol{r})$ or $\zeta_s(\boldsymbol{r})$. These rules can be simply extended to the Fourier transform of the fields (see Eq. (4.7)).

The picture just introduced is useful for the mean field approximation when we choose μ as the Fermi level of the superconductor. As we showed in Sec. 3.1.2, in this approximation we are able to diagonalize the Hamiltonian $\mathcal{H}_S = H_S - \mu N_S$ using the Bogoliubov transformation of Eq. (3.13) with

$$\begin{cases} u_k = \dfrac{1}{\sqrt{2}}\sqrt{1+\dfrac{\varepsilon_k}{\omega_k}}, \\ v_k = \dfrac{e^{i\delta}}{\sqrt{2}}\sqrt{1-\dfrac{\varepsilon_k}{\omega_k}}, \end{cases} \tag{4.20}$$

to get

$$\mathcal{H}_S = H_S - \mu N_S = \sum_{s=\uparrow,\downarrow}\int d^3\boldsymbol{k}\,\omega_k\alpha_{\boldsymbol{k}s}^\dagger\alpha_{\boldsymbol{k}s}, \tag{4.21a}$$

$$\mathcal{H}_V^{(l)} = H_V^{(l)} - \mu N_V^{(l)} = \sum_{s=\uparrow,\downarrow}\int d^3\boldsymbol{p}\,\varepsilon_p b_{\boldsymbol{p}s}^{\dagger(l)}b_{\boldsymbol{p}s}^{(l)}, \tag{4.21b}$$

$$\mathcal{H}_B = H_B - \mu N_B = \sum_{s=\uparrow,\downarrow}\int d^3\boldsymbol{p}\,\varepsilon_p c_{\boldsymbol{p}s}^\dagger c_{\boldsymbol{p}s}, \tag{4.21c}$$

where

$$\varepsilon_p = \frac{p^2}{2m} - \mu, \qquad \omega_k = \sqrt{\varepsilon_k^2 + |\Delta|^2} \tag{4.22}$$

are the energies of an emitted electron in vacuum and of a quasiparticle excitation in the superconducting emitter, respectively, measured relative to the Fermi level of the emitter, and

$$\Delta = W\langle\phi_\uparrow(\boldsymbol{r})\phi_\downarrow(\boldsymbol{r})\rangle = |\Delta|e^{i\delta} \tag{4.23}$$

is the gap parameter of the superconductor (for all these quantities see also Section 3.1).

In order to solve the dynamics of the system, we consider the operators $\tilde{\alpha}_{\boldsymbol{p}s}(t) = e^{i\mathcal{H}t}\alpha_{\boldsymbol{p}s}e^{-i\mathcal{H}t}$, $\tilde{b}^{(l)}_{\boldsymbol{p}s}(t) = e^{i\mathcal{H}t}b^{(l)}_{\boldsymbol{p}s}e^{-i\mathcal{H}t}$ and $\tilde{c}_{\boldsymbol{p}s}(t) = e^{i\mathcal{H}t}c_{\boldsymbol{p}s}e^{-i\mathcal{H}t}$ and their time-derivatives $\frac{d}{dt}\tilde{\alpha}_{\boldsymbol{p}s}(t) = i[\mathcal{H}, \tilde{\alpha}_{\boldsymbol{p}s}(t)]$, $\frac{d}{dt}\tilde{b}^{(l)}_{\boldsymbol{p}s}(t) = i[\mathcal{H}, \tilde{b}^{(l)}_{\boldsymbol{p}s}(t)]$ and $\frac{d}{dt}\tilde{c}_{\boldsymbol{p}s}(t) = i[\mathcal{H}, \tilde{c}_{\boldsymbol{p}s}(t)]$ which represent the equations of motion in the picture introduced above. After calculating explicitly the commutators using the rules in Eq. (4.19), we get the following equations:

$$\frac{d}{dt}\begin{pmatrix}\tilde{c}_{\boldsymbol{p}\uparrow}\\ \tilde{c}^\dagger_{\boldsymbol{p}\downarrow}\end{pmatrix} = -i\mathcal{E}_p\begin{pmatrix}\tilde{c}_{\boldsymbol{p}\uparrow}\\ \tilde{c}^\dagger_{\boldsymbol{p}\downarrow}\end{pmatrix} - i\lambda_2\int d^3\boldsymbol{k}\,\mathcal{F}_{\boldsymbol{pk}}\begin{pmatrix}\tilde{b}^{(R)}_{\boldsymbol{k}\uparrow}\\ \tilde{b}^{\dagger(R)}_{\boldsymbol{k}\downarrow}\end{pmatrix}, \tag{4.24a}$$

$$\frac{d}{dt}\begin{pmatrix}\tilde{b}^{(l)}_{\boldsymbol{p}\uparrow}\\ \tilde{b}^{\dagger(l)}_{\boldsymbol{p}\downarrow}\end{pmatrix} = -i\mathcal{E}_p\begin{pmatrix}\tilde{b}^{(l)}_{\boldsymbol{p}\uparrow}\\ \tilde{b}^{\dagger(l)}_{\boldsymbol{p}\downarrow}\end{pmatrix} - i\lambda_1\int d^3\boldsymbol{k}\,\mathcal{T}^{(l)}_{\boldsymbol{pk}}\begin{pmatrix}\tilde{\alpha}_{\boldsymbol{k}\uparrow}\\ \tilde{\alpha}^\dagger_{\boldsymbol{k}\downarrow}\end{pmatrix} - i\lambda_2\delta_{lR}\int d^3\boldsymbol{q}\,\mathcal{F}^\dagger_{\boldsymbol{qp}}\begin{pmatrix}\tilde{c}_{\boldsymbol{q}\uparrow}\\ \tilde{c}^\dagger_{\boldsymbol{q}\downarrow}\end{pmatrix}, \tag{4.24b}$$

$$\frac{d}{dt}\begin{pmatrix}\tilde{\alpha}_{\boldsymbol{k}\uparrow}\\ \tilde{\alpha}^\dagger_{\boldsymbol{k}\downarrow}\end{pmatrix} = -i\Omega_k\begin{pmatrix}\tilde{\alpha}_{\boldsymbol{k}\uparrow}\\ \tilde{\alpha}^\dagger_{\boldsymbol{k}\downarrow}\end{pmatrix} - i\lambda_1\sum_l\int d^3\boldsymbol{p}\,\mathcal{T}^{\dagger(l)}_{\boldsymbol{pk}}\begin{pmatrix}\tilde{b}^{(l)}_{\boldsymbol{p}\uparrow}\\ \tilde{b}^{\dagger(l)}_{\boldsymbol{p}\downarrow}\end{pmatrix}, \tag{4.24c}$$

where

$$\mathcal{E}_p = \begin{pmatrix}\varepsilon_p & 0\\ 0 & -\varepsilon_p\end{pmatrix}, \qquad \Omega_k = \begin{pmatrix}\omega_k & 0\\ 0 & -\omega_k\end{pmatrix}, \tag{4.25}$$

$$\mathcal{T}^{(l)}_{\boldsymbol{pk}} = \begin{pmatrix}T^{(l)}_{\boldsymbol{pk}}u_k & -T^{(l)}_{\boldsymbol{p}(-\boldsymbol{k})}v_k\\ -T^{*(l)}_{\boldsymbol{p}(-\boldsymbol{k})}v^*_k & -T^{*(l)}_{\boldsymbol{pk}}u^*_k\end{pmatrix}, \tag{4.26}$$

$$\mathcal{F}_{\boldsymbol{pk}} = \begin{pmatrix}F_{\boldsymbol{pk}} & 0\\ 0 & -F^*_{\boldsymbol{pk}}\end{pmatrix}. \tag{4.27}$$

This system of equations can be solved by means of the Laplace transform; let's introduce some notation. We define the 2D vectors

$$A_k \equiv \begin{pmatrix} \mathcal{L}[\tilde{\alpha}_{\boldsymbol{k}\uparrow}(t)](s) \\ \mathcal{L}[\tilde{\alpha}^\dagger_{\boldsymbol{k}\downarrow}(t)](s) \end{pmatrix}, \qquad A_{k0} \equiv \begin{pmatrix} \tilde{\alpha}_{\boldsymbol{k}\uparrow}(0) \\ \tilde{\alpha}^\dagger_{\boldsymbol{k}\downarrow}(0) \end{pmatrix}, \tag{4.28a}$$

$$B^{(l)}_p \equiv \begin{pmatrix} \mathcal{L}[\tilde{b}^{(l)}_{\boldsymbol{p}\uparrow}(t)](s) \\ \mathcal{L}[\tilde{b}^{\dagger(l)}_{\boldsymbol{p}\downarrow}(t)](s) \end{pmatrix}, \qquad B^{(l)}_{p0} \equiv \begin{pmatrix} \tilde{b}^{(l)}_{\boldsymbol{p}\uparrow}(0) \\ \tilde{b}^{\dagger(l)}_{\boldsymbol{p}\downarrow}(0) \end{pmatrix}, \tag{4.28b}$$

$$C_p \equiv \begin{pmatrix} \mathcal{L}[\tilde{c}_{\boldsymbol{p}\uparrow}(t)](s) \\ \mathcal{L}[\tilde{c}^\dagger_{\boldsymbol{p}\downarrow}(t)](s) \end{pmatrix}, \qquad C_{p0} \equiv \begin{pmatrix} \tilde{c}_{\boldsymbol{p}\uparrow}(0) \\ \tilde{c}^\dagger_{\boldsymbol{p}\downarrow}(0) \end{pmatrix}, \tag{4.28c}$$

where $\mathcal{L}[f(t)](s)$ is the Laplace transform of complex frequency s of the function $f(t)$.

In the weak coupling regime, which means $\lambda_1, \lambda_2 \ll 1$, we find the following solutions: up to second order in λ_1 and zero-th order in λ_2

$$\begin{aligned} B^{(l'')}_{k'} = &\sum_l \int d^3\boldsymbol{p}[\delta_{l''l}\delta(\boldsymbol{k'}-\boldsymbol{p}) - \lambda_1^2 \int d^3\boldsymbol{k}(s+i\mathcal{E}_{k'})^{-1} \\ &\times \mathcal{T}^{(l'')}_{\boldsymbol{k'k}}(s+i\Omega_k)^{-1}\mathcal{T}^{\dagger(l)}_{\boldsymbol{pk}}(s+i\mathcal{E}_p)^{-1}B^{(l)}_{p0} \\ &- i\int d^3\boldsymbol{p}[\delta(\boldsymbol{k'}-\boldsymbol{p})](s+i\mathcal{E}_p)^{-1}\lambda_1 \int d^3\boldsymbol{k}\mathcal{T}^{(l'')}_{\boldsymbol{pk}}(s+i\Omega_k)^{-1}A_{k0}. \end{aligned} \tag{4.29}$$

and up to first order in λ_1 and first order in λ_2

$$\begin{aligned} C_p = &(s+i\mathcal{E}_p)^{-1}C_{p0} - i\lambda_2(s+i\mathcal{E}_p)^{-1}\int d^3\boldsymbol{k'}\mathcal{F}_{\boldsymbol{pk'}} \\ &\times \Big\{ \sum_l \int d^3\boldsymbol{p'}[\delta_{Rl}\delta(\boldsymbol{k'}-\boldsymbol{p'})](s+i\mathcal{E}_{p'})^{-1}B^{(l)}_{p'0} \\ &- i\int d^3\boldsymbol{p'}[\delta(\boldsymbol{k'}-\boldsymbol{p'})](s+i\mathcal{E}_{p'})^{-1}\lambda_1 \int d^3\boldsymbol{k}\mathcal{T}^{(R)}_{\boldsymbol{p'k}}(s+i\Omega_k)^{-1}A_{k0}\Big\}. \end{aligned} \tag{4.30}$$

A detailed derivation of these results is given in Appendix A. Higher order terms in the perturbation parameters λ_1 and λ_2 have been neglected since they will just give higher order corrections to the quantities that we will analyze in the next sections (e.g. the anomalous correlation function of Eq. (4.35d)).

4.3 Correlation functions

Let's suppose to put the detectors in opposite directions with respect to the superconducting emitter, one behind the object in the position $\boldsymbol{r_1}$ (subsystem 4) and the other one on the other side in position $\boldsymbol{r_2}$ (subsystem 2). For now, let's not make any assumptions about the kind of detectors we use. In order to see some "ghost" effects, we fix the position of detector D1 and try to reconstruct the image by scanning with detector D2 on the other side.

As in the optical case (see Chapter 2), we are interested in the coincidences in the non-equilibrium steady state (NESS). The number of counts of two-particle detections, irrespectively of the spin states, is proportional to [33]

$$\rho^{(2)}(\boldsymbol{r}_1,t_1;\boldsymbol{r}_2,t_2)=\sum_{s_1,s_2=\uparrow,\downarrow}\langle\zeta^\dagger_{s_1}(\boldsymbol{r}_1,t_1)\psi^{\dagger(L)}_{s_2}(\boldsymbol{r}_2,t_2)\psi^{(L)}_{s_2}(\boldsymbol{r}_2,t_2)\zeta_{s_1}(\boldsymbol{r}_1,t_1)\rangle, \tag{4.31}$$

where the average is taken over the initial state, which is characterized by the Fermi distribution of the quasiparticle excitations for the superconductor and the vacuum state for the other subsystems,

$$\langle\alpha^\dagger_{\boldsymbol{k}s}\alpha_{\boldsymbol{k}'s'}\rangle=f(\omega_k)\delta_{ss'}\delta^3(\boldsymbol{k}-\boldsymbol{k}') \tag{4.32}$$

with

$$f(\omega_k)=\frac{1}{e^{\omega_k/k_BT}+1}, \tag{4.33}$$

where T is the temperature of the emitter and k_B the Boltzmann constant. Exploiting the generalized Wick's theorem, we may recast the two-particle distribution function in terms of two-point correlation functions:

$$\begin{aligned}\rho^{(2)}(\boldsymbol{r}_1,t_1;\boldsymbol{r}_2,t_2)&=4\gamma_2(\boldsymbol{r}_2,t_2;\boldsymbol{r}_2,t_2)\gamma_4(\boldsymbol{r}_1,t_1;\boldsymbol{r}_1,t_1)\\&\quad-2|\gamma_{24}(\boldsymbol{r}_1,t_1;\boldsymbol{r}_2,t_2)|^2+2|\chi(\boldsymbol{r}_1,t_1;\boldsymbol{r}_2,t_2)|^2.\end{aligned} \tag{4.34}$$

where

$$\gamma_2(\boldsymbol{r}_2,t_2;\boldsymbol{r}_2,t_2)=\langle\tilde\psi^{\dagger(L)}_\uparrow(\boldsymbol{r}_2,t_2)\tilde\psi^{(L)}_\uparrow(\boldsymbol{r}_2,t_2)\rangle=\langle\tilde\psi^{\dagger(L)}_\downarrow(\boldsymbol{r}_2,t_2)\tilde\psi^{(L)}_\downarrow(\boldsymbol{r}_2,t_2)\rangle \tag{4.35a}$$

$$\gamma_4(\boldsymbol{r}_1,t_1;\boldsymbol{r}_1,t_1)=\langle\tilde\zeta^\dagger_\uparrow(\boldsymbol{r}_1,t_1)\tilde\zeta_\uparrow(\boldsymbol{r}_1,t_1)\rangle=\langle\tilde\zeta^\dagger_\downarrow(\boldsymbol{r}_1,t_1)\tilde\zeta_\downarrow(\boldsymbol{r}_1,t_1)\rangle \tag{4.35b}$$

$$\gamma_{24}(\boldsymbol{r}_1,t_1;\boldsymbol{r}_2,t_2)=\langle\tilde\zeta^\dagger_\uparrow(\boldsymbol{r}_1,t_1))\tilde\psi^{(L)}_\uparrow(\boldsymbol{r}_2,t_2)\rangle=\langle\tilde\zeta^\dagger_\downarrow(\boldsymbol{r}_1,t_1)\tilde\psi^{(L)}_\downarrow(\boldsymbol{r}_2,t_2)\rangle \tag{4.35c}$$

$$\chi(\boldsymbol{r}_1,t_1;\boldsymbol{r}_2,t_2)=\langle\tilde\zeta_\uparrow(\boldsymbol{r}_1,t_1)\tilde\psi^{(L)}_\downarrow(\boldsymbol{r}_2,t_2)\rangle=-\langle\tilde\zeta_\downarrow(\boldsymbol{r}_1,t_1)\tilde\psi^{(L)}_\uparrow(\boldsymbol{r}_2,t_2)\rangle. \tag{4.35d}$$

The other two-point correlations vanish.

The function $\gamma_{24}(\boldsymbol{r}_1, t_1; \boldsymbol{r}_2, t_2)$ describes the antibunching due to Fermi statistics. It doesn't account for the superconductivity, in fact it is similar to the normal emitter case. As one can naturally expect, and as demonstrated in [18] in the absence of a diffracting object, this function rapidly goes to zero if the two detectors are not collinear. In our case they are almost opposite, so we can neglect this correlation function.

Since $\boldsymbol{r_1}$ is fixed, $\gamma_4(\boldsymbol{r}_1, t_1; \boldsymbol{r}_1, t_1)$ will be a constant.

The function $\gamma_2(\boldsymbol{r}_2, t_2; \boldsymbol{r}_2, t_2)$ will depend on the symmetry and the size of the emitter, but will not take into account the presence of the object. In the limiting case of an infinite plane emitter, from the transverse translational simmetry and from electric charge conservation follows directly that $\gamma_2(\boldsymbol{r}_2, t_2; \boldsymbol{r}_2, t_2)$ is a constant. In the case of a spherical emitter, instead, the function is proportional to $|\boldsymbol{r_2}|^{-2}$, as one would easily expect from charge conservation and has been demonstrated in [18]. Both these functions represent the detection of a single electron and take into account the quasiparticle emission from the superconductor.

Let's focus on the anomalous correlation function $\chi(\boldsymbol{r}_1, t_1; \boldsymbol{r}_2, t_2)$, which describes pair emission. Suppose for simplicity $T = 0$. Recalling the relations Eqs.(4.7),(4.28), we get

$$\begin{aligned}\chi(\boldsymbol{r}_1, t_1; \boldsymbol{r}_2, t_2) &= \langle \tilde{\zeta}_\uparrow(\boldsymbol{r}_1, t_1) \tilde{\psi}^{(L)}_\downarrow(\boldsymbol{r}_2, t_2) \rangle \\ &= \int d^3\boldsymbol{p} \int d^3\boldsymbol{k'} e^{i\boldsymbol{p}\cdot\boldsymbol{r}_1} e^{i\boldsymbol{k'}\cdot\boldsymbol{r}_2} \langle \mathcal{L}^{-1}[C^{(1)}_p](t_1) [\mathcal{L}^{-1}[B^{(L)(2)}_{k'}](t_2)]^\dagger \rangle,\end{aligned} \tag{4.36}$$

where $C^{(1)}_p$ and $B^{(L)(2)}_{k'}$ are the first and second component of the 2D vectors C_p and $B^{(L)}_{k'}$ of Eq. (4.28), respectively. $\mathcal{L}^{-1}[f(s)](t)$ is the inverse Laplace transform

$$\mathcal{L}^{-1}[f(s)](t) = \int_{C_B} \frac{ds}{2\pi i} f(s) e^{st} \tag{4.37}$$

with C_B the Bromwich path running parallel to the imaginary axis of s at the right of every pole of $f(s)$.

Since at $T = 0$ $f(\omega_k) = \theta(\omega_k)$, the initial state is the pure state formed by the tensor product of the BCS ground state (subsystem 1) and the vacuum states of the other subsystems.

As far as the anomalous correlation is concerned, it can be seen by inspection that the diagonal terms of $B^{(L)}_{k'}$ give zero contributions because they annihilate the ground state. From now on we can neglect these terms in the

discussion and write

$$B^{(L)}_{k'} = -\lambda_1^2 \sum_l \int d^3\boldsymbol{p} \int d^3\boldsymbol{k} (s+i\mathcal{E}_{k'})^{-1} \mathcal{T}^{(L)}_{\boldsymbol{k'k}} (s+i\Omega_k)^{-1} \mathcal{T}^{\dagger(l)}_{\boldsymbol{pk}} (s+i\mathcal{E}_p)^{-1} B^{(l)}_{p0}$$
$$- i(s+i\mathcal{E}_{k'})^{-1}\lambda_1 \int d^3\boldsymbol{k} \mathcal{T}^{(L)}_{\boldsymbol{k'k}} (s+i\Omega_k)^{-1} A_{k0}. \tag{4.38}$$

Let's notice that there are no terms in C_0 in Eq. (4.38), hence also the C_0 contributions given by Eq.(4.30) are null and we can drop those terms and write

$$C_p = -i\lambda_2 (s+i\mathcal{E}_p)^{-1} \int d^3\boldsymbol{k'} \mathcal{F}_{\boldsymbol{pk'}} (s+i\mathcal{E}_{k'})^{-1} B^{(R)}_{k'0}$$
$$- \lambda_1\lambda_2 (s+i\mathcal{E}_p)^{-1} \int d^3\boldsymbol{k'} \mathcal{F}_{\boldsymbol{pk'}} (s+i\mathcal{E}_{k'})^{-1} \int d^3\boldsymbol{k} \mathcal{T}^{(R)}_{\boldsymbol{k'k}} (s+i\Omega_k)^{-1} A_{k0}. \tag{4.39}$$

Making explicit the matrix products, we have

$$B^{(L)(2)}_{k'} = -\lambda_1^2 \sum_l \int d^3\boldsymbol{p} \int d^3\boldsymbol{k} (s-i\varepsilon_{k'})^{-1} \mathcal{T}^{(L)21}_{\boldsymbol{k'k}} (s+i\omega_k)^{-1}$$
$$\times (\mathcal{T}^{*(l)11}_{\boldsymbol{pk}} (s+i\varepsilon_p)^{-1} b^{(l)}_{\boldsymbol{p}\uparrow} + \mathcal{T}^{*(l)21}_{\boldsymbol{pk}} (s-i\varepsilon_p)^{-1} b^{(l)\dagger}_{\boldsymbol{p}\downarrow})$$
$$- \lambda_1^2 \sum_l \int d^3\boldsymbol{p} \int d^3\boldsymbol{k} (s-i\varepsilon_{k'})^{-1} \mathcal{T}^{(L)22}_{\boldsymbol{k'k}} (s-i\omega_k)^{-1}$$
$$\times (\mathcal{T}^{*(l)12}_{\boldsymbol{pk}} (s+i\varepsilon_p)^{-1} b^{(l)}_{\boldsymbol{p}\uparrow} + \mathcal{T}^{*(l)22}_{\boldsymbol{pk}} (s-i\varepsilon_p)^{-1} b^{\dagger(l)}_{\boldsymbol{p}\downarrow})$$
$$- i(s-i\varepsilon_{k'})^{-1}\lambda_1 \int d^3\boldsymbol{k} (\mathcal{T}^{(L)21}_{\boldsymbol{k'k}} (s+i\omega_k)^{-1} \alpha_{\boldsymbol{k}\uparrow} + \mathcal{T}^{(L)22}_{\boldsymbol{k'k}} (s-i\omega_k)^{-1} \alpha^\dagger_{\boldsymbol{k}\downarrow}). \tag{4.40}$$

and

$$C^{(1)}_p = -i\lambda_2 (s+i\varepsilon_p)^{-1} \int d^3\boldsymbol{k'} \mathcal{F}^{11}_{\boldsymbol{pk'}} (s+i\varepsilon_{k'})^{-1} b^{(R)}_{\boldsymbol{k'}\uparrow}$$
$$- \lambda_1\lambda_2 (s+i\varepsilon_p)^{-1} \int d^3\boldsymbol{k'} \mathcal{F}^{11}_{\boldsymbol{pk'}} (s+i\varepsilon_{k'})^{-1} \int d^3\boldsymbol{k}$$
$$\times (\mathcal{T}^{(R)11}_{\boldsymbol{k'k}} (s+i\omega_k)^{-1} \alpha_{\boldsymbol{k}\uparrow} + \mathcal{T}^{(R)12}_{\boldsymbol{k'k}} (s-i\omega_k)^{-1} \alpha^\dagger_{\boldsymbol{k}\downarrow}). \tag{4.41}$$

If we look at Eq. (4.36), we can see that all the terms with spin down in Eqs. (4.40),(4.41) do not contribute to the anomalous correlation, while the terms with spin up have the following expectation values on the ground state:

$$\langle \alpha_{\boldsymbol{k'}\uparrow} \alpha^\dagger_{\boldsymbol{p''}\uparrow} \rangle = \delta^3(\boldsymbol{k'} - \boldsymbol{p''}), \langle b^{(R)}_{\boldsymbol{p'}\uparrow} b^{\dagger(R)}_{\boldsymbol{p''}\uparrow} \rangle = \delta^3(\boldsymbol{p'} - \boldsymbol{p''}). \tag{4.42}$$

At $T = 0$ all the other expectation values vanish.

After a transient period, the electron emission approaches a NESS, which can be obtained in the limit $t \to \infty$. If $\mathcal{T}$ and $\mathcal{F}$ are sufficiently regular, following the procedure in [18], in the NESS we get

$$\begin{aligned}
\chi(\boldsymbol{r}_1, t_1; \boldsymbol{r}_2, t_2) &= \int d^3\boldsymbol{p} \int d^3\boldsymbol{k'} e^{i\boldsymbol{p}\cdot\boldsymbol{r}_1} e^{i\boldsymbol{k'}\cdot\boldsymbol{r}_2} \langle \mathcal{L}^{-1}[C_p^{(1)}](t_1) (\mathcal{L}^{-1}[B_{k'}^{(L)(2)}](t_2))^\dagger \rangle \\
&= \int d^3\boldsymbol{p} \int d^3\boldsymbol{k'} e^{i\boldsymbol{p}\cdot\boldsymbol{r}_1} e^{i\boldsymbol{k'}\cdot\boldsymbol{r}_2} \langle \mathcal{L}^{-1}\Big[- i\lambda_2 (s + i\varepsilon_p)^{-1} \\
&\times \int d^3\boldsymbol{k''} \mathcal{F}^{11}_{\boldsymbol{p}\boldsymbol{k''}} (s + i\varepsilon_{k''})^{-1} b^{(R)}_{\boldsymbol{k''}\uparrow} \\
&- \lambda_1\lambda_2 (s + i\varepsilon_p)^{-1} \int d^3\boldsymbol{k''} \mathcal{F}^{11}_{\boldsymbol{p}\boldsymbol{k''}} (s + i\varepsilon_{k''})^{-1} \\
&\times \int d^3\boldsymbol{k} \mathcal{T}^{(R)11}_{\boldsymbol{k''}\boldsymbol{k}} (s + i\omega_k)^{-1} \alpha_{\boldsymbol{k}\uparrow} \Big](t_1) \\
&\times \Big(\mathcal{L}^{-1}\Big[- \lambda_1^2 \sum_l \int d^3\boldsymbol{p'} \int d^3\boldsymbol{k'''} (s - i\varepsilon_{k'})^{-1} \mathcal{T}^{(L)21}_{\boldsymbol{k'}\boldsymbol{k'''}} \\
&\times (s + i\omega_{k'''})^{-1} \mathcal{T}^{*(l)11}_{\boldsymbol{p'}\boldsymbol{k'''}} (s + i\varepsilon_{p'})^{-1} b^{(l)}_{\boldsymbol{p'}\uparrow} \\
&- \lambda_1^2 \sum_l \int d^3\boldsymbol{p'} \int d^3\boldsymbol{k'''} (s - i\varepsilon_{k'})^{-1} \mathcal{T}^{(L)22}_{\boldsymbol{k'}\boldsymbol{k'''}} \\
&\times (s - i\omega_{k'''})^{-1} \mathcal{T}^{*(l)12}_{\boldsymbol{p'}\boldsymbol{k'''}} (s + i\varepsilon_{p'})^{-1} b^{(l)}_{\boldsymbol{p'}\uparrow} \\
&- i(s - i\varepsilon_{k'})^{-1} \lambda_1 \int d^3\boldsymbol{k'''} \mathcal{T}^{(L)21}_{\boldsymbol{k'}\boldsymbol{k'''}} (s + i\omega_{k'''})^{-1} \alpha_{\boldsymbol{k'''}\uparrow} \Big](t_2) \Big)^\dagger \rangle.
\end{aligned} \tag{4.43}$$

The Laplace inverse transform together with making explicit the scattering matrix elements $F_{\boldsymbol{p}\boldsymbol{p'}}$ of Eq. (4.10) and performing some of the integrations,

yields

$$\begin{aligned}\chi(\boldsymbol{r}_1,t_1;\boldsymbol{r}_2,t_2) = i4\pi^2 m\lambda_1^2\lambda_2 \int d^3\boldsymbol{k'}\int d^3\boldsymbol{r'}\frac{1}{(2\pi)^3}e^{i\boldsymbol{k'}\cdot\boldsymbol{r}_2}f(\boldsymbol{r'})\\ \times\Big[\int d^3\boldsymbol{p'}e^{i\boldsymbol{p'}\cdot\boldsymbol{r'}}e^{-i\varepsilon_{p'}t_1}\int d^3\boldsymbol{k}T^{(L)}_{\boldsymbol{k'-k}}v_k T^{(R)}_{\boldsymbol{p'k}}u_k\\ \times\frac{e^{i\varepsilon_{p'}t_2}}{(i(\varepsilon_{k'}+\varepsilon_{p'})+0^+)}M(\varepsilon_{p'})\frac{e^{ip(\varepsilon_{p'})|\boldsymbol{r}_1-\boldsymbol{r'}|}}{i|\boldsymbol{r}_1-\boldsymbol{r'}|}\\ \times\Big(\frac{1}{i(\varepsilon_{k'}+\omega_k)+0^+}+\frac{1}{(i(\omega_k+\varepsilon_{p'})+0^+)}\Big)\\ +\int d^3\boldsymbol{p'}e^{i\boldsymbol{p'}\cdot\boldsymbol{r'}}\int d^3\boldsymbol{k}T^{(R)}_{\boldsymbol{p'k}}u_k T^{(L)}_{\boldsymbol{k'-k}}v_k\\ \times\frac{1}{(i(\varepsilon_{p'}-\omega_k)+0^+)(i(\varepsilon_{k'}+\omega_k)+0^+)}\\ \times\Big(M(\omega_k)\frac{e^{ip(\omega_k)|\boldsymbol{r}_1-\boldsymbol{r'}|}}{i|\boldsymbol{r}_1-\boldsymbol{r'}|}e^{i\omega_k(t_2-t_1)}\\ -M(\varepsilon_{p'})\frac{e^{ip(\varepsilon_{p'})|\boldsymbol{r}_1-\boldsymbol{r'}|}}{i|\boldsymbol{r}_1-\boldsymbol{r'}|}e^{-i\varepsilon_{p'}(t_1-t_2)}\Big)\Big],\end{aligned}\tag{4.44}$$

where $p(E)\equiv\sqrt{2m(\mu+E)}$. The detailed calculation is performed in Appendix A.

So far we have kept the discussion quite general. Indeed, the only conditions we put are the weak coupling and the limit $t\to\infty$. The one other assumption we made is the independence of the left and right vacuum subsystems. Actually, up to this point of the calculations that condition is irrelevant and could even be relaxed. In fact, if we consider the two subsystems as one (which means losing all the sums over l and imposing $\boldsymbol{d}=0$, that leads to $T^{(R)}_{\boldsymbol{pk}}=T^{(L)}_{\boldsymbol{pk}}=T_{\boldsymbol{pk}}$), we arrive at the exact same formula (4.44). The independence will come in handy later for a specific case, but for now let's focus on a more general approach.

4.4 Formal approach

We will proceed in the extrapolation of a rather general form for the anomalous correlation in which each part has a clear and intuitive physical meaning. Let's substitute the matrix elements given by Eqs. (4.9),(4.8) in the expres-

sion of Eq. (4.44):

$$\begin{aligned}\chi(\boldsymbol{r}_1,t_1;\boldsymbol{r}_2,t_2) = \frac{im\lambda_1^2\lambda_2}{(2\pi)^4}\int d^3\boldsymbol{k'}\int d^3\boldsymbol{r'}\frac{1}{(2\pi)^3}e^{i\boldsymbol{k'}\cdot\boldsymbol{r}_2}f(\boldsymbol{r'})\\ \times\Big[\int d^3\boldsymbol{p'}e^{i\boldsymbol{p'}\cdot\boldsymbol{r'}}e^{-i\varepsilon_{p'}t_1}\int d^3\boldsymbol{k}\int d^3\boldsymbol{r''}\int d^3\boldsymbol{r'''}\\ \times h(\boldsymbol{p'})h(\boldsymbol{k'})e^{-i(\boldsymbol{k'}+\boldsymbol{k})\cdot\boldsymbol{r'''}}e^{-i(\boldsymbol{p'}-\boldsymbol{k})\cdot\boldsymbol{r''}}\\ \times g(\boldsymbol{r''}-\boldsymbol{d}/2)g(\boldsymbol{r'''}+\boldsymbol{d}/2)v_ku_kM(\varepsilon_{p'})\frac{e^{i\varepsilon_{p'}t_2}}{(i(\varepsilon_{k'}+\varepsilon_{p'})+0^+)}\\ \times\Big(\frac{1}{i(\varepsilon_{k'}+\omega_k)+0^+}+\frac{1}{(i(\omega_k+\varepsilon_{p'})+0^+)}\Big)\frac{e^{ip(\varepsilon_{p'})|\boldsymbol{r}_1-\boldsymbol{r'}|}}{i|\boldsymbol{r}_1-\boldsymbol{r'}|}\\ +\int d^3\boldsymbol{p'}e^{i\boldsymbol{p'}\cdot\boldsymbol{r'}}\int d^3\boldsymbol{k}\int d^3\boldsymbol{r''}\int d^3\boldsymbol{r'''}\\ \times h(\boldsymbol{p'})h(\boldsymbol{k'})e^{-i(\boldsymbol{k'}+\boldsymbol{k})\cdot\boldsymbol{r'''}}e^{-i(\boldsymbol{p'}-\boldsymbol{k})\cdot\boldsymbol{r''}}\\ \times g(\boldsymbol{r''}-\boldsymbol{d}/2)g(\boldsymbol{r'''}+\boldsymbol{d}/2)u_kv_k\\ \times\frac{1}{(i(\varepsilon_{p'}-\omega_k)+0^+)(i(\varepsilon_{k'}+\omega_k)+0^+)}\\ \times\Big(M(\omega_k)\frac{e^{ip(\omega_k)|\boldsymbol{r}_1-\boldsymbol{r'}|}}{i|\boldsymbol{r}_1-\boldsymbol{r'}|}e^{i\omega_k(t_2-t_1)}\\ -M(\varepsilon_{p'})\frac{e^{ip(\varepsilon_{p'})|\boldsymbol{r}_1-\boldsymbol{r'}|}}{i|\boldsymbol{r}_1-\boldsymbol{r'}|}e^{-i\varepsilon_{p'}(t_1-t_2)}\Big)\Big].\end{aligned} \tag{4.45}$$

This can now be simplified using the formula

$$\lim_{t\to\infty}\frac{e^{-ixt}}{x\pm i0^+} = \begin{cases}-2\pi i\,\delta(x),\\ 0,\end{cases} \tag{4.46}$$

which is valid in the sense of the distributions.

Let's then assume that $h(\boldsymbol{p'})$ and $M(\varepsilon_{p'})$ are regular functions and have spherical symmetry in $\boldsymbol{p'}$. If we have $|\mu(t_1-t_2)|, k_F|\boldsymbol{r_1}-\boldsymbol{r'}| \ll k_f|\boldsymbol{r'}-\boldsymbol{r''}|$ for each $\boldsymbol{r'},\boldsymbol{r''}$ such that$f(\boldsymbol{r'})g(\boldsymbol{r''}-\boldsymbol{d}/2)\neq 0$, we can integrate the second term over $\boldsymbol{p'}$ using the residue theorem or equivalently the formula (4.46), which stresses the fact that for large t the only relevant contributions are the on-shell ones ($\varepsilon_{p'}=\omega_k$). These are suppressed by the last parentheses, so the last term vanishes with the integration. As far as the first term is concerned,

the integration over the angular parts of $\boldsymbol{p'}$ and $\boldsymbol{k'}$ yields

$$\begin{aligned}\chi(\boldsymbol{r}_1,t_1;\boldsymbol{r}_2,t_2) = \frac{im\lambda_1^2\lambda_2}{(2\pi)^2}\int_{-\infty}^{\infty}dk'\,k'\int d^3\boldsymbol{r'}\frac{1}{(2\pi)^3}\frac{e^{ik'|\boldsymbol{r}_2-\boldsymbol{r'''}|}}{i|\boldsymbol{r}_2-\boldsymbol{r'''}|}f(\boldsymbol{r'})\\ \times\int_{-\infty}^{\infty}dp'\,p'\,\frac{e^{ip'|\boldsymbol{r'}-\boldsymbol{r''}|}}{i|\boldsymbol{r'}-\boldsymbol{r''}|}\int d^3\boldsymbol{k}\int d^3\boldsymbol{r''}\int d^3\boldsymbol{r'''}\\ \times h(p')h(k')e^{i\boldsymbol{k}\cdot(\boldsymbol{r''}-\boldsymbol{r'''})}g(\boldsymbol{r''}-\boldsymbol{d}/2)g(\boldsymbol{r'''}+\boldsymbol{d}/2)\\ \times\Big(\frac{1}{i(\varepsilon_{k'}+\omega_k)+0^+}+\frac{1}{(i(\omega_k+\varepsilon_{p'})+0^+)}\Big)\\ \times M(\varepsilon_{p'})\frac{e^{ip(\varepsilon_{p'})|\boldsymbol{r}_1-\boldsymbol{r'}|}}{i|\boldsymbol{r}_1-\boldsymbol{r'}|}v_ku_k\frac{e^{-i\varepsilon_{p'}(t_1-t_2)}}{(i(\varepsilon_{k'}+\varepsilon_{p'})+0^+)}.\end{aligned}\tag{4.47}$$

After a further integration and a change of variable, we get

$$\begin{aligned}\chi(\boldsymbol{r}_1,t_1;\boldsymbol{r}_2,t_2) = \frac{im^2\lambda_1^2\lambda_2}{(2\pi)^6}\int d^3\boldsymbol{k}\int d^3\boldsymbol{r''}\int d^3\boldsymbol{r'''}\int d^3\boldsymbol{r'}f(\boldsymbol{r'})\\ \times e^{i\boldsymbol{k}\cdot(\boldsymbol{r''}-\boldsymbol{r'''})}g(\boldsymbol{r''}-\boldsymbol{d}/2)g(\boldsymbol{r'''}+\boldsymbol{d}/2)v_ku_k\int_{-\infty}^{\infty}dq\,q\\ \times\Big(\frac{e^{iq|\boldsymbol{r}_2-\boldsymbol{r'''}|}}{i|\boldsymbol{r}_2-\boldsymbol{r'''}|}\frac{e^{ip(-\varepsilon_q)|\boldsymbol{r'}-\boldsymbol{r''}|}}{i|\boldsymbol{r'}-\boldsymbol{r''}|}e^{i\varepsilon_q(t_1-t_2)}\\ \times M(-\varepsilon_q)\frac{e^{ip(-\varepsilon_q)|\boldsymbol{r}_1-\boldsymbol{r'}|}}{i|\boldsymbol{r}_1-\boldsymbol{r'}|}\frac{h(p(-\varepsilon_q))h(q)}{i(\varepsilon_q+\omega_k)+0^+}\\ +\frac{e^{ip(-\varepsilon_q)|\boldsymbol{r}_2-\boldsymbol{r'''}|}}{i|\boldsymbol{r}_2-\boldsymbol{r'''}|}\frac{e^{iq|\boldsymbol{r'}-\boldsymbol{r''}|}}{i|\boldsymbol{r'}-\boldsymbol{r''}|}e^{-i\varepsilon_q(t_1-t_2)}\\ \times M(\varepsilon_q)\frac{e^{ip(\varepsilon_q)|\boldsymbol{r}_1-\boldsymbol{r'}|}}{i|\boldsymbol{r}_1-\boldsymbol{r'}|}\frac{h(q)h(p(-\varepsilon_q))}{(i(\omega_k+\varepsilon_q)+0^+)}\Big).\end{aligned}\tag{4.48}$$

4.4.1 Spectrum

Let's take a look at the spectral representation of the anomalous correlation defined by the Fourier transform

$$\chi(\boldsymbol{r}_1;\boldsymbol{r}_2;E)=\int_{-\infty}^{\infty}d\tau\,\chi(\boldsymbol{r}_1,t_1;\boldsymbol{r}_2,t_2)e^{-iE\tau},\tag{4.49}$$

where $\tau=t_1-t_2$. Since according to Eq. (4.48) the correlation depends only on the difference t_1-t_2, this definition is well-posed. From Eqs. (4.48),(4.49)

we get

$$\chi(\boldsymbol{r}_1;\boldsymbol{r}_2;E) = \frac{im^2\lambda_1^2\lambda_2}{(2\pi)^5}\int d^3\boldsymbol{k}\int d^3\boldsymbol{r''}\int d^3\boldsymbol{r'''}\int d^3\boldsymbol{r'} f(\boldsymbol{r'})$$
$$\times e^{i\boldsymbol{k}\cdot(\boldsymbol{r''}-\boldsymbol{r'''})} g(\boldsymbol{r''}-\boldsymbol{d}/2)g(\boldsymbol{r'''}+\boldsymbol{d}/2)v_k u_k \int_{-\infty}^{\infty} dq\, q$$
$$\times \Big(\frac{e^{iq|\boldsymbol{r}_2-\boldsymbol{r'''}|}}{i|\boldsymbol{r}_2-\boldsymbol{r'''}|}\frac{e^{ip(-\varepsilon_q)|\boldsymbol{r'}-\boldsymbol{r''}|}}{i|\boldsymbol{r'}-\boldsymbol{r''}|}$$
$$\times \delta(\varepsilon_q - E)M(-\varepsilon_q)\frac{e^{ip(-\varepsilon_q)|\boldsymbol{r}_1-\boldsymbol{r'}|}}{i|\boldsymbol{r}_1-\boldsymbol{r'}|}\frac{h(p(-\varepsilon_q))h(q)}{i(\varepsilon_q+\omega_k)+0^+}$$
$$+ \frac{e^{ip(-\varepsilon_q)|\boldsymbol{r}_2-\boldsymbol{r'''}|}}{i|\boldsymbol{r}_2-\boldsymbol{r'''}|}\frac{e^{iq|\boldsymbol{r'}-\boldsymbol{r''}|}}{i|\boldsymbol{r'}-\boldsymbol{r''}|}$$
$$\times \delta(\varepsilon_q + E)M(\varepsilon_q)\frac{e^{ip(\varepsilon_q)|\boldsymbol{r}_1-\boldsymbol{r'}|}}{i|\boldsymbol{r}_1-\boldsymbol{r'}|}\frac{h(q)h(p(-\varepsilon_q))}{(i(\omega_k+\varepsilon_q)+0^+)}\Big). \qquad (4.50)$$

Since $\delta(f(x)) = \sum_{x_i}\frac{\delta(x-x_i)}{|f'(x)|_{x_i}}$ for x_i such that $f(x_i)=0$, for $|E|<\mu$ the integration over q yields

$$\chi(\boldsymbol{r}_1;\boldsymbol{r}_2;E) = \frac{im^3\lambda_1^2\lambda_2}{(2\pi)^5}\int d^3\boldsymbol{k}\int d^3\boldsymbol{r''}\int d^3\boldsymbol{r'''}\int d^3\boldsymbol{r'} f(\boldsymbol{r'})e^{i\boldsymbol{k}\cdot(\boldsymbol{r''}-\boldsymbol{r'''})}$$
$$\times g(\boldsymbol{r''}-\boldsymbol{d}/2)g(\boldsymbol{r'''}+\boldsymbol{d}/2)v_k u_k M(-E)\frac{e^{ip(-E)|\boldsymbol{r}_1-\boldsymbol{r'}|}}{i|\boldsymbol{r}_1-\boldsymbol{r'}|}$$
$$\times \Big(\frac{e^{ip(E)|\boldsymbol{r}_2-\boldsymbol{r'''}|}}{i|\boldsymbol{r}_2-\boldsymbol{r'''}|}\frac{e^{ip(-E)|\boldsymbol{r'}-\boldsymbol{r''}|}}{i|\boldsymbol{r'}-\boldsymbol{r''}|}\frac{h(p(-E))h(p(E))}{i(E+\omega_k)+0^+}$$
$$- \frac{e^{-ip(E)|\boldsymbol{r}_2-\boldsymbol{r'''}|}}{i|\boldsymbol{r}_2-\boldsymbol{r'''}|}\frac{e^{ip(-E)|\boldsymbol{r'}-\boldsymbol{r''}|}}{i|\boldsymbol{r'}-\boldsymbol{r''}|}\frac{h(p(-E))h(-p(E))}{i(E+\omega_k)+0^+}$$
$$+ \frac{e^{ip(E)|\boldsymbol{r}_2-\boldsymbol{r'''}|}}{i|\boldsymbol{r}_2-\boldsymbol{r'''}|}\frac{e^{ip(-E)|\boldsymbol{r'}-\boldsymbol{r''}|}}{i|\boldsymbol{r'}-\boldsymbol{r''}|}\frac{h(p(-E))h(p(E))}{(i(\omega_k-E)+0^+)}$$
$$- \frac{e^{ip(E)|\boldsymbol{r}_2-\boldsymbol{r'''}|}}{i|\boldsymbol{r}_2-\boldsymbol{r'''}|}\frac{e^{-ip(-E)|\boldsymbol{r'}-\boldsymbol{r''}|}}{i|\boldsymbol{r'}-\boldsymbol{r''}|}\frac{h(-p(-E))h(p(E))}{(i(\omega_k-E)+0^+)}\Big). \qquad (4.51)$$

If $\boldsymbol{r}_1$ is such that $|\boldsymbol{r}_1-\boldsymbol{r'}| \ll (|\boldsymbol{r'}-\boldsymbol{r''}|+|\boldsymbol{r}_2-\boldsymbol{r'''}|)$ for each $\boldsymbol{r'},\boldsymbol{r''},\boldsymbol{r'''}$ such that $f(\boldsymbol{r'})g(\boldsymbol{r''}-\boldsymbol{d}/2)g(\boldsymbol{r'''}+\boldsymbol{d}/2)\neq 0$, for large $k_F|\boldsymbol{r'}-\boldsymbol{r''}|$ and $k_F|\boldsymbol{r}_2-\boldsymbol{r'''}|$, keeping $|\boldsymbol{r'}-\boldsymbol{r''}|-|\boldsymbol{r}_2-\boldsymbol{r'''}|$ finite, the second and fourth terms can be

neglected [see formula (4.46)]:

$$\chi(\boldsymbol{r}_1;\boldsymbol{r}_2;E) = \frac{m^3\lambda_1^2\lambda_2\Delta}{(2\pi)^5}\int d^3\boldsymbol{k}\int d^3\boldsymbol{r''}\int d^3\boldsymbol{r'''}\int d^3\boldsymbol{r'} f(\boldsymbol{r'}) e^{i\boldsymbol{k}\cdot(\boldsymbol{r''}-\boldsymbol{r'''})}$$
$$\times g(\boldsymbol{r''}-\boldsymbol{d}/2)g(\boldsymbol{r'''}+\boldsymbol{d}/2)M(-E)\frac{e^{ip(-E)|\boldsymbol{r}_1-\boldsymbol{r'}|}}{i|\boldsymbol{r}_1-\boldsymbol{r'}|}$$
$$\times \frac{e^{ip(E)|\boldsymbol{r}_2-\boldsymbol{r'''}|}}{i|\boldsymbol{r}_2-\boldsymbol{r'''}|}\frac{e^{ip(-E)|\boldsymbol{r'}-\boldsymbol{r''}|}}{i|\boldsymbol{r'}-\boldsymbol{r''}|}\frac{h(p(-E))h(p(E))}{(\omega_k^2-E^2)-i0^+}. \tag{4.52}$$

The last integration over momenta yields

$$\chi(\boldsymbol{r}_1;\boldsymbol{r}_2;E) = \frac{im^4\lambda_1^2\lambda_2\Delta}{2(2\pi)^3}\int d^3\boldsymbol{r''}\int d^3\boldsymbol{r'''}\int d^3\boldsymbol{r'} f(\boldsymbol{r'})$$
$$\times g(\boldsymbol{r''}-\boldsymbol{d}/2)g(\boldsymbol{r'''}+\boldsymbol{d}/2)M(-E)\frac{e^{ip(-E)|\boldsymbol{r}_1-\boldsymbol{r'}|}}{i|\boldsymbol{r}_1-\boldsymbol{r'}|}$$
$$\times \frac{e^{ip(E)|\boldsymbol{r}_2-\boldsymbol{r'''}|}}{i|\boldsymbol{r}_2-\boldsymbol{r'''}|}\frac{e^{ip(-E)|\boldsymbol{r'}-\boldsymbol{r''}|}}{i|\boldsymbol{r'}-\boldsymbol{r''}|}\frac{h(p(-E))h(p(E))}{\sqrt{E^2-|\Delta|^2}}$$
$$\times \left(\frac{e^{ik_+(E)|\boldsymbol{r''}-\boldsymbol{r'''}|}}{i|\boldsymbol{r''}-\boldsymbol{r'''}|}-\frac{e^{-ik_-(E)|\boldsymbol{r''}-\boldsymbol{r'''}|}}{i|\boldsymbol{r''}-\boldsymbol{r'''}|}\right), \tag{4.53}$$

where $k_\sigma(E)=\sqrt{2m\mu+\sigma 2m\sqrt{E^2-|\Delta|^2}}$.

For large distances the saddle point approximation assures that only the contributions for small E with respect to μ are relevant. Physically this means that only the energies near the Fermi level of the superconductor are important. So, it is possible to substitute the respective Taylor-series expansions in the exponentials for $E, |\Delta| \ll \mu$. This leads to

$$\chi(\boldsymbol{r}_1,t_1;\boldsymbol{r}_2,t_2) = \frac{-m^4\lambda_1^2\lambda_2\Delta}{(2\pi)^2}\int d^3\boldsymbol{r''}\int d^3\boldsymbol{r'''}\int d^3\boldsymbol{r'}\int_{-\infty}^{\infty} dE\, f(\boldsymbol{r'})$$
$$\times g(\boldsymbol{r''}-\boldsymbol{d}/2)g(\boldsymbol{r'''}+\boldsymbol{d}/2)M(-E)$$
$$\times \frac{e^{ik_F(|\boldsymbol{r}_1-\boldsymbol{r'}|+|\boldsymbol{r}_2-\boldsymbol{r'''}|+|\boldsymbol{r'}-\boldsymbol{r''}|)}}{|\boldsymbol{r}_1-\boldsymbol{r'}||\boldsymbol{r}_2-\boldsymbol{r'''}||\boldsymbol{r'}-\boldsymbol{r''}|}\frac{\sin k_F|\boldsymbol{r''}-\boldsymbol{r'''}|}{|\boldsymbol{r''}-\boldsymbol{r'''}|}$$
$$\times e^{i\frac{k_F E}{2\mu}(|\boldsymbol{r}_2-\boldsymbol{r'''}|-|\boldsymbol{r'}-\boldsymbol{r''}|-|\boldsymbol{r}_1-\boldsymbol{r'}|+\frac{2\mu\tau}{k_F})}$$
$$\times e^{i\frac{k_F\sqrt{E^2-|\Delta|^2}}{2\mu}|\boldsymbol{r''}-\boldsymbol{r'''}|}\frac{h(p(-E))h(p(E))}{\sqrt{E^2-|\Delta|^2}}, \tag{4.54}$$

where we extended the integration range $[-\mu,\mu]$ to the whole real axis. This limit is a good approximation since the integrand is relevant only for small E.

From the Fowler-Nordheim theory of electron field-emission [29] one can see that a good choice for the function $h(p)$ would be

$$h(\boldsymbol{p}) = e^{\varepsilon_p/2E_C}, \tag{4.55}$$

where E_C controls the low-energy cutoff of the tunneling spectrum. In this case $h(p(E))h(p(-E)) = 1$.

We can define the following function:

$$\Phi(x,y) = \int_{-\infty}^{\infty} ds\, \frac{e^{i\frac{s}{\pi\xi}x} e^{i\frac{\sqrt{s^2-1}}{\pi\xi}y}}{\sqrt{s^2-1}}, \tag{4.56}$$

where $\xi = \frac{2\mu}{\pi k_F|\Delta|}$ is the Pippard lenght, which characterises the spatial extension of a Cooper pair.

If we don't consider any energy filter in our setup ($M(-E) = 1$), we reach the general formula

$$\begin{aligned}\chi(\boldsymbol{r}_1,t_1;\boldsymbol{r}_2,t_2) = {} & \frac{-m^4\lambda_1^2\lambda_2\Delta}{(2\pi)^2}\int d^3\boldsymbol{r''}\int d^3\boldsymbol{r'''}\int d^3\boldsymbol{r'} f(\boldsymbol{r'}) \\ & \times g(\boldsymbol{r''}-\boldsymbol{d}/2)g(\boldsymbol{r'''}+\boldsymbol{d}/2)\frac{\sin k_F|\boldsymbol{r''}-\boldsymbol{r'''}|}{|\boldsymbol{r''}-\boldsymbol{r'''}|} \\ & \times \frac{e^{ik_F(|\boldsymbol{r}_1-\boldsymbol{r'}|+|\boldsymbol{r}_2-\boldsymbol{r'''}|+|\boldsymbol{r'}-\boldsymbol{r''}|)}}{|\boldsymbol{r}_1-\boldsymbol{r'}||\boldsymbol{r}_2-\boldsymbol{r'''}||\boldsymbol{r'}-\boldsymbol{r''}|} \\ & \times \Phi(|\boldsymbol{r}_2-\boldsymbol{r'''}|-|\boldsymbol{r'}-\boldsymbol{r''}|-|\boldsymbol{r}_1-\boldsymbol{r'}|+\frac{2\mu\tau}{k_F},|\boldsymbol{r''}-\boldsymbol{r'''}|).\end{aligned} \tag{4.57}$$

Let's isolate and analyse each part of this formula in order to understand its physical meaning.

The factor $\frac{e^{ik_F(|\boldsymbol{r}_1-\boldsymbol{r'}|+|\boldsymbol{r}_2-\boldsymbol{r'''}|+|\boldsymbol{r'}-\boldsymbol{r''}|)}}{|\boldsymbol{r}_1-\boldsymbol{r'}||\boldsymbol{r}_2-\boldsymbol{r'''}||\boldsymbol{r'}-\boldsymbol{r''}|}$ accounts for the free propagation in the vacuum regions.

The function $\Phi(|\boldsymbol{r}_2-\boldsymbol{r'''}|-|\boldsymbol{r'}-\boldsymbol{r''}|-|\boldsymbol{r}_1-\boldsymbol{r'}|+\frac{2\mu\tau}{k_F},|\boldsymbol{r''}-\boldsymbol{r'''}|)$ is the only part that considers the superconductive nature of the tip. Indeed, it expresses the correlation between the two electrons emitted by comparing the difference of their covered distances with the Pippard coherence length. If the ratio is big, Φ goes rapidly to zero. This means that we cannot measure coincidences if we move the detectors for more than a coherence lenght from the anti-symmetrical position. If that were the case, we would have attempted to measure a correlation between particles that never interact with each other and are uncorrelated from the beginning, because they were not originated by the same Cooper pair. A correction for a delay in the coincidence measurement is accounted for by the term with τ in the argument.

The factors $f(\boldsymbol{r'})$ and $g(\boldsymbol{r})$ describe the object and the emitting regions, respectively. They are accountable for any diffraction effect and for the profile of the emitted electron-beam.

The term $\frac{\sin k_F|\boldsymbol{r''}-\boldsymbol{r'''}|}{|\boldsymbol{r''}-\boldsymbol{r'''}|}$ is related to the propagation inside the superconductor of the bi-electron wavefunction. It is originated by the coherent superposition of two contributions which correspond to emission events involving a more electron-like or hole-like virtual bogoliubov quasiparticle state. Let's notice that the amplitude of the process is suppressed with a power law on the scale length of the Fermi wavelength, which is much smaller than the Pippard length. This effect is typical of the nonlocal Andreev reflection and has been observed in Refs. [20][22][26].

These interpretations will be more clear as soon as we consider some particular cases. Two limit configurations are studied in the following sections.

4.5 Particular case: infinite source

We consider an infinite planar superconductive emitter. We assume that the superconductor is thick ($k_F d \gg 1$) and so the relevant regions for the emission are those close to the surface. As already mentioned (see section 4.1), these assumptions ensure the independence of the electrons on the left side and on the right side, outside the superconductor, because they oppose the tunneling between vacuums through the tip and cancel border effects. The vector $\boldsymbol{d}$ is oriented in the longitudinal direction. Of course $\boldsymbol{d}$ should be shorter than the Pippard coherence length.

For the sake of the calculations, let's assume a gaussian shape of the emitting region in the longitudinal direction:

$$g(\boldsymbol{r}) = \frac{1}{\sqrt{(2\pi)w_z}} e^{-\frac{z^2}{2w_z^2}}, \tag{4.58}$$

so that from Eq. (4.9) we have

$$T_{\boldsymbol{p},\boldsymbol{k}} = h(\boldsymbol{p})\tilde{g}(\boldsymbol{p}-\boldsymbol{k}) = \frac{1}{2\pi} h(\boldsymbol{p}) e^{-\frac{w_z^2|p_z-k_z|^2}{2}} \delta(\boldsymbol{p}_\perp - \boldsymbol{k}_\perp), \tag{4.59}$$

where the subscript z indicates the longitudinal component of a vector, while $\perp$ stands for the transverse components. Suppose that the object is a planar, thin mask perpendicular to the z-axis, so that the filter function can be write down as follow:

$$f(\boldsymbol{r'}) = e^{-\frac{(z'-z0)^2}{2w_f^2}} A(\boldsymbol{r'}_\perp), \tag{4.60}$$

where w_f represents the thickness of the object and $A(\boldsymbol{r}'_\perp)$ describes the mask; no further hypothesis will be made on it until later. z_0 is the mean longitudinal distance between the object and the emitter. We must consider finite thickness of the emitting region and the object because otherwise the matrix elements $T_{\boldsymbol{pk}}$ and $F_{\boldsymbol{pk}}$ are not regular enough.

Our goal is to create the ghost image of the mask or to observe a ghost interference/diffraction effect, exploiting the correlation between electrons constituting the Cooper pairs emitted from the superconductor into vacuum. We would like to show that this is possible exploiting the study of the coincident clicks of two detectors placed on opposite sides with rispect to the emitter-object block. In fact, let's recall that the number of counts in this case is proportional to the two-particle distribution $\rho^{(2)}(\boldsymbol{r}_2, t_2; \boldsymbol{r}_1, t_1)$ and, in particular, $|\chi(\boldsymbol{r}_1, t_1; \boldsymbol{r}_2, t_2)|$ is related to the Cooper pair contribution. The latter is the function that will allow us to reconstruct the image.

This time let's try a different, more direct approach, which exploits the transverse translational invariance of the emitter. Let's assume the following conditions: the funtion $h(\boldsymbol{p})$ of Eq. (4.9) has spherical symmetry ($h(\boldsymbol{p}) = h(p)$); the object and the detectors are far from the emitter; the emitting region thickness is much smaller than the source's ($d_z \gg w_z$). Under these hypotheses the spectrum of the anomalous correlation of Eq. (4.44) is calculated to be

$$\begin{aligned}\chi(\boldsymbol{r}_1; \boldsymbol{r}_2; E) = i\frac{1}{2\sqrt{E^2 - |\Delta|^2}} m^4 \Delta \lambda_1^2 \lambda_2 \int d^3\boldsymbol{r'} \int d^2\boldsymbol{k}_\perp e^{i\boldsymbol{k}_\perp \cdot (\boldsymbol{r}'_\perp - \boldsymbol{r}_{2\perp})} f(\boldsymbol{r'}) \\ \times e^{ip^*(E)|r_{2z} + d_z/2|} h(p(E)) h(p(-E)) \\ \times M(-E) \frac{e^{ip(-E)|\boldsymbol{r}_1 - \boldsymbol{r'}|}}{i|\boldsymbol{r}_1 - \boldsymbol{r'}|} e^{ip^*(-E)(r'_z - d_z/2)} \frac{1}{p^*(-E)p^*(E)} \\ \times \Big(\frac{1}{k_+^*(E)} e^{ik_+^*(E)d_z} e^{-\frac{w_z^2|-p^*(E)+k_+^*(E)|^2}{2}} e^{-\frac{w_z^2|p^*(-E)-k_+^*(E)|^2}{2}} \\ + \frac{1}{k_-^*(E)} e^{-ik_-^*(E)d_z} e^{-\frac{w_z^2|p^*(E)+k_-^*(E)|^2}{2}} e^{-\frac{w_z^2|p^*(-E)+k_-^*(E)|^2}{2}}\Big). \qquad (4.61)\end{aligned}$$

where the following functions have been defined:

$$\mu^* = \mu - \frac{\boldsymbol{k}_\perp^2}{2m}, \qquad p^*(E) = \sqrt{2m(\mu^* + E)}, \qquad \varepsilon_p^* = \frac{p_z^2 + \boldsymbol{k}_\perp^2}{2m} - \mu = \frac{p_z^2}{2m} - \mu^*. \qquad (4.62)$$

Let's notice that placing the second detector far away at the left of the emitter implies $r_{2z} + d_z/2 < 0$. A thourough derivation of Eq. (4.61) is given in Appendix A. Thanks to the saddle point approximation, for large

distances only the small energy and transverse momenta contributions are significant. Moreover, the last term is negligible with repect to the other, as it can be easily seen by evaluating the ratio between the two at zero-th order in the small energy and transverse momenta expansion:

$$\begin{aligned}
&\left| \frac{\frac{1}{k_+^*(E)} e^{ik_+^*(E)d_z} e^{-\frac{w_z^2|-p^*(E)+k_+^*(E)|^2}{2}} e^{-\frac{w_z^2|p^*(-E)-k_+^*(E)|^2}{2}}}{\frac{1}{k_-^*(E)} e^{-ik_-^*(E)d_z} e^{-\frac{w_z^2|p^*(E)+k_-^*(E)|^2}{2}} e^{-\frac{w_z^2|p^*(-E)+k_-^*(E)|^2}{2}}} \right| \\
\simeq &\left| \frac{\frac{1}{k_F} e^{ik_F d_z} e^{-\frac{w_z^2|-k_F+k_F|^2}{2}} e^{-\frac{w_z^2|k_F-k_F|^2}{2}}}{\frac{1}{k_F} e^{-ik_F d_z} e^{-\frac{w_z^2|k_F+k_F|^2}{2}} e^{-\frac{w_z^2|k_F+k_F|^2}{2}}} \right| = e^{4w_z^2 k_F^2}. \qquad (4.63)
\end{aligned}$$

For w_z of the order of λ_F, the ratio is way bigger than one and the second term is suppressed. Recalling Eq.(4.55) we have $h(p(E))h(p(-E)) = 1$. Dropping the monochromatizing filter, at first order in E/μ and $|\boldsymbol{k}_\perp|^2/k_F^2$ we get

$$\begin{aligned}
\chi(\boldsymbol{r}_1;\boldsymbol{r}_2;E) = &\frac{m^4\Delta\lambda_1^2\lambda_2}{2k_F^3\sqrt{E^2-|\Delta|^2}} \int d^3\boldsymbol{r'} \int d^2\boldsymbol{k}_\perp e^{i\boldsymbol{k}_\perp\cdot(\boldsymbol{r'}_\perp-\boldsymbol{r}_{2\perp})} f(\boldsymbol{r'}) \\
&\times e^{ik_F|r_{2z}+d_z/2|} \frac{e^{ik_F|\boldsymbol{r}_1-\boldsymbol{r'}|}}{|\boldsymbol{r}_1-\boldsymbol{r'}|} e^{ik_F(r'_z-d_z/2)} e^{ik_F d_z} \\
&\times e^{i\frac{k_F E}{2\mu}|r_{2z}+d_z/2|} e^{-i\frac{k_F E}{2\mu}|\boldsymbol{r}_1-\boldsymbol{r'}|} e^{-i\frac{k_F E}{2\mu}(r'_z-d_z/2)} e^{i\frac{k_F\sqrt{E^2-|\Delta|^2}}{2\mu}d_z} \\
&\times e^{-i\frac{|\boldsymbol{k}_\perp|^2}{2k_F}|r_{2z}+d_z/2|} e^{-i\frac{|\boldsymbol{k}_\perp|^2}{2k_F}(r'_z-d_z/2)} e^{-i\frac{|\boldsymbol{k}_\perp|^2}{2k_F}d_z}. \qquad (4.64)
\end{aligned}$$

The integration over $\boldsymbol{k}_\perp$ and the fourier antitransform in energy give us

$$\begin{aligned}
\chi(\boldsymbol{r}_1;\boldsymbol{r}_2;\tau) = &\frac{-im^4\Delta\lambda_1^2\lambda_2}{2k_F^2} \int d^3\boldsymbol{r'} f(\boldsymbol{r'}) \\
&\times e^{ik_F|r_{2z}+d_z/2|} \frac{e^{ik_F|\boldsymbol{r}_1-\boldsymbol{r'}|}}{|\boldsymbol{r}_1-\boldsymbol{r'}|} e^{ik_F(r'_z-d_z/2)} e^{ik_F d_z} \\
&\times \Phi(|r_{2z}+d_z/2|-|\boldsymbol{r}_1-\boldsymbol{r'}|-(r'_z-d_z/2)+2\mu\tau/k_F, d_z) \\
&\times \frac{e^{i\frac{k_F|\boldsymbol{r'}_\perp-\boldsymbol{r}_{2\perp}|^2}{2(|r_{2z}+d_z/2|+(r'_z-d_z/2)+d_z)}}}{(|r_{2z}+d_z/2|+(r'_z-d_z/2)+d_z)}, \qquad (4.65)
\end{aligned}$$

where $\Phi(x,y)$ is defined by Eq. (4.56) and $\tau = t_1 - t_2$.

Keeping only the first order in $|\boldsymbol{k}_\perp|^2/k_F^2$ corresponds to making the paraxial approximation, which is equivalent to say that the electron beam has a small divergence. This implies that, if the object has a small transverse length compared to the distance from the source, we are only interested

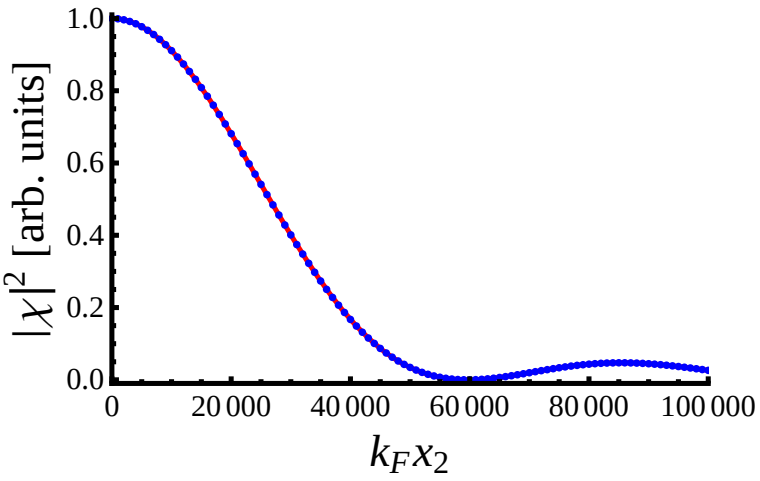

Figure 4.2: Simulation of a ghost diffraction setup with a single-slit object: Eq. (4.65) has been integrated numerically assuming a slit-width of $2\lambda_F$. The detector-source distances are of order $10^4\lambda_F$. In red, the classical cardinal sine diffraction pattern for a single slit is plotted considering as relevant the distance from the object to the second detector. The results from Eq. (4.65) seem to be fitted perfectly. [In the plot the function $|\chi|^2$ has been renormalized to its value in $x_2 = 0$. The same convention has been adopted in all the other numerical plots we present in the following.]

in the electron field near the longitudinal axis passing through the center of the object. In fact, let's notice that, since $r_{2z} + d_z/2 < 0$, we have $|r_{2z} + d_z/2| + (r'_z - d_z/2) + d_z = r'_z - r_{2z}$. For small transverse coordinates, the following expansion is valid:

$$\frac{e^{ik_F|\boldsymbol{r'}-\boldsymbol{r_2}|}}{|\boldsymbol{r'}-\boldsymbol{r_2}|} \simeq e^{ik_F(r'_z-d_z/2)}e^{ik_F d_z}e^{ik_F|r_{2z}+d_z/2|}\frac{e^{i\frac{k_F|\boldsymbol{r'_\perp}-\boldsymbol{r}_{2\perp}|^2}{2(|r_{2z}+d_z/2|+(r'_z-d_z/2)+d_z)}}}{(|r_{2z}+d_z/2|+(r'_z-d_z/2)+d_z)}. \tag{4.66}$$

That is to say, if $f(\boldsymbol{r'})$ is different from zero only in a small region and if $\boldsymbol{r_2}$ is not far from the longitudinal axis, Eq. (4.65) is just the first order expansion of

$$\chi(\boldsymbol{r}_1;\boldsymbol{r}_2;\tau) = \frac{-im^4\Delta\lambda_1^2\lambda_2}{2k_F^2}\int d^3\boldsymbol{r'}f(\boldsymbol{r'})\frac{e^{ik_F|\boldsymbol{r'}-\boldsymbol{r_2}|}}{|\boldsymbol{r'}-\boldsymbol{r_2}|}\frac{e^{ik_F|\boldsymbol{r}_1-\boldsymbol{r'}|}}{|\boldsymbol{r}_1-\boldsymbol{r'}|}$$
$$\times\,\Phi(|r_{2z}+d_z/2|-|\boldsymbol{r}_1-\boldsymbol{r'}|-(r'_z-d_z/2)+2\mu\tau/k_F,d_z). \tag{4.67}$$

The meaning of this formula is quite straightforward: the spherical waves represent free propagation, while the filter f is the object. Φ is a weighing

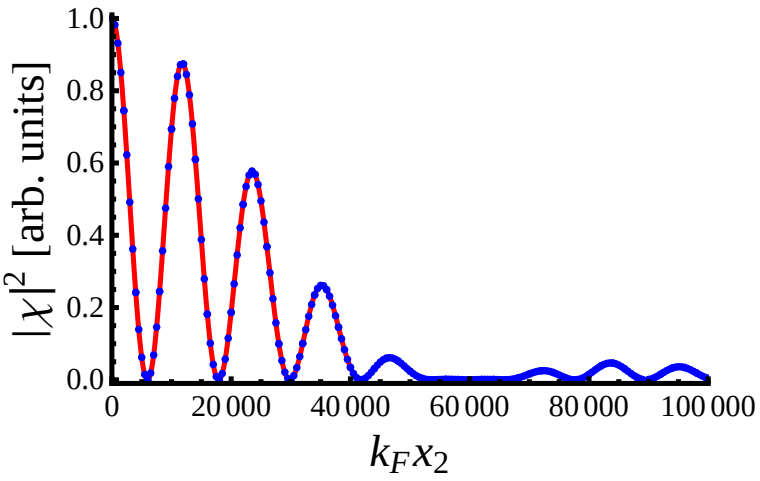

Figure 4.3: Simulation of a ghost interference/diffraction setup with a single-slit object: Eq. (4.65) has been integrated numerically assuming a slit-width of $2\lambda_F$. The detector-source distances are of order $10^4\lambda_F$. In red, the Young's double-slit interference pattern multiplied by the cardinal sine for the single-slit diffraction is plotted considering as relevant the distance from the object to the second detector. The results from Eq. (4.65) seem to be fitted perfectly.

function that takes into account the correlation of the electrons. Once again this is the only part that is concerned by the superconducting nature of the tip. Moreover, there is no track of the tip's shape elsewhere, so it appears like if the infinitely long source wasn't there, as long as the propagation is concerned. The tip only matters when we consider the correlation length.

Let's notice that, with the right choice of the position of the first detector $\boldsymbol{r_1}$, at first order Φ depends only on the longitudinal distances. If the object is infinitely thin ($w_f \simeq 0$), Φ can be considered a constant and taken outside of the integral. In this case, the anomalous correlation is proportional to the convolution of a spherical wave with an object and a free propagation, which is exactly the interference - diffraction effect due to the object from the point of view of the Huygens principle.

Let's examine the extreme case of a point-like double-slit object. This means taking the limit $w_f = 0$ and assuming a double delta-like aperture: $f(\boldsymbol{r'}) = \delta(z' - z_0)\delta(y')\delta(x' - a) + \delta(z' - z_0)\delta(y')\delta(x' + a)$, where a is the distance of the slit from the axis. Suppose to fix the first detector on the axis, which means midway between the slits in the transverse direction at a fixed longitudinal distance $r_{1z} - z_0$. So, by construction, considering the only two admitted values of $\boldsymbol{r'}$, the distance $|\boldsymbol{r}_1 - \boldsymbol{r'}|$ is a constant and so is Φ. If

we scan detector D2 over the plane $z = r_{2z}$, we have from Eq. (4.65)

$$\begin{aligned}|\chi(\boldsymbol{r}_1;\boldsymbol{r}_2;\tau)|^2 &\propto |e^{i\frac{k_F(r_{2x}-a)^2}{2(r'_z-r_{2z})}} + e^{i\frac{k_F(r_{2x}+a)^2}{2(r'_z-r_{2z})}}|^2 \\ &\propto \cos^2\left(\frac{k_F(r_{2x}-a)^2}{4(r'_z-r_{2z})} - \frac{k_F(r_{2x}+a)^2}{4(r'_z-r_{2z})}\right) \\ &= \cos^2\left(\frac{ak_F r_{2x}}{(r'_z-r_{2z})}\right) = \cos^2\left(\frac{2a\pi r_{2x}}{\lambda_F(r'_z-r_{2z})}\right). \end{aligned} \tag{4.68}$$

Recalling the fact that $2a$ is the distance between the slits, we obtain the well-known result for the double-slit interference pattern in classical optics for small r_{2x}. Let's notice that, analogously to Strekalov's experiment, the important distance in this case is the one between the object and the second detector, across the tip (which seems not to be present). Instead, the first detector acts like a point-like source. This is a typical example of ghost interference.

A situation a little bit closer to reality is the one with finite slit-width. In this case an analytical result is rather difficult and we decided to compute a numerical result for some fixed parameters. The simulations for a single slit and for a double-slit object are presented in Figs. 4.2, 4.3. The classical single- and double-slit interference/diffraction patterns are recovered: the data from Eq. (4.65) seem to be fitted perfectly by the classical expressions. This result is totally equivalent to the one obtained by Strekalov et al. using photons (see Section 2.2).

4.6 Particular case: finite spherical source

Let's suppose to have a small spherical source this time (see Fig. 4.4). If we don't insert any object, the system has a spherical simmetry and defining left and right doesn't make sense. In fact, in this case we can consider neither two distinguishable emitting region inside the superconductor nor two independent vacuum regions outside. Even when we break the simmetry by inserting the object, since the latter is small compared to the source-detector distances, the independence assumption is not valid. Of course, the initial discussion should be slightly modified, but as we already pointed out at the end of section 4.3, the result of Eq. (4.44) is still valid with the condition $\boldsymbol{d} = 0$. For sake of simplicity, we describe the source region with a 3D gaussian distribution:

$$g(\boldsymbol{r}) = \frac{1}{\sqrt{(2\pi w)^3}} e^{-\frac{|\boldsymbol{r}|^2}{2w^2}}. \tag{4.69}$$

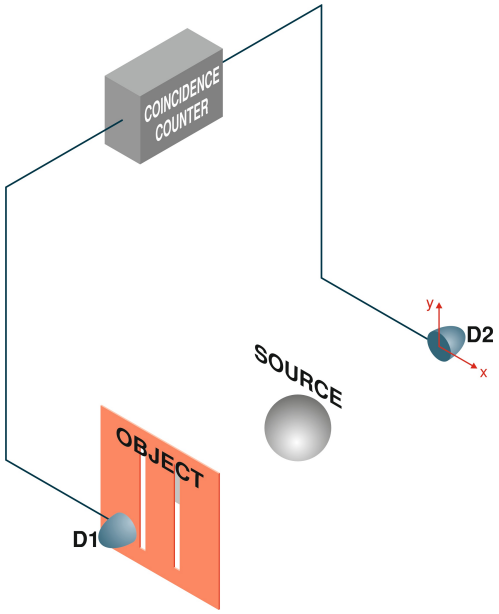

Figure 4.4: Correlated electrons are emitted in opposite directions from a small spherical superconducting tip and are detected in coincidence by two point-like detectors $D1$ and $D2$. An object is placed in front of $D1$, which is held fix. $D2$ moves on the transverse plane.

Keeping the other definitions of the previous case, following a procedure similar to the Sec. 4.5 and to [18], under the far field conditions $k_f z_0 \gg 1$ and $k_F \boldsymbol{r_2} \gg 1$, we obtain the following spectrum:

$$\begin{aligned}\chi(\boldsymbol{r}_1;\boldsymbol{r}_2;E) = &\frac{i\pi}{4(2\pi)^2\sqrt{E^2-|\Delta|^2}q(E)w^2}m^3\lambda_1^2\lambda_2\Delta\int d^3\boldsymbol{r'}\frac{e^{ip(E)|\boldsymbol{r_2}|}}{i|\boldsymbol{r_2}|}f(\boldsymbol{r'})\\
&\times\frac{e^{ip(-E)|\boldsymbol{r'}|}}{i|\boldsymbol{r'}|}M(-E)\frac{e^{ip(-E)|\boldsymbol{r}_1-\boldsymbol{r'}|}}{i|\boldsymbol{r}_1-\boldsymbol{r'}|}e^{-w^2(2m\mu-q(E)^2)}\\
&\times\sum_{\sigma=+,-}[e^{-(wq(E)+wk_\sigma(E))^2}(i\sigma\,\mathrm{erfi}(wq(E)+wk_\sigma(E))+1)\\
&-e^{-(wq(E)-wk_\sigma(E))^2}(i\sigma\,\mathrm{erfi}(-wq(E)+wk_\sigma(E))+1)], \qquad (4.70)\end{aligned}$$

where we have defined

$$q(E)=\sqrt{m\mu-p(E)p(-E)\hat{\boldsymbol{r'}}\cdot\hat{\boldsymbol{r}}_{\boldsymbol{2}}/2}. \qquad (4.71)$$

The derivation is presented in Appendix A. The expansion at first order in $|E|/\mu$ and $|\Delta|/\mu$ of the previous equation is

$$\begin{aligned}\chi(\boldsymbol{r}_1;\boldsymbol{r}_2;E) \simeq & \sum_{\sigma=+,-}\int d^3\boldsymbol{r'} f(\boldsymbol{r'})\frac{\pi m^3\lambda_1^2\lambda_2\Delta}{4(2\pi)^3 k_F\sqrt{\frac{1-\hat{\boldsymbol{r'}}\cdot\hat{\boldsymbol{r_2}}}{2}}w^2} \\ & \times e^{ik_F(|\boldsymbol{r_2}|+|\boldsymbol{r'}|+|\boldsymbol{r}_1-\boldsymbol{r'}|)}|\boldsymbol{r_2}||\boldsymbol{r'}||\boldsymbol{r}_1-\boldsymbol{r'}|\frac{e^{i\frac{k_F E}{2\mu}(|\boldsymbol{r_2}|-|\boldsymbol{r'}|-|\boldsymbol{r}_1-\boldsymbol{r'}|)}}{\sqrt{E^2-|\Delta|^2}} \\ & \times [e^{-2w^2k_F^2(1-\sqrt{\frac{1-\hat{\boldsymbol{r'}}\cdot\hat{\boldsymbol{r_2}}}{2}})(1+\sigma\frac{\sqrt{E^2-|\Delta|^2}}{2\mu})} \\ & - e^{-2w^2k_F^2(1+\sqrt{\frac{1-\hat{\boldsymbol{r'}}\cdot\hat{\boldsymbol{r_2}}}{2}})(1+\sigma\frac{\sqrt{E^2-|\Delta|^2}}{2\mu})}] \\ & + \int d^3\boldsymbol{r'} f(\boldsymbol{r'})\frac{i\sqrt{\pi}m^3\lambda_1^2\lambda_2\Delta\Lambda e^{-w^2k_F^2\frac{1+\hat{\boldsymbol{r'}}\cdot\hat{\boldsymbol{r_2}}}{2}}}{2(2\pi)^3\sqrt{\frac{1-\hat{\boldsymbol{r'}}\cdot\hat{\boldsymbol{r_2}}}{2}}w\mu} \\ & \times \frac{e^{ik_F(|\boldsymbol{r_2}|+|\boldsymbol{r'}|+|\boldsymbol{r}_1-\boldsymbol{r'}|)}}{|\boldsymbol{r_2}||\boldsymbol{r'}||\boldsymbol{r}_1-\boldsymbol{r'}|}e^{i\frac{k_F E}{2\mu}(|\boldsymbol{r_2}|-|\boldsymbol{r'}|-|\boldsymbol{r}_1-\boldsymbol{r'}|+\frac{2\mu\tau}{k_F})}. \end{aligned} \tag{4.72}$$

The profile of the emitted electron beam is related to the term in the squared brackets, which at zero-th order in energy is proportional to $\cosh(2w^2k_F^2\sqrt{\frac{1-\hat{\boldsymbol{r'}}\cdot\hat{\boldsymbol{r_2}}}{2}})$. This function is sharply peaked around its maximum which occurs at $\hat{\boldsymbol{r'}}\cdot\hat{\boldsymbol{r_2}} = -1$. This means that when we fix the direction for one of the emitted electrons, the other one will be emitted almost in the opposite direction, with some spread related to the size of the source: the bigger the tip, the more collimated is the beam.

Keeping all that in mind, we can focus our attention on the relevant range $\hat{\boldsymbol{r'}}\cdot\hat{\boldsymbol{r_2}} \simeq -1$ and expand the integrand around its maximum. In that case, the second term in the squared brackets is negligible with respect to to first one. In fact their ratio, neglecting the contributions in $|E|/\mu$, $|\Delta|/\mu$ and $(1+\hat{\boldsymbol{r'}}\cdot\hat{\boldsymbol{r_2}})$, is

$$\frac{e^{-2w^2k_F^2(1-\sqrt{\frac{1-\hat{\boldsymbol{r'}}\cdot\hat{\boldsymbol{r_2}}}{2}})(1+\sigma\frac{\sqrt{E^2-|\Delta|^2}}{2\mu})}}{e^{-2w^2k_F^2(1+\sqrt{\frac{1-\hat{\boldsymbol{r'}}\cdot\hat{\boldsymbol{r_2}}}{2}})(1+\sigma\frac{\sqrt{E^2-|\Delta|^2}}{2\mu})}} = e^{4w^2k_F^2(\sqrt{\frac{1-\hat{\boldsymbol{r'}}\cdot\hat{\boldsymbol{r_2}}}{2}})(1+\sigma\frac{\sqrt{E^2-|\Delta|^2}}{2\mu})} \simeq e^{4w^2k_F^2} \gg 1. \tag{4.73}$$

The last inequality holds for w of the order or greater than λ_F. Since $(1-\sqrt{\frac{1-\hat{\boldsymbol{r'}}\cdot\hat{\boldsymbol{r_2}}}{2}}) \ll 1$, if we want to keep only first order terms in the exponential, we should also neglect the contribution given by $\frac{\sqrt{E^2-|\Delta|^2}}{2\mu} \ll 1$.

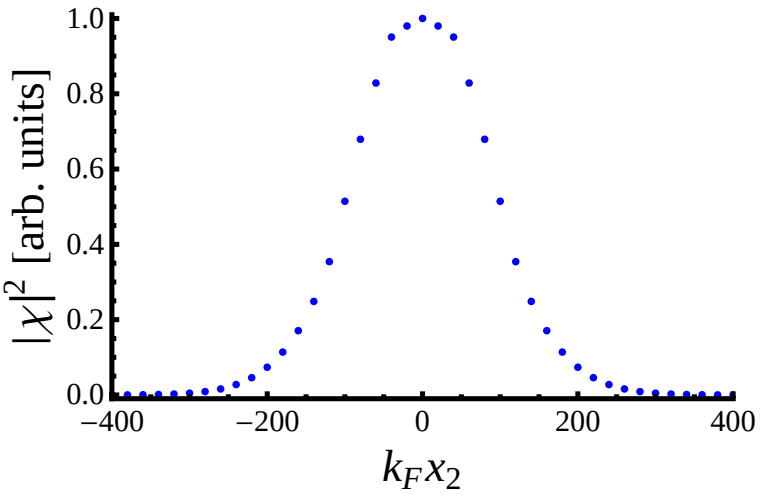

Figure 4.5: Simulation of a ghost image reconstruction of a single-slit object: Eq. (4.74) has been integrated numerically assuming a slit-width of $2\lambda_F$ and a source size of the order of $100\lambda_F$. The detector-source distances are of order $10^4\lambda_F$.

Back in the correlation time picture we have

$$\chi(\boldsymbol{r}_1;\boldsymbol{r}_2;\tau) \simeq \int d^3\boldsymbol{r'} f(\boldsymbol{r'}) \frac{\pi m^3 \lambda_1^2 \lambda_2 \Delta}{4(2\pi)^3 k_F \sqrt{\frac{1-\hat{\boldsymbol{r'}}\cdot\hat{\boldsymbol{r_2}}}{2}} w^2} \frac{e^{ik_F(|\boldsymbol{r_2}|+|\boldsymbol{r'}|+|\boldsymbol{r}_1-\boldsymbol{r'}|)}}{|\boldsymbol{r_2}||\boldsymbol{r'}||\boldsymbol{r}_1-\boldsymbol{r'}|}$$
$$\times [e^{-2w^2k_F^2(1-\sqrt{\frac{1-\hat{\boldsymbol{r'}}\cdot\hat{\boldsymbol{r_2}}}{2}})} \Phi(|\boldsymbol{r_2}|-|\boldsymbol{r'}|-|\boldsymbol{r}_1-\boldsymbol{r'}|+\frac{2\mu\tau}{k_F},0)$$
$$+ 4\sqrt{\pi} i k_F w \Lambda e^{-w^2k_F^2\frac{1+\hat{\boldsymbol{r'}}\cdot\hat{\boldsymbol{r_2}}}{2}} \delta(\frac{k_F}{2}(|\boldsymbol{r_2}|-|\boldsymbol{r'}|-|\boldsymbol{r}_1-\boldsymbol{r'}|+\frac{2\mu\tau}{k_F}))]. \tag{4.74}$$

The term with the delta function is zero almost everywhere, besides some specific values of $\boldsymbol{r'}$ that don't always exist. In fact, if we don't choose the position of the detectors satisfying $|\boldsymbol{r_2}|+\frac{2\mu\tau}{k_F} > |\boldsymbol{r_1}|$, that term is always zero. Of course this condition can be relaxed if we consider also the second order in energy, so that the delta function is smoothed into a gaussian. However, this is just a correction to the main term, which is the first one. Let's analyse it.

The factor $\frac{e^{ik_F(|\boldsymbol{r_2}|+|\boldsymbol{r'}|+|\boldsymbol{r}_1-\boldsymbol{r'}|)}}{|\boldsymbol{r_2}||\boldsymbol{r'}||\boldsymbol{r}_1-\boldsymbol{r'}|}$ represents the free propagation in the vacuum, while $f(\boldsymbol{r'})$ is the object. Let's notice that $\Phi(x,0) = -i\pi H_0^{(2)}(|\frac{x}{\pi\xi}|)$ diverges in 0 logarithmically in its real part. It represents the correlation between the electrons and has its origin in the superconductive nature of

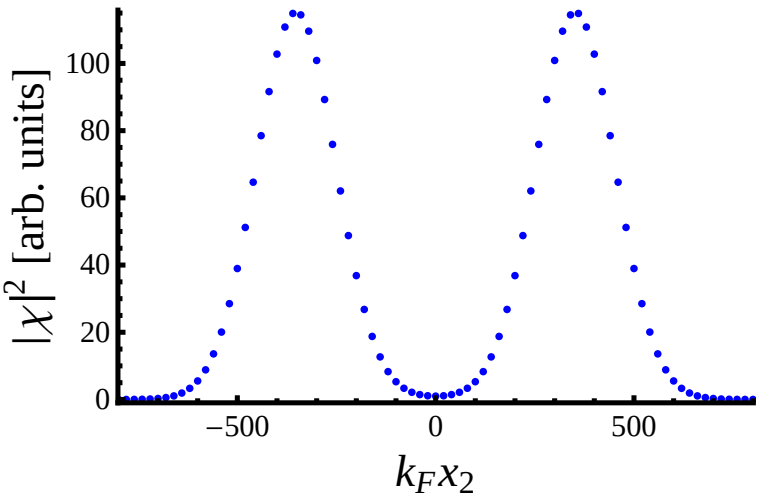

Figure 4.6: Simulation of a ghost image reconstruction of a double-slit object: Eq. (4.74) has been integrated numerically assuming a slit-width of $2\lambda_F$, a separation of $100\lambda_F$ and a source size of the order of $100\lambda_F$. The detector-source distances are of order $10^4\lambda_F$.

the tip. This time the lateral correlation, that dipends only on the shape of the emitter, is expressed by the factor $\frac{e^{-2w^2k_F^2(1-\sqrt{\frac{1-\hat{\boldsymbol{r}'}\cdot\hat{\boldsymbol{r}_2}}{2}})}}{\sqrt{\frac{1-\hat{\boldsymbol{r}'}\cdot\hat{\boldsymbol{r}_2}}{2}}}$. The details of this function have already been discussed.

Considering only the main term, let's see what happens if we consider a double point-like aperture (let's call the two points $\boldsymbol{r_A}$ and $\boldsymbol{r_B}$) symmetrical with respect to the line that joins detector 1 to the source. From Eq. (4.74) we have:

$$|\chi(\boldsymbol{r}_1;\boldsymbol{r}_2;\tau)| \propto |\frac{e^{-2w^2k_F^2(1-\sqrt{\frac{1-\hat{\boldsymbol{r_A}}\cdot\hat{\boldsymbol{r_2}}}{2}})}}{\sqrt{\frac{1-\hat{\boldsymbol{r_A}}\cdot\hat{\boldsymbol{r_2}}}{2}}} + \frac{e^{-2w^2k_F^2(1-\sqrt{\frac{1-\hat{\boldsymbol{r_B}}\cdot\hat{\boldsymbol{r_2}}}{2}})}}{\sqrt{\frac{1-\hat{\boldsymbol{r_B}}\cdot\hat{\boldsymbol{r_2}}}{2}}}| \qquad (4.75)$$

If the distance between the two points is big, we will see two separate peaks corresponding to each one of the points. In fact only one of the two addends can be substantially different from zero at the time, according to which position we choose for detector two. So we obtain an inverted image with some diffraction effects due to the finite size of the tip. This is a typical case of ghost imaging.

On the other hand, if the two points are close to each other, for $\boldsymbol{r_2}$ in the

opposite direction near the line mentioned before, we get at first order

$$|\chi(\boldsymbol{r}_1;\boldsymbol{r}_2;\tau)| \propto |e^{-w^2k_F^2\frac{\hat{\boldsymbol{r_A}}\cdot\hat{\boldsymbol{r_2}}}{2}} + e^{-w^2k_F^2\frac{\hat{\boldsymbol{r_B}}\cdot\hat{\boldsymbol{r_2}}}{2}}|$$
$$= 2e^{-w^2k_F^2\frac{(\hat{\boldsymbol{r_A}}+\hat{\boldsymbol{r_B}})\cdot\hat{\boldsymbol{r_2}}}{4}}\cosh(w^2k_F^2\frac{(\hat{\boldsymbol{r_A}}-\hat{\boldsymbol{r_B}})\cdot\hat{\boldsymbol{r_2}}}{4}). \qquad (4.76)$$

In this case we substantially see only one peak, symmetrical with respect to the D1-tip line (the hyperbolic cosine is almost a constant if the two points are close). Either way, we won't see any kind of oscillatory pattern, typical of the double-slit interference.

In the numerical simulations of Figs. 4.5 and 4.6 the finite width of the slits is taken into account. We can see one single peak for the single-slit case and two symmetric peaks for the double-slit case. The image of the object is reconstructed without evidencing any kind of interference due to the object; the only diffraction effect is the one related to the size of the source, that determines the width of the peaks. Qualitatively, it seems that the system behaves like a pinhole camera, i.e. the same image would be obtained if $D1$ were substituted by a point-like single-particle source and the tip by some sort of pinhole. However let's keep in mind that no Airy oscillatory pattern is observed; a possible explanation relies on the choice of the function $g(\boldsymbol{r})$ of Eq. (4.9) as a gaussian distribution[1], instead of a finite spherical function.

[1]The Fourier transform of a real gaussian is also a real gaussian, which is a function that doesn't oscillate but goes exponentially to zero, as the one in Fig. 4.5.

Chapter 5

Conclusions

The thesis work is set in the framework of quantum imaging, an area of quantum optics that exploits quantum correlations (such as quantum entanglement) to reconstruct images of object, with resolution or other characteristics that exceed the limits of classical optics.

Recently, several experiments demonstrated the possibility of implementing ghost imaging and ghost diffraction schemes with photonic fields.

The goal of this thesis was to analyze diffraction effects and to reconstruct images in the case of electronic sources. The basic idea is to observe ghost diffraction effects exploiting the quantum correlation of a Cooper pair emitted by a superconductive source in such a way that one electron goes in opposite direction with respect to the other. This idea originates from a formal analogy with systems having biphotonic correlated sources (twin-beams).

After a brief review of the relevant experiments about ghost imaging, ghost interference and electron field emission, we introduced an effective model for the emission of Cooper pairs in the vacuum. This model exploits the matrix element formalism, where the Hamiltonian is composed of an unperturbed term for each single separated region and an effective term that couples the separated regions allowing the electrons to transfer between them. A perturbation approach is mandatory for this kind of theory and has been exploited in the hypothesis of weak coupling.

We studied the dynamics of the system in the presence of an object (e.g. a single- or double-slit aperture) and we particularly focalized on the non equilibrium steady state and on the far field limit.

A gedanken-experiment is proposed in different configurations, where we tried to reconstruct the image or the diffraction pattern through coincidence counting measurements of particles from different directions.

The fundamental aspect is that we move only the second detector, the one

that detects particles that do not "see" the object, while the other is held fix. The first obtained result is just formal: various contributions, depending on the parameters of the system, are isolated and analyzed one by one. It seems that the model can be interpreted in a Huygens-like picture: we have the convolution of free propagation in the vacuum and three "spatial filters", the two emitting (not necessarily distinguishable) regions and the object. Two corrective terms are peculiar: the first one is the only one that takes into account the correlation of the Cooper pair, in fact it is suppressed exponentially on the scale of the Pippard coherence length; the second term is suppressed with a power law on the very much smaller scale of the Fermi wavelength and is deeply connected with the dynamics of the emission process.

An analytic expression for this convolution, even if approximated, is not easy to get, unless we study some limit cases: we discussed two of them. The first one is the one with a planar infinite source. Numerical simulations and the direct analytic calculation of the point-like case, both showed patterns similar to that of classical optics, with the exception of the object-second detector distance being the relevant one. The result is totally analogous to the photonic case; the ghost diffraction/interference effect is verified.

The second setup is the one with a space-limited spherical-symmetric superconductive source. The exact shape of this tip determines the divergence of the emitted electron beam: this is the dominant overall observed effect. We do not see interference fringes; instead, in case of not too small objects, one can reconstruct the image of the aperture. The specific cases of single and double slits are discussed: for our choice of the parameters, only one peak is visible in the single slit case, as expected, while two distinguishable ones have been observed in the other case. The resolution is strictly related to the size of the emitter and can be increased by enlarging the tip. It is interesting to note that one can switch from the ghost diffraction regime to the ghost imaging regime simply by changing tip.

Appendix A

Derivation of some intermediate results

Derivation of Equations (4.29) and (4.30)

Since $\mathcal{L}[f(t)'](s) = s\mathcal{L}[f(t)](s) - f(0)$, after Laplace-transforming the system in Eq. (4.24) and keeping in mind the definitions of Eq. (4.28), we have

$$\begin{cases} sA_p - A_{p0} = -i\Omega_p A_p - i\lambda_1 \sum_l \int d^3\boldsymbol{q} \mathcal{T}^{\dagger(l)}_{\boldsymbol{qp}} B^{(l)}_q \\ sB^{(l)}_p - B^{(l)}_{p0} = -i\mathcal{E}_p B^{(l)}_p - i\lambda_1 \int d^3\boldsymbol{k} \mathcal{T}^{(l)}_{\boldsymbol{pk}} A_k - i\lambda_2 \delta_{lR} \int d^3\boldsymbol{q} \mathcal{F}^{\dagger}_{\boldsymbol{qp}} C_q \\ sC_p - C_{p0} = -i\mathcal{E}_p C_p - i\lambda_2 \int d^3\boldsymbol{k} \mathcal{F}_{\boldsymbol{pk}} B^{(R)}_k, \end{cases} \tag{A.1}$$

which is equivalent to

$$\begin{cases} A_p &= (s+i\Omega_p)^{-1} A_{p0} - i\lambda_1 (s+i\Omega_p)^{-1} \sum_l \int d^3\boldsymbol{q} \mathcal{T}^{\dagger(l)}_{\boldsymbol{qp}} B^{(l)}_q \\ B^{(l)}_p &= (s+i\mathcal{E}_p)^{-1} B^{(l)}_{p0} - i\lambda_1 (s+i\mathcal{E}_p)^{-1} \int d^3\boldsymbol{k} \mathcal{T}^{(l)}_{\boldsymbol{pk}} A_k \\ &\quad -i\lambda_2 \delta_{lR} (s+i\mathcal{E}_p)^{-1} \int d^3\boldsymbol{q} \mathcal{F}^{\dagger}_{\boldsymbol{qp}} C_q \\ C_p &= (s+i\mathcal{E}_p)^{-1} C_{p0} - i\lambda_2 (s+i\mathcal{E}_p)^{-1} \int d^3\boldsymbol{k} \mathcal{F}_{\boldsymbol{pk}} B^{(R)}_k. \end{cases} \tag{A.2}$$

After substituting the first and the last equations in the second one, we get

$$
\begin{aligned}
B_p^{(l)} &= (s+i\mathcal{E}_p)^{-1}B_{p0}^{(l)} - i\lambda_1(s+i\mathcal{E}_p)^{-1}\int d^3\boldsymbol{k}\mathcal{T}_{\boldsymbol{pk}}^{(l)}[(s+i\Omega_k)^{-1}A_{k0} \\
&- i\lambda_1(s+i\Omega_k)^{-1}\sum_{l'}\int d^3\boldsymbol{q}\mathcal{T}_{\boldsymbol{qk}}^{\dagger(l')}B_q^{(l')}] \\
&- i\lambda_2(s+i\mathcal{E}_p)^{-1}\delta_{lR}\int d^3\boldsymbol{q}\mathcal{F}_{\boldsymbol{qp}}^{\dagger}[(s+i\mathcal{E}_q)^{-1}C_{q0} \\
&- i\lambda_2(s+i\mathcal{E}_q)^{-1}\int d^3\boldsymbol{k}\mathcal{F}_{\boldsymbol{qk}}B_k^{(R)}]. \qquad \text{(A.3)}
\end{aligned}
$$

This is equivalent to

$$
\begin{aligned}
&\sum_{l'}\int d^3\boldsymbol{q}[\delta_{ll'}\delta(\boldsymbol{q}-\boldsymbol{p}) + \lambda_1^2(s+i\mathcal{E}_p)^{-1}\int d^3\boldsymbol{k}\mathcal{T}_{\boldsymbol{pk}}^{(l)}(s+i\Omega_k)^{-1}\mathcal{T}_{\boldsymbol{qk}}^{\dagger(l')} \\
&+ \delta_{ll'}\lambda_2^2\delta_{lR}(s+i\mathcal{E}_p)^{-1}\int d^3\boldsymbol{k}\mathcal{F}_{\boldsymbol{kp}}^{\dagger}(s+i\mathcal{E}_k)^{-1}\mathcal{F}_{\boldsymbol{kq}}]B_q^{(l')} \\
&= (s+i\mathcal{E}_p)^{-1}B_{p0}^{(l)} - i\lambda_1(s+i\mathcal{E}_p)^{-1}\int d^3\boldsymbol{k}\mathcal{T}_{\boldsymbol{pk}}^{(l)}(s+i\Omega_k)^{-1}A_{k0} \\
&- i\lambda_2\delta_{lR}(s+i\mathcal{E}_p)^{-1}\int d^3\boldsymbol{q}\mathcal{F}_{\boldsymbol{qp}}^{\dagger}(s+i\mathcal{E}_q)^{-1}C_{q0}. \qquad \text{(A.4)}
\end{aligned}
$$

Let's define the matrix $\mathcal{G}_{pq}^{ll'}$ such that its inverse is

$$
\begin{aligned}
[\mathcal{G}^{-1}]_{pq}^{ll'} = [&\delta_{ll'}\delta(\boldsymbol{q}-\boldsymbol{p}) + \lambda_1^2(s+i\mathcal{E}_p)^{-1}\int d^3\boldsymbol{k}\mathcal{T}_{\boldsymbol{pk}}^{(l)}(s+i\Omega_k)^{-1}\mathcal{T}_{\boldsymbol{qk}}^{\dagger(l')} \\
&+ \delta_{ll'}\lambda_2^2\delta_{lR}(s+i\mathcal{E}_p)^{-1}\int d^3\boldsymbol{k}\mathcal{F}_{\boldsymbol{kp}}^{\dagger}(s+i\mathcal{E}_k)^{-1}\mathcal{F}_{\boldsymbol{kq}}],
\end{aligned}
$$

so that $\sum_l \int d^3\boldsymbol{p}\mathcal{G}_{kp}^{l''l}[\mathcal{G}^{-1}]_{pq}^{ll'} = \delta_{l''l'}\delta(\boldsymbol{k}-\boldsymbol{q})$.

Multiplying on the left by $\mathcal{G}_{k'p}^{l''l}$ and summing over l and $\boldsymbol{p}$ yields

$$
\begin{aligned}
B_{k'}^{(l'')} =& \sum_l\int d^3\boldsymbol{p}\mathcal{G}_{k'p}^{l''l}\sum_{l'}\int d^3\boldsymbol{q}[\mathcal{G}^{-1}]_{pq}^{ll'}B_q^{(l')} \\
=& \sum_l\int d^3\boldsymbol{p}\mathcal{G}_{k'p}^{l''l}(s+i\mathcal{E}_p)^{-1}B_{p0}^{(l)} \\
&-i\sum_l\int d^3\boldsymbol{p}\mathcal{G}_{k'p}^{l''l}\lambda_1(s+i\mathcal{E}_p)^{-1}\int d^3\boldsymbol{k}\mathcal{T}_{\boldsymbol{pk}}^{(l)}(s+i\Omega_k)^{-1}A_{k0} \\
&-i\sum_l\int d^3\boldsymbol{p}\mathcal{G}_{k'p}^{l''l}\lambda_2\delta_{lR}(s+i\mathcal{E}_p)^{-1}\int d^3\boldsymbol{q}\mathcal{F}_{\boldsymbol{qp}}^{\dagger}(s+i\mathcal{E}_q)^{-1}C_{q0}. \qquad \text{(A.5)}
\end{aligned}
$$

Let's assume a weak coupling regime, which means $\lambda_1, \lambda_2 \ll 1$. Up to second order in λ_1 and λ_2, for regular $T_{\boldsymbol{pk}}$ and $F_{\boldsymbol{pk}}$ [18], we have

$$\begin{aligned}\mathcal{G}^{ll'}_{pq} = \delta_{ll'}\delta(\boldsymbol{q}-\boldsymbol{p}) - \lambda_1^2 \int d^3\boldsymbol{k}(s+i\mathcal{E}_p)^{-1}\mathcal{T}^{(l)}_{\boldsymbol{pk}}(s+i\Omega_k)^{-1}\mathcal{T}^{\dagger(l')}_{\boldsymbol{qk}} \\ - \delta_{ll'}\lambda_2^2\delta_{lR}\int d^3\boldsymbol{k}(s+i\mathcal{E}_p)^{-1}\mathcal{F}^{\dagger}_{\boldsymbol{kp}}(s+i\mathcal{E}_k)^{-1}\mathcal{F}_{\boldsymbol{kq}} \qquad \text{(A.6)}\end{aligned}$$

After defining the 2x2 matrix product $\mathcal{B}^{ll'}_{pq} = \mathcal{G}^{ll'}_{pq}(s+i\mathcal{E}_q)^{-1}$, we have

$$\begin{aligned}B^{(l'')}_{k'} = \sum_l \int d^3\boldsymbol{p}\mathcal{B}^{l''l}_{k'p}B^{(l)}_{p0} - i\sum_l \int d^3\boldsymbol{p}\mathcal{B}^{l''l}_{k'p}\lambda_1 \int d^3\boldsymbol{k}\mathcal{T}^{(l)}_{\boldsymbol{pk}}(s+i\Omega_k)^{-1}A_{k0} \\ - i\int d^3\boldsymbol{p}\mathcal{B}^{l''R}_{k'p}\lambda_2 \int d^3\boldsymbol{q}\mathcal{F}^{\dagger}_{\boldsymbol{qp}}(s+i\mathcal{E}_q)^{-1}C_{q0} \qquad \text{(A.7)}\end{aligned}$$

and

$$\begin{aligned}C_p = (s+i\mathcal{E}_p)^{-1}C_{p0} - i\lambda_2(s+i\mathcal{E}_p)^{-1}\int d^3\boldsymbol{k'}\mathcal{F}_{\boldsymbol{pk'}}[\sum_l \int d^3\boldsymbol{p}\mathcal{B}^{Rl}_{k'p}B^{(l)}_{p0} \\ - i\sum_l \int d^3\boldsymbol{p}\mathcal{B}^{Rl}_{k'p}\lambda_1 \int d^3\boldsymbol{k}\mathcal{T}^{(l)}_{\boldsymbol{pk}}(s+i\Omega_k)^{-1}A_{k0} \\ - i\int d^3\boldsymbol{p}\mathcal{B}^{RR}_{k'p}\lambda_2 \int d^3\boldsymbol{q}\mathcal{F}^{\dagger}_{\boldsymbol{qp}}(s+i\mathcal{E}_q)^{-1}C_{q0}]. \qquad \text{(A.8)}\end{aligned}$$

If we keep only the terms relevant for the anomalous correlation of Eq. (4.35d), we get Eqs. (4.29) and (4.30).

Derivation of Equation (4.44)

The Laplace inverse transform of Eq. (4.43) yields

$$
\begin{aligned}
\chi(\boldsymbol{r}_1,t_1;\boldsymbol{r}_2,t_2) = & \int d^3\boldsymbol{p}\int d^3\boldsymbol{k'}e^{i\boldsymbol{p}\cdot\boldsymbol{r}_1}e^{i\boldsymbol{k'}\cdot\boldsymbol{r}_2}\langle[-i\lambda_2\int d^3\boldsymbol{k''}\mathcal{F}^{11}_{\boldsymbol{pk''}} \\
& \times \frac{e^{-i\varepsilon_{k''}t_1}}{i(\varepsilon_p-\varepsilon_{k''})+0^+}b^{(R)}_{\boldsymbol{k''}\uparrow} - \lambda_1\lambda_2\int d^3\boldsymbol{k''}\mathcal{F}^{11}_{\boldsymbol{pk''}}\int d^3\boldsymbol{k}\mathcal{T}^{(R)11}_{\boldsymbol{k''k}} \\
& \times \frac{e^{-i\omega_k t_1}}{(i(\varepsilon_p-\omega_k)+0^+)(i(\varepsilon_{k''}-\omega_k)+0^+)}\alpha_{\boldsymbol{k}\uparrow}] \\
& \times [-\lambda_1^2\sum_l\int d^3\boldsymbol{p'}\int d^3\boldsymbol{k'''}\mathcal{T}^{*(L)21}_{\boldsymbol{k'k'''}}\mathcal{T}^{(l)11}_{\boldsymbol{p'k'''}} \\
& \times \frac{e^{i\varepsilon_{p'}t_2}}{(i(\varepsilon_{k'}+\varepsilon_{p'})+0^+)(-i(\omega_{k'''}-\varepsilon_{p'})+0^+)}b^{\dagger(l)}_{\boldsymbol{p'}\uparrow} \\
& - \lambda_1^2\sum_l\int d^3\boldsymbol{p'}\int d^3\boldsymbol{k'''}\mathcal{T}^{*(L)22}_{\boldsymbol{k'k'''}}\mathcal{T}^{(l)12}_{\boldsymbol{p'k'''}} \\
& \times \frac{e^{i\varepsilon_{p'}t_2}}{(i(\varepsilon_{k'}+\varepsilon_{p'})+0^+)(i(\omega_{k'''}+\varepsilon_{p'})+0^+)}b^{\dagger(l)}_{\boldsymbol{p'}\uparrow} \\
& + i\lambda_1\int d^3\boldsymbol{k'''}\mathcal{T}^{*(L)21}_{\boldsymbol{k'k'''}}\frac{e^{i\omega_{k'''}t_2}}{i(\varepsilon_{k'}+\omega_{k'''})+0^+}\alpha^\dagger_{\boldsymbol{k'''}\uparrow}]\rangle \\
= & \int d^3\boldsymbol{p}\int d^3\boldsymbol{k'}e^{i\boldsymbol{p}\cdot\boldsymbol{r}_1}e^{i\boldsymbol{k'}\cdot\boldsymbol{r}_2}[\langle(-i\lambda_2\int d^3\boldsymbol{k''}\mathcal{F}^{11}_{\boldsymbol{pk''}} \\
& \times \frac{e^{-i\varepsilon_{k''}t_1}}{i(\varepsilon_p-\varepsilon_{k''})+0^+}b^{(R)}_{\boldsymbol{k''}\uparrow})(-\lambda_1^2\int d^3\boldsymbol{p'}\int d^3\boldsymbol{k'''}\mathcal{T}^{*(L)21}_{\boldsymbol{k'k'''}}\mathcal{T}^{(R)11}_{\boldsymbol{p'k'''}} \\
& \times \frac{e^{i\varepsilon_{p'}t_2}}{(i(\varepsilon_{k'}+\varepsilon_{p'})+0^+)(-i(\omega_{k'''}-\varepsilon_{p'})+0^+)}b^{\dagger(R)}_{\boldsymbol{p'}\uparrow})\rangle \\
& + \langle(-i\lambda_2\int d^3\boldsymbol{k''}\mathcal{F}^{11}_{\boldsymbol{pk''}}\frac{e^{-i\varepsilon_{k''}t_1}}{i(\varepsilon_p-\varepsilon_{k''})+0^+}b^{(R)}_{\boldsymbol{k''}\uparrow}) \\
& \times (-\lambda_1^2\int d^3\boldsymbol{p'}\int d^3\boldsymbol{k'''}\mathcal{T}^{*(L)22}_{\boldsymbol{k'k'''}}\mathcal{T}^{(R)12}_{\boldsymbol{p'k'''}} \\
& \times \frac{e^{i\varepsilon_{p'}t_2}}{(i(\varepsilon_{k'}+\varepsilon_{p'})+0^+)(i(\omega_{k'''}+\varepsilon_{p'})+0^+)}b^{\dagger(R)}_{\boldsymbol{p'}\uparrow})\rangle \\
& + \langle(-\lambda_1\lambda_2\int d^3\boldsymbol{k''}\mathcal{F}^{11}_{\boldsymbol{pk''}}\int d^3\boldsymbol{k}\mathcal{T}^{(R)11}_{\boldsymbol{k''k}} \\
& \times \frac{e^{-i\omega_k t_1}}{(i(\varepsilon_p-\omega_k)+0^+)(i(\varepsilon_{k''}-\omega_k)+0^+)}\alpha_{\boldsymbol{k}\uparrow}) \\
& \times (i\lambda_1\int d^3\boldsymbol{k'''}\mathcal{T}^{*(L)21}_{\boldsymbol{k'k'''}}\frac{e^{i\omega_{k'''}t_2}}{i(\varepsilon_{k'}+\omega_{k'''})+0^+}\alpha^\dagger_{\boldsymbol{k'''}\uparrow})\rangle]. \qquad \text{(A.9)}
\end{aligned}
$$

After evaluating the expectation values and integrating over $\boldsymbol{k''}$ in the first two terms and $\boldsymbol{k'''}$ in the last one, we obtain

$$\begin{aligned}\chi(\boldsymbol{r}_1,t_1;\boldsymbol{r}_2,t_2) = i\lambda_1^2\lambda_2 \int d^3\boldsymbol{p}\int d^3\boldsymbol{k'} e^{i\boldsymbol{p}\cdot\boldsymbol{r}_1}e^{i\boldsymbol{k'}\cdot\boldsymbol{r}_2}\\
\times[\int d^3\boldsymbol{p'}(\mathcal{F}^{11}_{\boldsymbol{pp'}}\frac{e^{-i\varepsilon_{p'}t_1}}{i(\varepsilon_p-\varepsilon_{p'})+0^+}\\
\times\int d^3\boldsymbol{k}\mathcal{T}^{*(L)21}_{\boldsymbol{k'k}}\mathcal{T}^{(R)11}_{\boldsymbol{p'k}}\frac{e^{i\varepsilon_{p'}t_2}}{(i(\varepsilon_{k'}+\varepsilon_{p'})+0^+)(-i(\omega_k-\varepsilon_{p'})+0^+)})\\
+\int d^3\boldsymbol{p'}(\mathcal{F}^{11}_{\boldsymbol{pp'}}\frac{e^{-i\varepsilon_{p'}t_1}}{i(\varepsilon_p-\varepsilon_{p'})+0^+}\\
\times\int d^3\boldsymbol{k}\mathcal{T}^{*(L)22}_{\boldsymbol{k'k}}\mathcal{T}^{(R)12}_{\boldsymbol{p'k}}\frac{e^{i\varepsilon_{p'}t_2}}{(i(\varepsilon_{k'}+\varepsilon_{p'})+0^+)(i(\omega_k+\varepsilon_{p'})+0^+)})\\
-(\int d^3\boldsymbol{p'}\mathcal{F}^{11}_{\boldsymbol{pp'}}\int d^3\boldsymbol{k}\mathcal{T}^{(R)11}_{\boldsymbol{p'k}}\frac{e^{-i\omega_k t_1}}{(i(\varepsilon_p-\omega_k)+0^+)(i(\varepsilon_{p'}-\omega_k)+0^+)}\\
\times\mathcal{T}^{*(L)21}_{\boldsymbol{k'k}}\frac{e^{i\omega_k t_2}}{i(\varepsilon_{k'}+\omega_k)+0^+})].\end{aligned}\tag{A.10}$$

The definitions of Eqs. (4.26),(4.27) yield

$$\begin{aligned}\chi(\boldsymbol{r}_1,t_1;\boldsymbol{r}_2,t_2) = i\lambda_1^2\lambda_2 \int d^3\boldsymbol{p}\int d^3\boldsymbol{k'} e^{i\boldsymbol{p}\cdot\boldsymbol{r}_1}e^{i\boldsymbol{k'}\cdot\boldsymbol{r}_2}\\
\times[-\int d^3\boldsymbol{p'}F_{\boldsymbol{pp'}}\frac{e^{-i\varepsilon_{p'}t_1}}{i(\varepsilon_p-\varepsilon_{p'})+0^+}\\
\times\int d^3\boldsymbol{k}T^{(L)}_{\boldsymbol{k'-k}}v_k T^{(R)}_{\boldsymbol{p'k}}u_k\frac{e^{i\varepsilon_{p'}t_2}}{(i(\varepsilon_{k'}+\varepsilon_{p'})+0^+)}\\
\times(\frac{1}{(i(-\omega_k+\varepsilon_{p'})+0^+)}-\frac{1}{(i(\omega_k+\varepsilon_{p'})+0^+)})\qquad\text{(A.11)}\\
+\int d^3\boldsymbol{p'}F_{\boldsymbol{pp'}}\int d^3\boldsymbol{k}T^{(R)}_{\boldsymbol{p'k}}u_k\frac{e^{-i\omega_k t_1}}{(i(\varepsilon_p-\omega_k)+0^+)(i(\varepsilon_{p'}-\omega_k)+0^+)}\\
\times T^{(L)}_{\boldsymbol{k'-k}}v_k\frac{e^{i\omega_k t_2}}{i(\varepsilon_{k'}+\omega_k)+0^+}].\qquad\text{(A.12)}\end{aligned}$$

Let's add and subtract the term $\frac{1}{i(\varepsilon_{k'}+\omega_k)+0^+}$ in the parenthesis in the first addend and notice that

$$\frac{1}{i(\varepsilon_{k'}+\omega_k)+0^+}+\frac{1}{i(\varepsilon_{p'}-\omega_k)+0^+}=\frac{i(\varepsilon_{p'}+\varepsilon_{k'})+0^+}{(i(\varepsilon_{p'}-\omega_k)+0^+)(i(\varepsilon_{k'}+\omega_k)+0^+)}.\tag{A.13}$$

$$\chi(\boldsymbol{r}_1,t_1;\boldsymbol{r}_2,t_2) = i\lambda_1^2\lambda_2 \int d^3\boldsymbol{p} \int d^3\boldsymbol{k'} e^{i\boldsymbol{p}\cdot\boldsymbol{r}_1} e^{i\boldsymbol{k'}\cdot\boldsymbol{r}_2}$$
$$\times [\int d^3\boldsymbol{p'} F_{\boldsymbol{p}\boldsymbol{p'}} \frac{e^{-i\varepsilon_{p'}t_1}}{i(\varepsilon_p - \varepsilon_{p'}) + 0^+}$$
$$\times \int d^3\boldsymbol{k} T^{(L)}_{\boldsymbol{k'}-\boldsymbol{k}} v_k T^{(R)}_{\boldsymbol{p'}\boldsymbol{k}} u_k \frac{e^{i\varepsilon_{p'}t_2}}{(i(\varepsilon_{k'} + \varepsilon_{p'}) + 0^+)}$$
$$\times (\frac{1}{i(\varepsilon_{k'} + \omega_k) + 0^+} + \frac{1}{(i(\omega_k + \varepsilon_{p'}) + 0^+)}) \tag{A.14}$$
$$- \int d^3\boldsymbol{p'} F_{\boldsymbol{p}\boldsymbol{p'}} \frac{e^{-i\varepsilon_{p'}t_1}}{i(\varepsilon_p - \varepsilon_{p'}) + 0^+}$$
$$\times \int d^3\boldsymbol{k} T^{(L)}_{\boldsymbol{k'}-\boldsymbol{k}} v_k T^{(R)}_{\boldsymbol{p'}\boldsymbol{k}} u_k \frac{e^{i\varepsilon_{p'}t_2}}{(i(\varepsilon_{p'} - \omega_k) + 0^+)(i(\varepsilon_{k'} + \omega_k) + 0^+)}$$
$$+ \int d^3\boldsymbol{p'} F_{\boldsymbol{p}\boldsymbol{p'}} \int d^3\boldsymbol{k} T^{(R)}_{\boldsymbol{p'}\boldsymbol{k}} u_k \frac{e^{-i\omega_k t_1}}{(i(\varepsilon_p - \omega_k) + 0^+)(i(\varepsilon_{p'} - \omega_k) + 0^+)}$$
$$\times T^{(L)}_{\boldsymbol{k'}-\boldsymbol{k}} v_k \frac{e^{i\omega_k t_2}}{i(\varepsilon_{k'} + \omega_k) + 0^+}]. \tag{A.15}$$

Rearranging the terms we have

$$\chi(\boldsymbol{r}_1,t_1;\boldsymbol{r}_2,t_2) = i\lambda_1^2\lambda_2 \int d^3\boldsymbol{p} \int d^3\boldsymbol{k'} e^{i\boldsymbol{p}\cdot\boldsymbol{r}_1} e^{i\boldsymbol{k'}\cdot\boldsymbol{r}_2}$$
$$\times [\int d^3\boldsymbol{p'} F_{\boldsymbol{p}\boldsymbol{p'}} \frac{e^{-i\varepsilon_{p'}t_1}}{i(\varepsilon_p - \varepsilon_{p'}) + 0^+}$$
$$\times \int d^3\boldsymbol{k} T^{(L)}_{\boldsymbol{k'}-\boldsymbol{k}} v_k T^{(R)}_{\boldsymbol{p'}\boldsymbol{k}} u_k \frac{e^{i\varepsilon_{p'}t_2}}{(i(\varepsilon_{k'} + \varepsilon_{p'}) + 0^+)}$$
$$\times (\frac{1}{i(\varepsilon_{k'} + \omega_k) + 0^+} + \frac{1}{(i(\omega_k + \varepsilon_{p'}) + 0^+)}) \tag{A.16}$$
$$+ \int d^3\boldsymbol{p'} F_{\boldsymbol{p}\boldsymbol{p'}} \int d^3\boldsymbol{k} T^{(R)}_{\boldsymbol{p'}\boldsymbol{k}} u_k \frac{1}{(i(\varepsilon_{p'} - \omega_k) + 0^+)(i(\varepsilon_{k'} + \omega_k) + 0^+)}$$
$$\times T^{(L)}_{\boldsymbol{k'}-\boldsymbol{k}} v_k (\frac{e^{i\omega_k(t_2-t_1)}}{(i(\varepsilon_p - \omega_k) + 0^+)} - \frac{e^{-i\varepsilon_{p'}(t_1-t_2)}}{i(\varepsilon_p - \varepsilon_{p'}) + 0^+})]. \tag{A.17}$$

The last term vanishes on the energy shell $\varepsilon_{p'} = \omega_k$. Let's explicit the

scattering matrix elements $F_{\boldsymbol{p}\boldsymbol{p}'}$ exploiting Eq. (4.10):

$$\begin{aligned}\chi(\boldsymbol{r}_1,t_1;\boldsymbol{r}_2,t_2) = i\lambda_1^2\lambda_2 \int d^3\boldsymbol{p} \int d^3\boldsymbol{k}' \int d^3\boldsymbol{r}' \frac{1}{(2\pi)^3} M(\varepsilon_p) \\ \times e^{i\boldsymbol{p}\cdot(\boldsymbol{r}_1-\boldsymbol{r}')} e^{i\boldsymbol{k}'\cdot\boldsymbol{r}_2} f(\boldsymbol{r}') [\int d^3\boldsymbol{p}' e^{i\boldsymbol{p}'\cdot\boldsymbol{r}'} \frac{e^{-i\varepsilon_{p'}t_1}}{i(\varepsilon_p-\varepsilon_{p'})+0^+} \\ \times \int d^3\boldsymbol{k} T^{(L)}_{\boldsymbol{k}'-\boldsymbol{k}} v_k T^{(R)}_{\boldsymbol{p}'\boldsymbol{k}} u_k \frac{e^{i\varepsilon_{p'}t_2}}{(i(\varepsilon_{k'}+\varepsilon_{p'})+0^+)} \\ \times (\frac{1}{i(\varepsilon_{k'}+\omega_k)+0^+} + \frac{1}{(i(\omega_k+\varepsilon_{p'})+0^+)} \\ + \int d^3\boldsymbol{p}' e^{i\boldsymbol{p}'\cdot\boldsymbol{r}'} \int d^3\boldsymbol{k} \frac{1}{(i(\varepsilon_{p'}-\omega_k)+0^+)(i(\varepsilon_{k'}+\omega_k)+0^+)} \\ \times T^{(R)}_{\boldsymbol{p}'\boldsymbol{k}} u_k T^{(L)}_{\boldsymbol{k}'-\boldsymbol{k}} v_k (\frac{e^{i\omega_k(t_2-t_1)}}{(i(\varepsilon_p-\omega_k)+0^+)} - \frac{e^{-i\varepsilon_{p'}(t_1-t_2)}}{i(\varepsilon_p-\varepsilon_{p'})+0^+})].\end{aligned} \tag{A.18}$$

The integration over the momentum $\boldsymbol{p}$ of the electron behind the object yields Eq. (4.44).

Derivation of Equation (4.70)

Let's substitute Eqs. (4.8),(4.59) in Eq. (4.44):

$$
\begin{aligned}
\chi(\boldsymbol{r}_1,t_1;\boldsymbol{r}_2,t_2) = i\frac{1}{(2\pi)^3}m\lambda_1^2\lambda_2 \int d^3\boldsymbol{k'}\int d^3\boldsymbol{r'}e^{i\boldsymbol{k'}\cdot\boldsymbol{r}_2}f(\boldsymbol{r'})\\
\times [\int d^3\boldsymbol{p'}e^{i\boldsymbol{p'}\cdot\boldsymbol{r'}}e^{-i\varepsilon_{p'}t_1}\int d^3\boldsymbol{k}\, h(\boldsymbol{k'})\delta(\boldsymbol{k'}_\perp+\boldsymbol{k}_\perp)h(\boldsymbol{p'})\\
\times e^{-\frac{w_z^2|p'_z-k_z|^2}{2}}\delta(\boldsymbol{p'}_\perp-\boldsymbol{k}_\perp)e^{i(\boldsymbol{k'}+\boldsymbol{k})\cdot\boldsymbol{d}/2}e^{-i(\boldsymbol{p'}-\boldsymbol{k})\cdot\boldsymbol{d}/2}v_ku_k\\
\times \frac{e^{i\varepsilon_{p'}t_2}}{(i(\varepsilon_{k'}+\varepsilon_{p'})+0^+)}\frac{e^{ip(\varepsilon_{p'})|\boldsymbol{r}_1-\boldsymbol{r'}|}}{i|\boldsymbol{r}_1-\boldsymbol{r'}|}e^{-\frac{w_z^2|k'_z+k_z|^2}{2}}\\
\times (\frac{1}{i(\varepsilon_{k'}+\omega_k)+0^+}+\frac{1}{(i(\omega_k+\varepsilon_{p'})+0^+)})M(\varepsilon_{p'})\\
+\int d^3\boldsymbol{p'}e^{i\boldsymbol{p'}\cdot\boldsymbol{r'}}\int d^3\boldsymbol{k}h(\boldsymbol{k'})e^{-\frac{w_z^2|k'_z+k_z|^2}{2}}\delta(\boldsymbol{k'}_\perp+\boldsymbol{k}_\perp)h(\boldsymbol{p'})\\
\times e^{-\frac{w_z^2|p'_z-k_z|^2}{2}}\delta(\boldsymbol{p'}_\perp-\boldsymbol{k}_\perp)\frac{e^{i(\boldsymbol{k'}+\boldsymbol{k})\cdot\boldsymbol{d}/2}e^{-i(\boldsymbol{p'}-\boldsymbol{k})\cdot\boldsymbol{d}/2}v_ku_k}{(i(\varepsilon_{p'}-\omega_k)+0^+)(i(\varepsilon_{k'}+\omega_k)+0^+)}\\
\times (M(\omega_k)\frac{e^{ip(\omega_k)|\boldsymbol{r}_1-\boldsymbol{r'}|}}{i|\boldsymbol{r}_1-\boldsymbol{r'}|}e^{i\omega_k(t_2-t_1)}\\
-M(\varepsilon_{p'})\frac{e^{ip(\varepsilon_{p'})|\boldsymbol{r}_1-\boldsymbol{r'}|}}{i|\boldsymbol{r}_1-\boldsymbol{r'}|}e^{-i\varepsilon_{p'}(t_1-t_2)})]. \qquad \text{(A.19)}
\end{aligned}
$$

Assuming a spherical simmetry for the function $h(\boldsymbol{p}) = h(p)$, the integration over $\boldsymbol{k'}_\perp$ and $\boldsymbol{p'}_\perp$ yields

$$\begin{aligned}
\chi(\boldsymbol{r}_1, t_1; \boldsymbol{r}_2, t_2) = \frac{im\lambda_1^2\lambda_2}{(2\pi)^3} \int_{-\infty}^{\infty} dk'_z \int d^3\boldsymbol{r'} \int d^3\boldsymbol{k} e^{ik'_z r_{2z}} e^{i\boldsymbol{k}_\perp \cdot (\boldsymbol{r'}_\perp - \boldsymbol{r}_{2\perp})} f(\boldsymbol{r'}) \\
\times [\int_{-\infty}^{\infty} dp'_z \, e^{ip'_z r'_z} e^{-i\varepsilon^*_{p'} t_1} h(p(\varepsilon^*_{k'})) e^{-\frac{w_z^2 |k'_z + k_z|^2}{2}} h(p(\varepsilon^*_{p'})) \\
\times e^{-\frac{w_z^2 |p'_z - k_z|^2}{2}} e^{i(k'_z + k_z)d_z/2} e^{-i(p'_z - k_z)d_z/2} v_k u_k \\
\times \frac{e^{i\varepsilon^*_{p'} t_2}}{(i(\varepsilon^*_{k'} + \varepsilon^*_{p'}) + 0^+)} \frac{e^{ip(\varepsilon^*_{p'})|\boldsymbol{r}_1 - \boldsymbol{r'}|}}{i|\boldsymbol{r}_1 - \boldsymbol{r'}|} \\
\times (\frac{1}{i(\varepsilon^*_{k'} + \omega_k) + 0^+} + \frac{1}{(i(\omega_k + \varepsilon^*_{p'}) + 0^+)}) M(\varepsilon^*_{p'}) \\
+ \int_{-\infty}^{\infty} dp'_z \, e^{ip'_z r'_z} h(p(\varepsilon^*_{k'})) e^{-\frac{w_z^2 |k'_z + k_z|^2}{2}} h(p(\varepsilon^*_{p'})) e^{-\frac{w_z^2 |p'_z - k_z|^2}{2}} \\
\times \frac{e^{i(k'_z + k_z)d_z/2} e^{-i(p'_z - k_z)d_z/2} v_k u_k}{(i(\varepsilon^*_{p'} - \omega_k) + 0^+)(i(\varepsilon^*_{k'} + \omega_k) + 0^+)} \\
\times (M(\omega_k) \frac{e^{ip(\omega_k)|\boldsymbol{r}_1 - \boldsymbol{r'}|}}{i|\boldsymbol{r}_1 - \boldsymbol{r'}|} e^{i\omega_k (t_2 - t_1)} \\
- M(\varepsilon^*_{p'}) \frac{e^{ip(\varepsilon^*_{p'})|\boldsymbol{r}_1 - \boldsymbol{r'}|}}{i|\boldsymbol{r}_1 - \boldsymbol{r'}|} e^{-i\varepsilon^*_{p'}(t_1 - t_2)})], \qquad \text{(A.20)}
\end{aligned}$$

where the following functions have been defined:

$$\mu^* = \mu - \frac{\boldsymbol{k}_\perp^2}{2m}, \qquad p^*(E) = \sqrt{2m(\mu^* + E)}, \qquad \varepsilon^*_p = \frac{p_z^2 + \boldsymbol{k}_\perp^2}{2m} - \mu = \frac{p_z^2}{2m} - \mu^*. \qquad \text{(A.21)}$$

As for the general case, thanks to formula (4.46), for large $(r'_z - d_z/2)$ the last term can be neglected. This is valid if the object is far from the emitter, which is the case here. Noticing that placing the second detector far away at the left of the emitter implies $r_{2z} + d_z/2 < 0$, a further integration and a

change of variable yield

$$\begin{aligned}\chi(\boldsymbol{r}_1,t_1;\boldsymbol{r}_2,t_2) = i\frac{1}{(2\pi)^2}m^2\lambda_1^2\lambda_2\int d^3\boldsymbol{r'}\int d^3\boldsymbol{k}e^{ik_zd_z}e^{i\boldsymbol{k}_\perp\cdot(\boldsymbol{r'}_\perp-\boldsymbol{r}_{2\perp})}f(\boldsymbol{r'})\\ \times(\int_{-\infty}^{\infty}dq_z\,e^{iq_z(r_{2z}+d_z/2)}e^{ip^*(-\varepsilon_q^*)(r'_z-d_z/2)}e^{i\varepsilon_q^*t_1}\\ \times h(p(\varepsilon_q^*))e^{-\frac{w_z^2|q_z+k_z|^2}{2}}h(p(-\varepsilon_q^*))e^{-\frac{w_z^2|p^*(-\varepsilon_q^*)-k_z|^2}{2}}v_ku_k\\ \times e^{-i\varepsilon_q^*t_2}\frac{1}{i(\varepsilon_q^*+\omega_k)+0^+}M(-\varepsilon_q^*)\frac{e^{ip(-\varepsilon_q^*)|\boldsymbol{r}_1-\boldsymbol{r'}|}}{i|\boldsymbol{r}_1-\boldsymbol{r'}|p^*(-\varepsilon_q^*)}\\ +\int_{-\infty}^{\infty}dq_z\,e^{-ip^*(-\varepsilon_q^*)(r_{2z}+d_z/2)}e^{iq_z(r'_z-d_z/2)}e^{-i\varepsilon_q^*t_1}\\ \times h(p(-\varepsilon_q^*))e^{-\frac{w_z^2|-p^*(-\varepsilon_q^*)+k_z|^2}{2}}h(p(\varepsilon_q^*))e^{-\frac{w_z^2|q_z-k_z|^2}{2}}v_ku_k\\ \times e^{i\varepsilon_q^*t_2}\frac{1}{(i(\omega_k+\varepsilon_q^*)+0^+)}M(\varepsilon_q^*)\frac{e^{ip(\varepsilon_q^*)|\boldsymbol{r}_1-\boldsymbol{r'}|}}{i|\boldsymbol{r}_1-\boldsymbol{r'}|p^*(-\varepsilon_q^*)}).\end{aligned}\tag{A.22}$$

Using the same technique as Section (4.4), the spectral representation of the anomalous correlation for $|E|<\mu$ is

$$\begin{aligned}\chi(\boldsymbol{r}_1;\boldsymbol{r}_2;E) = i\frac{1}{2\pi}m^3\lambda_1^2\lambda_2\int d^3\boldsymbol{r'}\int d^3\boldsymbol{k}e^{ik_zd_z}e^{i\boldsymbol{k}_\perp\cdot(\boldsymbol{r'}_\perp-\boldsymbol{r}_{2\perp})}f(\boldsymbol{r'})\\ \times(e^{ip^*(-E)(r'_z-d_z/2)}h(p(E))h(p(-E))e^{-\frac{w_z^2|p^*(-E)-k_z|^2}{2}}v_ku_k\\ \times\frac{1}{i(E+\omega_k)+0^+}M(-E)\frac{e^{ip(-E)|\boldsymbol{r}_1-\boldsymbol{r'}|}}{i|\boldsymbol{r}_1-\boldsymbol{r'}|p^*(-E)}\\ \times(-e^{-ip^*(E)|r_{2z}+d_z/2|}e^{-\frac{w_z^2|p^*(E)+k_z|^2}{2}}\frac{1}{p^*(E)}\\ +e^{ip^*(E)|r_{2z}+d_z/2|}e^{-\frac{w_z^2|-p^*(E)+k_z|^2}{2}}\frac{1}{p^*(E)})\\ +e^{ip^*(E)|r_{2z}+d_z/2|}h(p(E))e^{-\frac{w_z^2|-p^*(E)+k_z|^2}{2}}h(p(-E))v_ku_k\\ \times\frac{1}{(i(\omega_k-E)+0^+)}M(-E)\frac{e^{ip(-E)|\boldsymbol{r}_1-\boldsymbol{r'}|}}{i|\boldsymbol{r}_1-\boldsymbol{r'}|p^*(E)}\\ \times(e^{ip^*(-E)(r'_z-d_z/2)}e^{-\frac{w_z^2|p^*(-E)-k_z|^2}{2}}\frac{1}{p^*(-E)}\\ -e^{-ip^*(-E)(r'_z-d_z/2)}e^{-\frac{w_z^2|p^*(-E)+k_z|^2}{2}}\frac{1}{p^*(-E)})).\end{aligned}\tag{A.23}$$

For large distances, the first and fourth addends are negligible due to formula (4.46). Since $d_z \gg w_z$, using the residue theorem we get Eq. (4.61).

Starting from Eq. (4.44), with the definitions given in Section 4.5, under the far field conditions $k_f z_0 \gg 1$ and $k_F \boldsymbol{r_2} \gg 1$ one get

$$\begin{aligned}\chi(\boldsymbol{r}_1;\boldsymbol{r}_2;\tau) = i2\pi m\lambda_1^2\lambda_2 \int dk'\, k' \int d^3\boldsymbol{r'} \frac{e^{ik'|\boldsymbol{r_2}|}}{i|\boldsymbol{r_2}|} f(\boldsymbol{r'}) \\ \times \int dp'\, p' \, \frac{e^{ip'|\boldsymbol{r'}|}}{i|\boldsymbol{r'}|} \int d^3\boldsymbol{k} T_{(k'\hat{\boldsymbol{r_2}})-\boldsymbol{k}} v_k T_{(p'\hat{\boldsymbol{r'}})\boldsymbol{k}} u_k \\ \times \frac{e^{-i\varepsilon_{p'}\tau}}{(i(\varepsilon_{k'}+\varepsilon_{p'})+0^+)} \frac{e^{ip(\varepsilon_{p'})|\boldsymbol{r}_1-\boldsymbol{r'}|}}{i|\boldsymbol{r}_1-\boldsymbol{r'}|} \\ \times \left(\frac{1}{i(\varepsilon_{k'}+\omega_k)+0^+} + \frac{1}{(i(\omega_k+\varepsilon_{p'})+0^+)}\right) M(\varepsilon_{p'}). \end{aligned} \tag{A.24}$$

After integrating with the residue theorem, we get

$$\begin{aligned}\chi(\boldsymbol{r}_1;\boldsymbol{r}_2;\tau) = i(2\pi)^2 m^2\lambda_1^2\lambda_2 \Big[\int dk'\, k' \int d^3\boldsymbol{r'} \frac{e^{ik'|\boldsymbol{r_2}|}}{i|\boldsymbol{r_2}|} f(\boldsymbol{r'}) \\ \times \frac{e^{ip(-\varepsilon_{k'})|\boldsymbol{r'}|}}{i|\boldsymbol{r'}|} \int d^3\boldsymbol{k} T_{(k'\hat{\boldsymbol{r_2}})-\boldsymbol{k}} v_k T_{(p(-\varepsilon_{k'})\hat{\boldsymbol{r'}})\boldsymbol{k}} u_k \\ \times e^{i\varepsilon_{k'}\tau} \frac{1}{i(\varepsilon_{k'}+\omega_k)+0^+} M(-\varepsilon_{k'}) \frac{e^{ip(-\varepsilon_{k'})|\boldsymbol{r}_1-\boldsymbol{r'}|}}{i|\boldsymbol{r}_1-\boldsymbol{r'}|} \\ + \int d^3\boldsymbol{r'} \frac{e^{ip(-\varepsilon_{p'})|\boldsymbol{r_2}|}}{i|\boldsymbol{r_2}|} f(\boldsymbol{r'}) \int dp'\, p' \, \frac{e^{ip'|\boldsymbol{r'}|}}{i|\boldsymbol{r'}|} \\ \times \int d^3\boldsymbol{k} T_{(p(-\varepsilon_{p'})\hat{\boldsymbol{r_2}})-\boldsymbol{k}} v_k T_{(p'\hat{\boldsymbol{r'}})\boldsymbol{k}} u_k \\ \times e^{-i\varepsilon_{p'}\tau} \frac{1}{(i(\omega_k+\varepsilon_{p'})+0^+)} M(\varepsilon_{p'}) \frac{e^{ip(\varepsilon_{p'})|\boldsymbol{r}_1-\boldsymbol{r'}|}}{i|\boldsymbol{r}_1-\boldsymbol{r'}|} \Big]. \end{aligned} \tag{A.25}$$

The spectral representation of the previous quantity for $|E| < \mu$ is

$$\begin{aligned}\chi(\boldsymbol{r}_1;\boldsymbol{r}_2;E) = (2\pi)^3 m^2\lambda_1^2\lambda_2\Delta \int d^3\boldsymbol{r'} \frac{e^{ip(E)|\boldsymbol{r_2}|}}{i|\boldsymbol{r_2}|} f(\boldsymbol{r'}) \\ \times \frac{e^{ip(-E)|\boldsymbol{r'}|}}{i|\boldsymbol{r'}|} \int d^3\boldsymbol{k} T_{(p(E)\hat{\boldsymbol{r_2}})-\boldsymbol{k}} T_{(p(-E)\hat{\boldsymbol{r'}})\boldsymbol{k}} \\ \times \frac{1}{(\omega_k^2-E^2)-i0^+} M(-E) \frac{e^{ip(-E)|\boldsymbol{r}_1-\boldsymbol{r'}|}}{i|\boldsymbol{r}_1-\boldsymbol{r'}|}. \end{aligned} \tag{A.26}$$

Let's substitute Eq. (4.9) in Eq. (A.26) and integrate over the orientation

of $\boldsymbol{k}$:

$$\begin{aligned}\chi(\boldsymbol{r}_1;\boldsymbol{r}_2;E) = &\frac{1}{(2\pi)^2}m^2\lambda_1^2\lambda_2\Delta\int d^3\boldsymbol{r'}\frac{e^{ip(E)|\boldsymbol{r_2}|}}{i|\boldsymbol{r_2}|}f(\boldsymbol{r'})\\ &\times\frac{e^{ip(-E)|\boldsymbol{r'}|}}{i|\boldsymbol{r'}|}M(-E)\frac{e^{ip(-E)|\boldsymbol{r}_1-\boldsymbol{r'}|}}{i|\boldsymbol{r}_1-\boldsymbol{r'}|}e^{-w^2(2m\mu)}\\ &\times\int_0^\infty dk\,k\,\frac{1}{(\omega_k^2-E^2)-i0^+}\\ &\times e^{-w^2k^2}\frac{e^{|p(-E)\hat{\boldsymbol{r}}'-p(E)\hat{\boldsymbol{r}}_2|kw^2}-e^{-|p(-E)\hat{\boldsymbol{r}}'-p(E)\hat{\boldsymbol{r}}_2|kw^2}}{|p(-E)\hat{\boldsymbol{r}}'-p(E)\hat{\boldsymbol{r}}_2|w^2}.\end{aligned}\tag{A.27}$$

With some manipulations we obtain

$$\begin{aligned}\chi(\boldsymbol{r}_1;\boldsymbol{r}_2;E) = &\frac{1}{2(2\pi)^2\sqrt{E^2-|\Delta|^2}}m^3\lambda_1^2\lambda_2\Delta\int d^3\boldsymbol{r'}\frac{e^{ip(E)|\boldsymbol{r_2}|}}{i|\boldsymbol{r_2}|}f(\boldsymbol{r'})\\ &\times\frac{e^{ip(-E)|\boldsymbol{r'}|}}{i|\boldsymbol{r'}|}M(-E)\frac{e^{ip(-E)|\boldsymbol{r}_1-\boldsymbol{r'}|}}{i|\boldsymbol{r}_1-\boldsymbol{r'}|}e^{-w^2(2m\mu-q(E)^2)}\\ &\times\int_{-\infty}^\infty dk\,\Big(pv\frac{1}{k-k_+(E)}+i\pi\delta(k-k_+(E))\\ &+pv\frac{1}{k+k_+(E)}-i\pi\delta(k+k_+(E))\\ &-pv\frac{1}{k-k_-(E)}+i\pi\delta(k-k_-(E))\\ &-pv\frac{1}{k+k_-(E)}-i\pi\delta(k+k_-(E))\Big)\frac{e^{-w^2(k+q(E))^2}}{2q(E)w^2},\end{aligned}\tag{A.28}$$

where we have defined

$$q(E)=\sqrt{m\mu-p(E)p(-E)\hat{\boldsymbol{r'}}\cdot\hat{\boldsymbol{r}}_{\boldsymbol{2}}/2}.\tag{A.29}$$

A simple change of variables yields

$$\begin{aligned}\chi(\boldsymbol{r}_1;\boldsymbol{r}_2;E) = &\frac{1}{4(2\pi)^2\sqrt{E^2-|\Delta|^2}q(E)w^2}m^3\lambda_1^2\lambda_2\Delta\int d^3\boldsymbol{r'}\frac{e^{ip(E)|\boldsymbol{r_2}|}}{i|\boldsymbol{r_2}|}f(\boldsymbol{r'})\\
&\times\frac{e^{ip(-E)|\boldsymbol{r'}|}}{i|\boldsymbol{r'}|}M(-E)\frac{e^{ip(-E)|\boldsymbol{r}_1-\boldsymbol{r'}|}}{i|\boldsymbol{r}_1-\boldsymbol{r'}|}e^{-w^2(2m\mu-q(E)^2)}\\
&\times\int_{-\infty}^{\infty}dk\,(pv\frac{e^{-w^2k^2}}{k-q(E)-k_+(E)}+i\pi\delta(k-q(E)-k_+(E))e^{-w^2k^2}\\
&+pv\frac{e^{-w^2k^2}}{k-q(E)+k_+(E)}-i\pi\delta(k-q(E)+k_+(E))e^{-w^2k^2}\\
&-pv\frac{e^{-w^2k^2}}{k-q(E)-k_-(E)}+i\pi\delta(k-q(E)-k_-(E))e^{-w^2k^2}\\
&-pv\frac{e^{-w^2k^2}}{k-q(E)+k_-(E)}-i\pi\delta(k-q(E)+k_-(E)))e^{-w^2k^2}).\end{aligned}\tag{A.30}$$

Recalling the integral representation on the real axis of the imaginary error function, we have Eq.(4.70).

Bibliography

[1] E. Schrodinger, Naturwissenschafter **23**, 807 (1935).

[2] A. Einstein, B. Podolsky, and N. Rosen, Phys. Rev. **47**, 777 (1935).

[3] A. Peres, *Quantum Theory: Concepts and Methods* (Springer, 1995).

[4] R. Horodecki et al., Rev. Mod. Phys. **81**, 865 (2009).

[5] O. Guhne ang G. Toht, Physics Reports **474**, 1 (2009).

[6] J. S. Bell, Physics **1**, 195-200 (1964).

[7] J. F. Clauser et al., Phys. Rev. Lett. **23**, 880884 (1969).

[8] A. Aspect et al., Phys. Rev. Lett. **49**, 9194 (1982).

[9] M. A. Nielsen and I. L. Chuang, *Quantum Computation and Quantum Information* (Cambridge University Press,Cambridge, 2000).

[10] M. D'Angelo et al., Phys. Rev. Lett. **87**, 013602 (2001).

[11] T. B. Pittman et al., Phys. Rev. A **52**, R3429 (1995).

[12] A. N. Bolo et al., Phys. Rev. Lett. **85**, 2733 (2000).

[13] D. N. Klyshko, *Photons and Nonlinear Optics* (Gordon and Breach, New York 1988).

[14] Y. Shih, IEEE J. Sel. Topics Quantum Electron. **13**, 1016 (2008).

[15] D. N. Klyshko, Sov. Phys. Usp. **31**, 74 (1988).

[16] D. V. Strekalov et al., Phys. Rev. Lett. **74**, 3600 (1995).

[17] Z. L. Wang, J. Phys. Chem. B **104**, 11531175 (2000).

[18] K. Yuasa, Phys Rev B **80**, 104516 (2009).

[19] J. Bardeen, L. N. Cooper and J. R. Schrieffer, Phys. Rev. **108**, 1175 (1957).

[20] P. Recher et al., Phys. Rev. B **63**, 165314 (2001).

[21] P. Recher et al., Phys. Rev. B **65**, 165327 (2002).

[22] O. Sauret et al., Phys. Rev. B **70**, 245313 (2004).

[23] P. Samuelsson et al., Phys. Rev. Lett. **91**, 157002 (2003).

[24] P. Samuelsson et al., Phys. Rev. B **70**, 115330 (2004).

[25] P. Samuelsson et al., New J. Phys. **7**, 176 (2005).

[26] E. Prada and F. Sols, Eur. Phys. J. B **40**, 379 (2004).

[27] E. Prada and F. Sols, New J. Phys. **7**, 231 (2005).

[28] L. Faoro, F. Taddei and R. Fazio, Phys. Rev. B **69**, 125326 (2004).

[29] R. H. Fowler, L. Nordheim, Proceedings of the Royal Society of London **119** (781): 173181 (1928).

[30] K. Nagaoka et al., Nature **396**, 557 (1998).

[31] J. Bardeen, Phys. Rev. Lett. **6**, 57 (1961).

[32] J. W. Goodman, *Introduction to Fourier Optics*, McGraw-Hill Publishing Company, New York (1968).

[33] R. J. Glauber, Phys. Rev. **130**, 2529 (1963).

[34] L. Mandel and E. Wolf, *Optical Coherence and Quantum Optics* (Cambridge University Press, 1995)

[35] M. H. Rubin, Phys. Rev. A **54**, 5439 (1996).

[36] L. N. Cooper, Phys. Rev. **104**, 1189 (1956).

[37] H. Frolich, Phys. Rev. **79**, 845 (1950).

[38] N. N. Bogoliubov, Nuovo Cimento **7**, 794 (1958).

[39] M. Tinkham, *Introduction to Superconductivity* (Dover Publications, New York 1996).

[40] G. Grosso and G. Pastori Parravicini, *Solid state physics* (Academic Press, 2000).

[41] I. Giaever, Phys. Rev. Lett. **5**, 147, 464 (1960).

[42] M. H. Cohen et al., Phys. Rev. Lett. **8**, 316 (1962).

[43] I. Giaever et al., Phys. Rev. **122**, 1101 (1961).

[44] J. W. Gadzuk, Surf. Sci. **15**, 466 (1969).

[45] J. Tersoff and D. R. Hamann, Phys. Rev. Lett. **50**, 1998 (1983).

[46] J. Tersoff and D. R. Hamann, Phys. Rev. B **31**, 805 (1985).

[47] E. Wigner and J. Bardeen, Phys. Rev. **48**, 8487 (1935).

[48] J. Bardeen, Phys. Rev. **49**, 653 (1936).

[49] R. E. Prange, Phys. Rev. **131**, 1083 (1963).

[50] R. D. Young, Phys. Rev. **113**, 110 (1959).

[51] V. Ambegaokar and A. Baratoff, Phys. Rev. Lett. **10**, 486 (1963).

[52] R. D. Young, Phys. Rev. **113**, 115 (1959).

[53] K. Nagaoka et al., Surf. Sci. **357-358**, 218 (1996).

[54] M. Iazzi, *Higher Order Processes in Field Emission Spectroscopy from Superconductors* (Tesi di laurea specialistica, Università di Pisa, 2008).

[55] A. F. Andreev, Sov. Phys. JETP **19**, 1228 (1964).

[56] H. Kiesel et al., Nature **418**, 392 (2002).

Acknowledgements

I would like to thank my supervisor, Prof. Vittorio Giovannetti, for always being so patient and available for me in the last years. I would like to acknowledge his great role in the realization of this thesis for all the things he taught me and for all the useful discussions about this work. His support has been a precious constant and has really helped me in many occasions. I would also like to thank Prof. Giovannetti for guiding me through the world of scientific research and for always stimulating me to participate to seminars and discussions, encouraging me to interact with international colleagues and experts. Most of all, I would like to thank him for being a role model as a physicist, for transmitting me a passion, for teaching me a method and for giving me all those inestimable little advices.

I would also like to thank Dr. Kazuya Yuasa, who has been like a second supervisor for this thesis. I'm pleased to acknowledge his fundamental role in our research for the precious discussions on every detail and for his useful tips and ideas that represented a turning point towards the conclusion of this work. I would also like to thank Dr. Yuasa for being so patient and available and for giving me so much time during his visits.

Finally, I would like to thank my family and friends who always believed in me, supported me and made all this such a wonderful journey.

Stefano Valentini